



# Hydrological Study for Tuban Catchment in Yemen

Final Report



# Hydrological study for the Tuban Basin, Yemen

## Executive summary

Yemen's Tuban Basin faces increasing water stress due to arid conditions, growing demand, and limited groundwater regulation. To support sustainable water planning, this study applied modelling approach, combining a reconnaissance-level SWAT model for the entire basin with detailed models for four priority districts: Al-Mawaset, Al-Selw, Al-Musaymir, and Tuban. The basin-wide model provides a first estimate of the water balance and key hydrological processes using global datasets and satellite-derived inputs. It reveals a strong north-south gradient in water availability, with higher rainfall and runoff in the uplands and increasing scarcity in the delta. While groundwater contributions appear low in the model, actual abstraction is likely much higher. Data limitations, especially for streamflow and groundwater, restricted full calibration but highlight areas for targeted monitoring and analysis. The detailed district models incorporate field data and stakeholder input to better represent irrigation practices, crop patterns, and water infrastructure. They help identify potential zones for water harvesting and groundwater recharge, and offer a strategic basis for planning future interventions. A coupled SWAT-MODFLOW model in Tuban district further supports analysis of aquifer behaviour. While not yet ready for site-specific planning, the models provide essential guidance for prioritising water resource management actions. Continued calibration, improved monitoring networks, and local engagement will be critical for moving toward resilient and sustainable water use in the Tuban Basin.

## Colophon

### Client

United Nations Development Programme (UNDP)

### Status

Final Report

### Date

August 13, 2025

### Reference number

AW25\_201\_NU\_251590

### Author(s)

Uribe, N., Waterloo, M.J., Sandfort, N., Exterkate, K., Al-Washali, T., Noman, A., Al-Wathaf, Y., Al-Jailani, O., Al-Madhji, Z.

# Table of contents

<b>1. Introduction</b>	<b>1</b>
1.1 Objectives	1
1.2 Outline report	2
<b>2. Summary of Desk Review and Existing Studies</b>	<b>3</b>
2.1 Desk Review Key Findings	3
2.2 Summary of Available Data and Identified Gaps - Phase 1.	4
2.3 Highlights from Relevant Studies	4
2.4 Recommendations from the Desk Review	5
<b>3. Water Balance Methodology</b>	<b>7</b>
3.1 Description of Wadi Tuban catchment	7
3.2 Approach to water balance assessment: reconnaissance-level and detailed sub-catchment hydrological modelling	8
<b>4. The SWAT hydrological model and tools used</b>	<b>10</b>
4.1 Model description	10
4.2 Model calibration approach	12
4.3 HAWQS cloud-based interface	13
<b>5. Data sources</b>	<b>14</b>
5.1 Field data collection	14
5.2 Input data for SWAT modelling	17
<b>6. Hydrological modelling at reconnaissance level</b>	<b>27</b>
6.1 Methods	27
6.2 Results	31
6.3 General conclusions of the Hydrological modelling at reconnaissance level	41
<b>7. Detailed sub-catchment hydrological assessment</b>	<b>43</b>
7.1 Description study area	43
7.2 Materials and Methods	44
7.3 Results	45
<b>8. Water harvesting options</b>	<b>71</b>
8.1 Current surface water harvesting	71
8.2 Potential groundwater recharge and Integrated Water Harvesting approaches	72

8.3	Water Harvesting Potential Areas	74
8.4	Water Harvesting Potential Areas under Climate Change Scenario	78
<b>9.</b>	<b>Conclusions</b>	<b>83</b>
<b>10.</b>	<b>Recommendations</b>	<b>85</b>
<b>References</b>		<b>86</b>
<b>Annex 1 – Desk Review</b>		<b>89</b>
<b>Annex 2 - Input Data Preparation and Processing for the SWAT Model</b>		<b>90</b>
<b>Annex 3 – Monte Carlo Calibration</b>		<b>91</b>

## **List of figures**

Figure 1.	Map of Wadi Tuban catchment area with the four target districts.	7
Figure 2.	Proposed methodology for the water balance computation.	9
Figure 3.	SWAT model description inputs, configuration and outputs.	10
Figure 4.	SWAT model process interaction in the water balance.	11
Figure 5.	HAWQS cloud-based interface.	13
Figure 6.	Field data collected from Al-Mawaset and Al-Selw Districts	15
Figure 7.	Field data collected from Tuban and Al- Al-Mosaymer Districts	15
Figure 8.	Photos taken during field work in the targeted districts.	17
Figure 9.	Comparison between a global terrace mapping database shown as red areas (Li et al., 2025) and the terrace mapping done in this study (green polygons) for the northern part of the Tuban Basin. The global database does not include many terrace areas and lumps distinct terrace areas together.	19
Figure 10.	Digital Elevation map of the Tuban basin, Yemen.	20
Figure 11.	Land use land cover (LULC) map of the Tuban basin, Yemen.	21
Figure 12.	Soil map of the Tuban Basin, Yemen.	24
Figure 13.	Annual average maps (top) and monthly mean values graphs (bottom) for precipitation (right) and temperature (left) across the Tuban Basin, Yemen.	25
Figure 14.	SWAT model setup map of the Tuban basin, Yemen.	28
Figure 15.	Monthly ET time series for six subbasins comparing SWAT simulations and WaPOR estimates.	32
Figure 16.	Portions of land use types per subbasin	33
Figure 17.	Annual average water balance component schematic for Tuban catchment model over the 20-year period 1999-2018.	34
Figure 18.	Average annual precipitation (left) and actual evapotranspiration-ET (right) spatial distribution over the Tuban Basin as simulated by SWAT for 1999 - 2018.	36
Figure 19.	Average annual potential evaporation (PET) as modelled with SWAT for the Tuban basin for the period 1999-2018.	36
Figure 20.	Average annual water yield over the Tuban catchment as simulated by SWAT for the period 1999 - 2018.	37

Figure 21. Average monthly surface runoff generation and subbasin stream outflow over the Tuban Basin as simulated by SWAT for the period 1999 - 2018.	38
Figure 22. Map of the Tuban Basin showing water harvesting infrastructure.	39
Figure 23. Average annual dep aquifer recharge estimates for the Tuban Basin as simulated by SWAT for the period 1999 - 2018.	40
Figure 24. Annual average irrigation water use in the Tuban Basin for 1999-2018.	41
Figure 25. Location in the Tuban Basin of detailed hydrological models covering the districts of interest.	43
Figure 26. Subbasin (red lines), reservoir (blue circles), inlet (red triangle) and outlets (blue triangles) of Al-Mosaymer district catchment model, as overlain on the soil map.	44
Figure 27. Annual average water balance schematic for the Al-Selw / Al Mawaset district model over the period 1999-2018.	46
Figure 28. Monthly variation in precipitation (Precip [mm]), soil water content (SW [mm]), actual evapotranspiration (ET [mm]) and surface runoff (SURQ [mm]) for subbasin 11, and wadi outflow FLOW_OUT [ $m^3 s^{-1}$ ] and wadi bed infiltration (TLOSS [ $m^3 s^{-1}$ ]) for reach 18 over the period 1999-2108.	47
Figure 29. Average monthly outflow and total annual outflow of reach 18 in the Al Selw - Al Mawaset region over the period 1999-2018.	48
Figure 30. Average annual precipitation distribution over the Al Selw / Al Mawaset Districts (black line) for the period 1999 - 2018.	48
Figure 31. Average annual actual evapotranspiration distribution over the Al Selw / Al Mawaset Districts (black line) as simulated by SWAT for the period 1999 - 2018.	49
Figure 32. Average annual water yield distribution over the Al Selw / Al Mawaset Districts (black lines) as simulated by SWAT for the period 1999 - 2018.	50
Figure 33. Average annual surface runoff generation and river runoff for the Al Selw / Al Mawaset Districts (black lines) as simulated by SWAT for the period 1999 - 2018.	51
Figure 34. Average annual groundwater recharge in the Al Selw / Al Mawaset Districts (black lines) as simulated by SWAT for the period 1999 - 2018.	52
Figure 35. Annual average water balance schematic for the Al Mosaymer district model over the period 1999-2018.	53
Figure 36. Average annual precipitation distribution over the Al Mosaymer District (black line) for the period 1999 - 2018.	55
Figure 37. Average annual actual evapotranspiration distribution over the Al Mosaymer District (black line) as simulated by SWAT for the period 1999 - 2018.	55
Figure 38. Monthly variation in precipitation (Precip [mm]), soil water content (SW [mm]), actual evapotranspiration (ET [mm]) and surface runoff (SURQ [mm]) for subbasin 11, and wadi outflow FLOW_OUT [ $m^3 s^{-1}$ ] and wadi bed infiltration (TLOSS [ $m^3 s^{-1}$ ]) for reach 18 over the period 1999-2108.	56
Figure 39. Average annual water yield distribution over the Al Mosaymer District (black line) as simulated by SWAT for the period 1999 - 2018.	57
Figure 40. Impact of terraces (black-lined polygons) on the water yield in the north of the Al Mosaymer District region.	57
Figure 41. Average annual surface runoff generation and river runoff for the Al Mosaymer District (black line) as simulated by SWAT for the period 1999 - 2018.	58
Figure 42. Average monthly outflow and total annual outflow of reach 18 in the Al Mosaymer region over the period 1999-2018.	58

Figure 43. Average annual groundwater recharge over the Al Mosaymer District (black line) as simulated by SWAT for the period 1999 - 2018.	59
Figure 44. Annual average water balance schematic for the Tuban District model over the period 1999-2018.	60
Figure 45. Average annual precipitation distribution over the Tuban District (black line) for the period 1999 - 2018.	62
Figure 46. Average annual actual evapotranspiration distribution over the Tuban District (black line) as simulated by SWAT for the period 1999 - 2018.	62
Figure 47. Monthly variation in precipitation (Precip [mm]), soil water content (SW [mm]), actual evapotranspiration (ET [mm]) and surface runoff (SURQ [mm]) for subbasin 6, and wadi outflow FLOW_OUT [ $m^3 s^{-1}$ ] and wadi bed infiltration (TLOSS [ $m^3 s^{-1}$ ]) for reach 6 over the period 1999-2108.	63
Figure 48. Average annual water yield distribution over the Tuban District (black line) as simulated by SWAT for the period 1999 - 2018.	64
Figure 49. Average annual irrigation distribution over the Tuban District (black line) as simulated by SWAT for the period 1999 - 2018.	64
Figure 50. Average annual surface runoff generation over Tuban District (black line) as simulated by SWAT for the period 1999 - 2018.	65
Figure 51. Average monthly outflow and total annual outflow of reach 6 in the Tuban District over the period 1999-2018.	66
Figure 52. Average annual groundwater recharge over the Tuban District (black line) as simulated by SWAT for the period 1999 - 2018.	67
Figure 53. Phreatic hydraulic heads [m.a.s.l.] (left) and EC salinity [ $\mu S cm^{-1}$ ] (right) in boreholes measured during the UNDP reconnaissance mission in May 2025.	68
Figure 54. Map of the boreholes in the Tuban Delta and the land use classification.	69
Figure 55. Hydraulic head in 2018 in the Tuban District. The MODFLOW model grid shows inactive cells in grey.	70
Figure 56. Modeled hydraulic head at observation point from 1998 to 2017.	70
Figure 57. Map of rainwater harvesting structures (blue dots) and terrace agriculture (purple) displayed on the land use map.	72
Figure 58. Map of potential water harvesting for Tuban Basin.	75
Figure 59. Map of potential water harvesting for Al Selw / Al Mawaset Districts.	76
Figure 60. Map of potential water harvesting for Mosaymer District.	77
Figure 61. Map of potential water harvesting for Tuban District.	78
Figure 62. Global CO <sub>2</sub> emissions of SSP scenarios (Rogelj et al., 2018).	79
Figure 63. Map of potential precipitation change under SSP2-4.5 Climate Change Scenario for Yemen.	80
Figure 64. Map of potential temperature change under ssp2-4.5 Climate Change Scenario for Yemen.	80
Figure 65. Comparison between current (upper) and future (lower) climate with a +1.0 °C temperature increase for water balance components for the Tuban Basin in the period 1999 – 2018.	81
Figure 66. Comparison of current climate potential water harvesting map (left) and map for a significant temperature increase of 1.0 °C as predicted for 2050 by the CMIP6 dataset. Simulation data periods 1999-2018.	82

## List of tables

Table 1. Overview of district areas, along with the area of the districts falling within the total Tuban catchment area.	8
Table 2. Calibration parameters adjusted during the Monte Carlo runs to optimize SWAT evaporation simulation. For each parameter, the table shows the range of relative changes applied, the physically valid value range, and the initial value used to start the calibration.	12
Table 3. Global datasets used for the input data for the SWAT model.	18
Table 4. Slope classes defined for the SWAT model of the Tuban Basin and associated areas.	20
Table 5. Land use codes, types and corresponding SWAT land use code.	22
Table 6. Overview of the crop rotation operations schedules used for the upland and delta target areas. Auto irrigation is the start of irrigation at a certain soil moisture level, HI is harvesting index, Target BMS is the biomass attained for harvesting, Max. irr and Irr. Eff. Are the maximum irrigation quantity and the efficiency, respectively.	22
Table 7. WRB soil codes and SWAT Name code associated to the Soil map, in the Tuban Basin.	23
Table 8. Average monthly water balance component values for Tuban Basin. SURF Q is surface runoff, LATQ is lateral flow, EY is actual evapotranspiration, PET is potential evapotranspiration.	35
Table 9. Information on the three sub-models developed for the districts in the Tuban Basin and for the entire Tuban Basin.	44
Table 10. Monthly overview of water balance components for the Al Selw / Al Mawaset region for the period 1999-2018.	46
Table 11. Overview of simulated outputs of SWAT for the Al Selw / Al Mawaset district catchment over the period 1999-2018 for each land use type (LULC). CN is the curve number, BIOM is the biomass of the vegetation, whereas YLD is the crop yield.	47
Table 12. Monthly overview of water balance components for the Al Mosaymer catchment for the period 1999-2018.	53
Table 13. Overview of simulated outputs of SWAT for the Al Mosaymer district catchment over the period 1999-2018 for each land use (LULC). CN is the curve number, BIOM is the biomass of the vegetation, whereas YLD is the crop yield.	54
Table 14. Monthly overview of water balance components for the Tuban District catchment for the period 1999-2018.	60
Table 15. Overview of simulated outputs of SWAT for the Tuban District catchment in the delta over the period 1999-2018 for each land use (LULC). CN is the curve number, BIOM is the biomass of the vegetation, whereas YLD is the crop yield.	61
Table 16. QSWATMOD MODFLOW model input variables.	69

# List of acronyms

AREA	Agriculture Research Extension Authority
ASL	Above Sea Level
BGR	Federal Institute for Geosciences and Natural Resources (Germany)
ET	Actual evapotranspiration
FAO	Food and Agriculture Organization
HRU	Hydrological Response Unit
KfW	German Development Bank
LATQ	Lateral runoff
MoAIF	Ministry of Agriculture, Irrigation, and Fisheries
MoWE	Ministry of Water and Environment
NDVI	Normalised Differential Vegetation Index
NWRA	National Water Resources Authority
PET	Potential evapotranspiration
RVO	Rijksdienst voor Ondernemend Nederland (The Netherlands Enterprise Agency)
SURFQ	Surface runoff
SWAT	Soil Water Assessment Tool
UNDP	United Nations Development Programme

# 1. Introduction

Yemen faces extreme pressure on its water resources due to its arid climate, limited and uneven rainfall, and increasing demand from agriculture and domestic use. These pressures have far-reaching impacts—not only on water availability but also on food production, public health, and long-term resilience. The resulting challenges, including declining agricultural productivity and rising malnutrition, are particularly acute in rural areas, where access to water is essential for both livelihoods and local food systems. To support Yemen in addressing these challenges, the German Development Bank (KfW) and UNDP Yemen, with funding from the Federal Government of Germany through BMZ, have partnered to improve water resource management and food security in the country. Within this broader programme, understanding the availability, use, and risks associated with water resources is a key step toward informed planning and sustainable investment.

In this context, MetaMeta and Acacia Water were contracted to carry out a hydrological assessment of the Wadi Tuban basin—an agriculturally and strategically important watershed in southern Yemen. Given the limited availability of consistent hydrological data across the region, a tiered modelling approach was adopted. This includes both a reconnaissance-level model, covering the entire Tuban catchment using global datasets, and more detailed models for four targeted districts where field data and stakeholder input allowed for a deeper analysis.

The hydrological modelling conducted under this assignment provides essential insights into the current water balance, seasonal flow patterns, and spatial distribution of key hydrological processes across the basin. These findings serve not only to identify critical gaps and vulnerabilities but also to support more targeted, climate-resilient water and agricultural planning in the years to come.

## 1.1 Objectives

The primary objectives of this assignment are as follows:

1. **Reconnaissance-Level Hydrological Modeling and Water Balance Assessment:** To conduct a preliminary hydrological modeling and water balance assessment of Wadi Tuban, providing a broad understanding of the catchment's behavior.
2. **Detailed Sub-Catchment Hydrological Analysis:** To carry out in-depth hydrological assessments for selected sub-catchments within the targeted districts. This includes a detailed water balance analysis that considers the potential impacts of upstream developments on downstream flow regimes.  
The targeted districts :
  - o Al-Mawaset and Al-Selw districts (upstream) in Taiz governorate, and
  - o Al-Musaymir and Tuban districts (downstream) in Lahj governorate.
3. **Stakeholder Engagement and Data Enhancement:** To incorporate findings from four participatory workshops held in the targeted districts. These workshops aim to engage local authorities and stakeholders, while also supporting the collection of spatial data necessary for building robust and detailed hydrological models.

## **1.2 Outline report**

This report outlines the introduction and main objectives (Chapter 1), Summary of the desk review (Chapter 2), the overview of the methodology (Chapter 3), the SAWT hydrological model and tools (Chapter 4), Data sources (Chapter 5), Hydrological modeling at reconnaissance level (Chapter 6), detailed sub-catchment hydrological assessment (Chapter 7), Water harvesting options (Chapter 8), and conclusions and recommendations (Chapter 9).

## **2. Summary of Desk Review and Existing Studies**

This chapter summarizes key insights from over 60 reports, assessments, and studies concerning water resources in Wadi Tuban. It covers various themes, including hydrology, groundwater management, climate variability, agricultural water use, and infrastructure performance. These sources include government records, international agency reports, academic research, and geospatial datasets. Annex 1 presents the full list of reviewed documents and their relevance to the basin's hydrology, infrastructure, and governance.

The main objective of the review was to gather existing knowledge on water availability, use, and management in the Tuban basin, identify data gaps, and extract lessons learned to guide ongoing fieldwork and model development.

Based on this review, a set of strategic, evidence-based recommendations is proposed, focusing on improving hydrological monitoring, strengthening groundwater governance, enhancing water and sanitation infrastructure—especially in Aden—and promoting institutional integration and the adoption of modern technology. These strategies aim to improve water security, operational efficiency, and sustainability throughout the Wadi Tuban basin.

### **2.1 Desk Review Key Findings**

The desk review compiled and analysed over 60 documents from government institutions, international agencies, and academic studies related to water resources in the Wadi Tuban basin. The objective was to extract lessons learned, identify systemic challenges, and define priority areas for intervention. The findings reveal that water resource management in the basin is hindered by several structural issues.

First, groundwater depletion is occurring at an alarming rate, with an average decline of about 1 meter per year across many areas of the Tuban Delta. The over-reliance on groundwater, combined with increasing abstraction from solar-powered wells, is accelerating aquifer exhaustion without adequate monitoring or regulation.

Second, institutional fragmentation limits coordination between stakeholders. Customary water rights, legal ambiguities, and weak enforcement mechanisms contribute to unequal access, particularly between upstream and downstream users.

Third, irrigation inefficiencies remain widespread. Traditional irrigation methods dominate, leading to significant water loss. Despite the existence of 182 dams and water structures, most operate well below their capacity due to sedimentation, poor maintenance, and lack of integrated planning.

Finally, climate change is compounding water stress through increased variability in rainfall, a rising frequency of droughts and floods, and saltwater intrusion in the coastal

aquifers. These risks pose direct threats to agricultural productivity, drinking water supply, and long-term sustainability.

## **2.2 Summary of Available Data and Identified Gaps - Phase 1.**

The review of existing datasets underscores serious limitations in the availability, continuity, and quality of hydrological and related data. Although some historical records exist—such as rainfall data from 13 stations (1981–2008) and groundwater level measurements from the 1990s—most of the data is outdated, incomplete, or geographically limited.

Climate data is particularly deficient. After 2008, there is minimal rainfall or temperature monitoring, with only two stations providing recent records. This has required reliance on satellite-derived datasets, which—while helpful—lack the spatial precision and temporal detail needed for high-confidence modelling.

Streamflow data are limited to the Dukeim gauging station and only cover select years between 1955 and 2000. Similarly, groundwater data lacks updated measurements on aquifer recharge rates, abstraction volumes, salinity levels, and well depth distribution. The piezometric network for long-term monitoring is essentially non-existent.

Geological and soil data are drawn from older, low-resolution maps, which are insufficient for modelling aquifer boundaries, infiltration processes, or soil-water interactions. Detailed land use and agricultural water demand data are also lacking, particularly in terms of crop cycles, irrigation methods, and actual usage at farm level.

Water infrastructure data, including the location, function, and performance of dams, reservoirs, and weirs, requires significant updating. The database lacks insights into seasonal operation, recharge potential, and maintenance status.

Overall, this section confirms that while a foundation of historical data exists, it must be significantly updated and expanded. The next phase of the project will focus on targeted fieldwork, stakeholder consultations, and integration of remote sensing to close these gaps and enable robust hydrological modelling.

## **2.3 Highlights from Relevant Studies**

Several key studies reviewed under this section offer detailed analyses of the challenges and potential solutions for the Wadi Tuban basin. The most recent assessments, particularly from UN-Habitat (2024) and the Ministry of Agriculture, provide alarming projections and urgent calls for action.

One study estimates that in 2022 alone, the Tuban Delta experienced a groundwater deficit of over 80 million m<sup>3</sup>, primarily due to over-abstraction, weak regulation, and upstream surface water retention. Future climate models predict increasing frequencies of extreme weather events—both floods and droughts—between 2029 and 2076, putting further strain on infrastructure and ecosystems.

Another study documented that more than 1,200 of the 3,600 wells in the basin have already gone dry. This is particularly concerning for Aden city, which depends heavily on groundwater from the Tuban basin. The situation is worsened by rising salinity, land degradation, and loss of agricultural productivity in the lower delta.

Infrastructure studies identified that only 40% of irrigation water reaches intended agricultural fields, due to poor design, sediment accumulation, and lack of operation protocols. Although 182 dams and water structures exist, many face structural and environmental challenges, and 89% lack proper environmental protection measures.

In terms of governance, several studies stress the urgent need to update legal frameworks, enhance stakeholder participation (including gender equity), and strengthen coordination between water user associations, local authorities, and national agencies. Some documents propose innovative solutions such as solar-powered desalination, artificial recharge, and wastewater reuse, though these require feasibility assessments and long-term investment.

Overall, these studies confirm that Wadi Tuban is at a critical tipping point. Without strategic, multi-sectoral interventions, the basin risks irreversible damage to its water resources, food systems, and population well-being.

## 2.4 Recommendations from the Desk Review

Based on the insights gathered through the desk review and the identification of data and governance gaps, a comprehensive set of recommendations was formulated to strengthen water resource management and planning in the Wadi Tuban basin.

### 1. Enhance Hydrological and Meteorological Monitoring

Filling long-term data gaps is a priority. This includes restoring and upgrading rainfall and temperature monitoring stations, expanding the surface water gauging network from two to at least five stations, and implementing automated data collection and transmission systems. Evapotranspiration monitoring should be supplemented through remote sensing platforms (e.g., MODIS, WaPOR), and field validation is necessary to improve model accuracy.

### 2. Strengthen Groundwater Monitoring and Regulation

Groundwater abstraction must be tracked more systematically. Recommendations include installing digital meters on key wells, developing a central database to monitor pumping volumes, salinity, and piezometric levels, and reactivating historical monitoring points. It is also essential to map recharge areas and conduct pumping tests to estimate safe yields.

### 3. Improve Surface–Groundwater Interaction Understanding

To address recharge deficits, studies recommend the use of artificial recharge structures, such as check dams and infiltration galleries, especially in upstream areas. Seasonal flood monitoring and sediment control are also crucial for increasing recharge efficiency and reducing degradation of surface infrastructure.

### 4. Promote Infrastructure Rehabilitation and Efficiency

Many existing dams and water structures operate below capacity. Upgrading their performance requires sediment removal, technical audits, and the integration of smart

monitoring technologies. Irrigation efficiency can be improved by replacing traditional surface systems with drip or sprinkler methods, supported by training and incentives for farmers.

### **5. Modernise Pumping Systems and Reduce Energy Costs**

The growing use of solar-powered wells highlights the need to balance energy access with water sustainability. Replacing old pumps with energy-efficient models and regulating solar irrigation use is recommended. Vibration and temperature sensors can be installed to enable predictive maintenance and reduce breakdowns.

### **6. Improve Urban Water Supply Integration**

Aden's dependency on groundwater from Tuban makes it critical to integrate wellfield operations with urban water planning. This includes analysing supply reliability, conducting well-by-well feasibility studies, and prioritising investment in productive sources. A centralised platform linking technical, operational, and planning data is necessary to guide decision-making.

### **7. Strengthen Institutional Coordination and Data Sharing**

Governance reforms should aim to enhance inter-agency coordination, standardise procedures, and improve data transparency. Establishing joint technical committees, linking databases, and engaging local communities in monitoring efforts are recommended to build shared accountability.

### **8. Build Climate Resilience and Risk Preparedness**

Given the basin's exposure to floods, droughts, and sea-level rise, the development of a basin-wide disaster risk management strategy is essential. Early warning systems, scenario-based planning, and adaptive infrastructure (e.g., solar-powered desalination, treated wastewater reuse) are proposed to reduce long-term vulnerability.

# 3. Water Balance Methodology

## 3.1 Description of Wadi Tuban catchment

The Wadi Tuban catchment covers around 7,169 km<sup>2</sup>, including about 700 km<sup>2</sup> of delta area along the coast (Comparison Between the Main Results of UN-Habitat & BGR Studies of Tuban Delta 2013, n.d.). It stretches between latitudes 13°59'54" N and 12°56'33" N and longitudes 44°5'57" E and 45°5'58" E. Elevation ranges from 3,209 m above sea level in the highlands down to sea level at the Arabian Sea. The wadi is about 156 km long, running from Ibb in the north, through Taizz in the west, and toward Abawil in the east. It flows into the Arabian Sea near Aden.

This study focuses on the Wadi Tuban catchment and the four areas within it that represent the selected districts: 1) Al-Mawaset and 2) Al-Selw (upstream) in Taiz governorate, and 3) Al-Mosaymer and 4) Tuban (downstream) in Lahj governorate (Figure 1). With support from UNDP, we completed the delineation of the Tuban catchment.

To carry out the hydrological modelling for each district of interest, we developed separate models covering only the part of each district that falls within the Tuban catchment. The aim was to include as much of the district area as possible within Tuban, while minimizing areas falling outside. Table 1 gives an overview of the total area of each district, how much of it is included within the Tuban catchment, and the percentage. This helps define the area each model is based on.

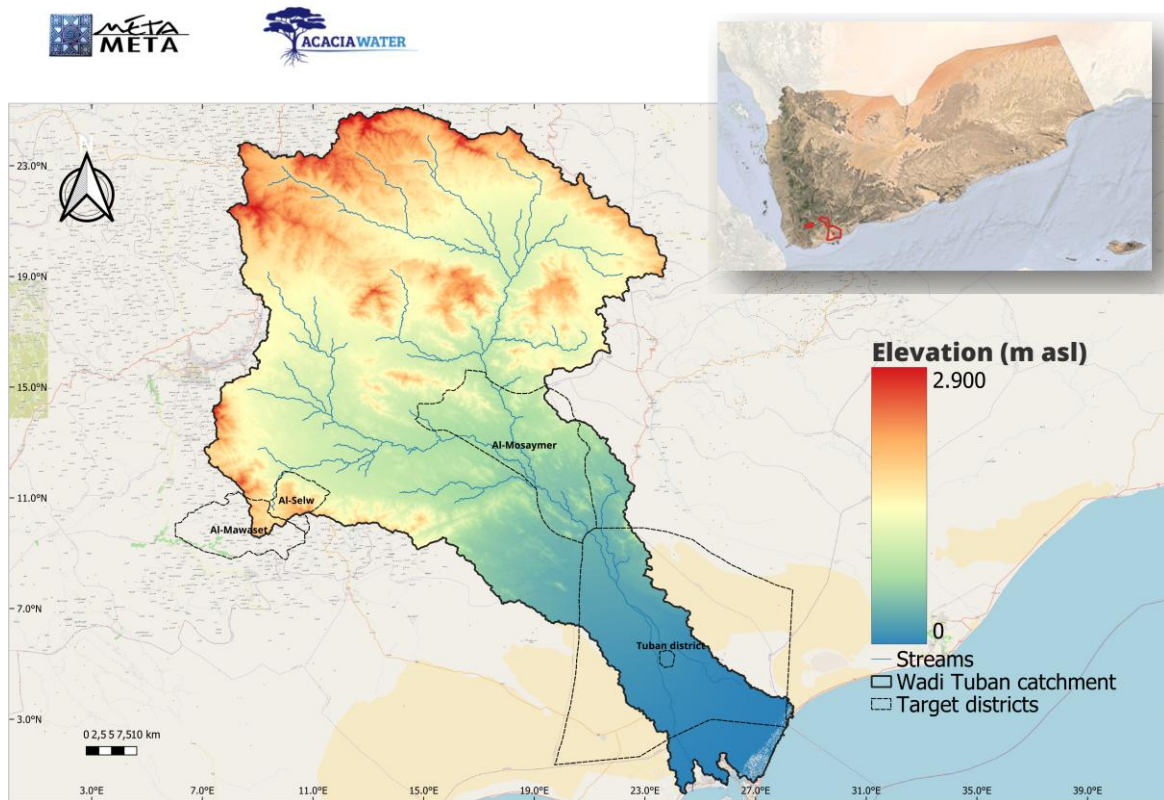


Figure 1. Map of Wadi Tuban catchment area with the four target districts.

Table 1. Overview of district areas, along with the area of the districts falling within the total Tuban catchment area.

District	Area district	Area district within	Tuban catchment
	km <sup>2</sup>	km <sup>2</sup>	%
<b>Al-Mawaset</b>	216	32	15
<b>Al-Selw</b>	83	73	88
<b>Al-Mosaymer</b>	559	538	96
<b>Tuban</b>	1626	804	49

### 3.2 Approach to water balance assessment: reconnaissance-level and detailed sub-catchment hydrological modelling

Assessing the water balance in a catchment involves quantifying the major hydrological components—precipitation, evapotranspiration, runoff, infiltration, and changes in water storage. This process is especially complex in arid and semi-arid regions like the Tuban Basin, where water management practices such as irrigation and groundwater abstraction heavily influence the hydrological regime.

For this study, we adopt the open-source Soil and Water Assessment Tool (SWAT) model (Arnold et al., 2012; Arnold and Fohrer, 2005) as the primary tool to simulate hydrological processes and estimate the water balance in the Tuban basin. SWAT is well-suited for semi-arid environments and allows the integration of surface water, groundwater, land use, and water management practices in a single modelling framework.

The approach will consist of two levels of analysis:

#### 1. Reconnaissance-Level Assessment (Entire Tuban Catchment)

**Objective:** Develop a baseline understanding of the overall hydrological behaviour of the Tuban Basin.

**Process:**

- Delineation of the catchment and sub-basins using a DEM;
- Definition of Hydrological Response Units (HRUs) based on land use, soil, and slope bands;
- Definition of channel and management parameters, e.g. crop rotations;
- Calibration Using Satellite-Based evapotranspiration data, such as from MODIS (Mu et al., n.d.) and WaPOR (FAO, 2020);
- Use of global datasets of the climate data (precipitation, temperature, etc.), land use, soils maps and digital elevation model to simulate key water balance components;
- Placing the model into the HAWQS (The Hydrologic And Water Modeling System) cloud-based interface setup;

**Output:** Annual and seasonal estimates of precipitation patterns, runoff, evapotranspiration, groundwater recharge, and water yield.

## **2. Detailed Sub-Catchment Assessments (Four Target Areas in Taiz and Lahj Governorates)**

**Objective:** Conduct a detailed hydrological assessments in priority sub-catchments.

**Process:**

- Inclusion of detailed data collected on field: irrigation, water transfers, reservoirs, irrigated areas, terraces, surface impoundments, and groundwater abstraction;
- A coupled SWAT-MODFLOW model (Park et al., 2019) for the Tuban District to achieve more accurate representation of land surface processes and spatially explicit groundwater flow dynamics;
- Where available, observed hydrological data will be used to calibrate and validate model outputs. Field data collected will help improve parameterization, especially for groundwater use, irrigation schedules, and crop types;
- Focused analysis of consumptive water use to assess irrigation efficiency and potential water deficits.

**Output:**

- Seasonal estimates of precipitation patterns, runoff, evapotranspiration, groundwater recharge, and water yield.
- Recommendations for Conjunctive Water Use in Irrigation.
- Upstream/downstream dependencies between the governorates

## **3. Results Interpretation and Reporting**

Model results will be analyzed spatially and temporally to understand key hydrological dynamics. Graphical outputs—such as water balance diagrams, hydrographs, and sub-basin water yield maps—will be used to present findings clearly. The final report will document the methodology, data sources, assumptions, limitations, and recommendations for future water resource management in the Tuban Basin.

Figure 2 provides a concise step-by-step outline of the proposed water balance methodology, aligned with UNDP requirements. It includes a reconnaissance-level hydrological assessment for the Tuban primary basin and detailed assessments for the four sub-catchments in the target districts of Taiz and Lahj governorates.

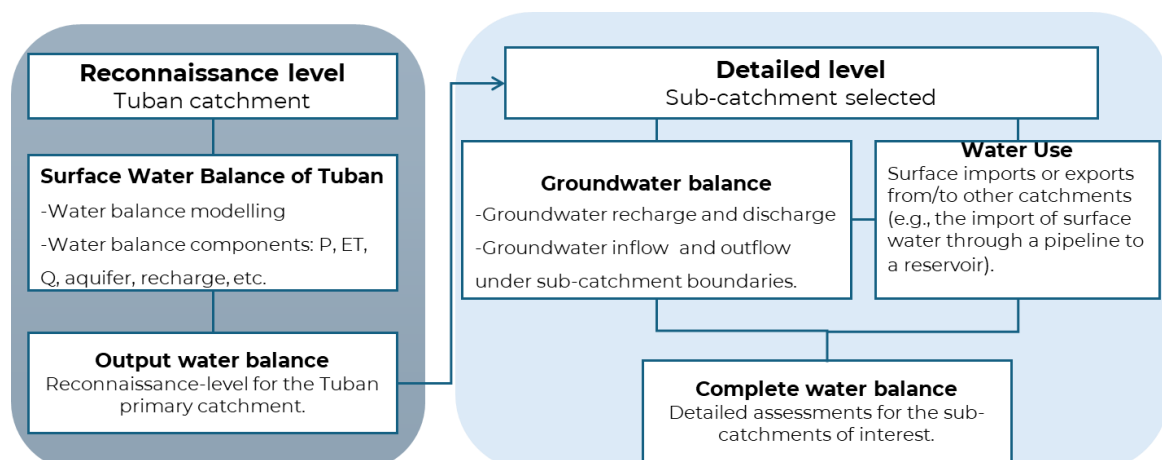


Figure 2. Proposed methodology for the water balance computation.

# 4. The SWAT hydrological model and tools used

## 4.1 Model description

The Soil and Water Assessment Tool (SWAT), developed by the United States Department of Agriculture – Agricultural Research Service, was used in this study (Arnold et al., 1998; Neitsch et al., 2011). SWAT is a process-driven, semi-distributed, continuous-time, and process-based watershed-scale model designed to simulate the effects of water management decisions on water quantity and quality. SWAT is capable of operating on a daily basis, and newer versions support sub-daily time steps to improve the representation of rapid hydrological processes (Jeong et al., 2010). The model is particularly well-suited for assessing how land management practices affect water quantity, sediment transport, and the movement of agricultural chemicals within large river basins.

SWAT divides the entire watershed into several subbasins, which are further broken down into Hydrologic Response Units (HRUs), as is showed in Figure 3. These HRUs are defined by unique combinations of land use, soil type, and slope, allowing the model to accurately reflect spatial variations in hydrological behaviour, particularly evapotranspiration and surface runoff (Arnold et al., 1998). The hydrological cycle is based on the following water balance equation.

$$SW_t = SW_{t-1} + \sum_{i=1}^t (R_{day} - Q_{surf} - E_a - W_{seep} - Q_{gw}), SW_t = SW_{t-1} + \sum_{i=1}^t R_{day} - Q_{surf} - E_a - W_{seep} - Q_{gw} \quad (1)$$

where  $SW_t$  is the soil water content (mm),  $SW_{t-1}$  is the soil water content on day  $t$  in the previous period (mm),  $t$  is the time step (days),  $R_{day}$  indicates the amount of precipitation on day  $t$  (mm),  $Q_{surf}$  represents the surface streamflow on day  $t$  (mm),  $E_a$  indicates the AET on day  $t$  (mm),  $W_{seep}$  is the percolation and bypass flow on day  $t$  (mm), and  $Q_{gw}$  represents the return flow on day  $t$  (mm).

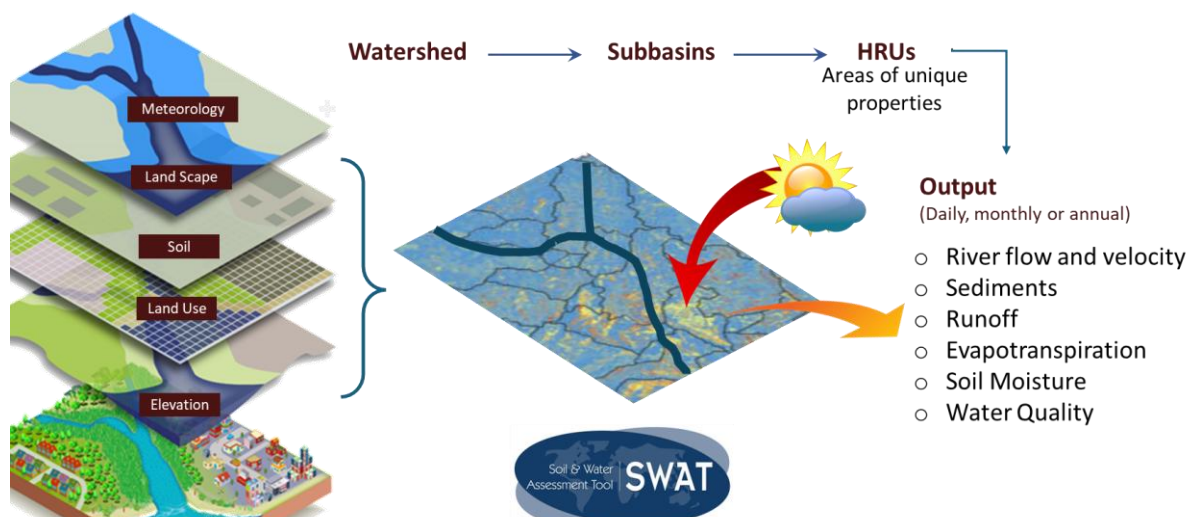


Figure 3. SWAT model description inputs, configuration and outputs.

The model simulates watershed hydrology through two main components: the land phase and the routing phase (Figure 4). The land phase includes processes such as precipitation, infiltration, surface runoff, evapotranspiration, and the generation of sediment and pollutant loads. These are computed on a daily time step using a quasi-steady approach. The routing phase simulates the movement of water, sediment, and pollutants through the stream network to the watershed outlet using a simplified hydrologic routing method, rather than full hydrodynamic equations (Neitsch et al., 2011).

Each HRU functions independently and simulates processes like canopy interception, infiltration, soil moisture redistribution, lateral flow, percolation to groundwater, and baseflow contributions from aquifers. A unified plant growth model is used for all vegetation types, distinguishing between annual and perennial species and estimating water and nutrient uptake, as well as biomass and yield production (Gassman et al., 2007).

SWAT calculates surface runoff differently depending on the temporal resolution. For daily time steps, it uses the Soil Conservation Service Curve Number (SCS-CN) method, which is empirical and requires data on land use, soil properties, topography, and daily precipitation. For sub-daily simulations, the model adopts the Green-Ampt and Mein-Larson (GAML) infiltration method, which is physically based and requires more detailed soil profiles and high-resolution rainfall data (Mein and Larson, 1973).

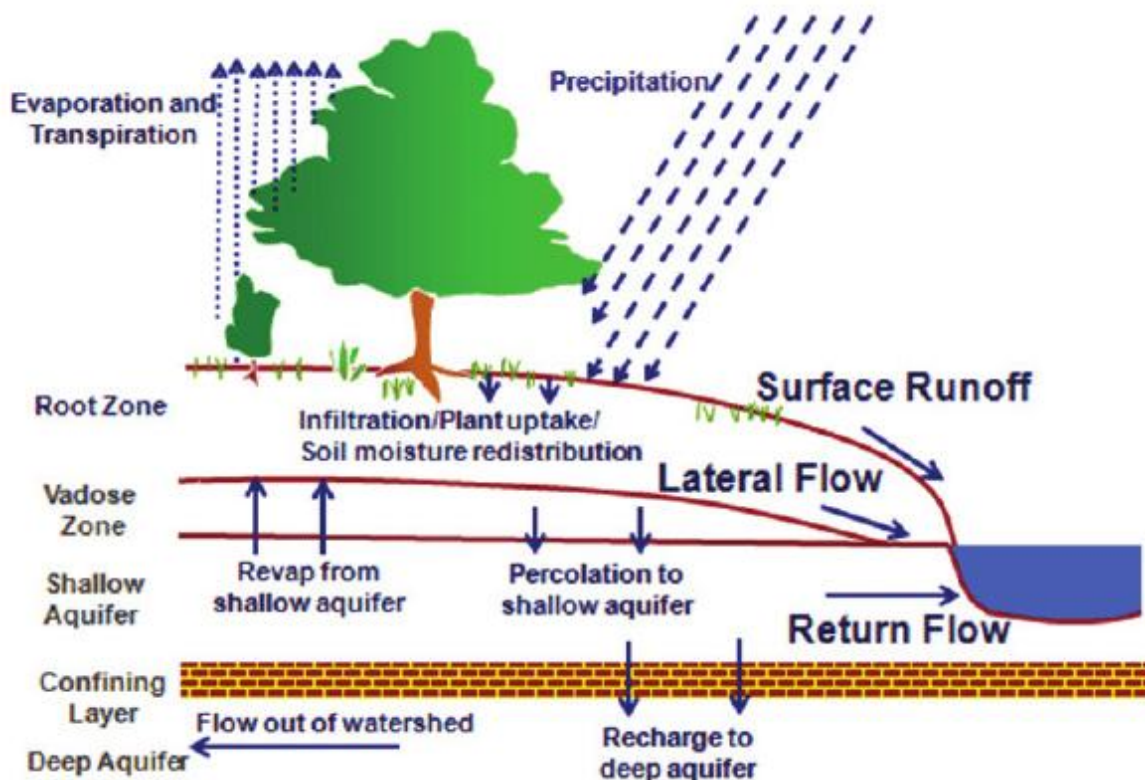


Figure 4. SWAT model process interaction in the water balance.

For more comprehensive information on SWAT's structure, algorithms, and applications, key reference is <https://swat.tamu.edu/media/99192/swat2009-theory.pdf>

## 4.2 Model calibration approach

An approach has been developed to calibrate the SWAT model using evapotranspiration data, as seasonal rivers in Tuban do not consistently provide river discharge measurements throughout the year and flow data are missing to calibrate and validate against. To calibrate the SWAT model to evapotranspiration (ET), a Monte Carlo simulation approach was implemented using satellite-based ET observations as reference. The calibration focused on SWAT model parameters known to affect soil and plant evaporation dynamics, namely ESCO (Soil Evaporation Compensation factor), EPCO (Plant Evaporation Compensation factor), CANMX (maximum canopy water storage [mm]), and CN2 (Initial SCS curve number II value). The parameter ranges in Table 2 were used to guide the calibration. During the Monte Carlo runs, each parameter was changed within these set limits to test different combinations and compare these to the model simulations.

Table 2. Calibration parameters adjusted during the Monte Carlo runs to optimize SWAT evaporation simulation. For each parameter, the table shows the range of relative changes applied, the physically valid value range, and the initial value used to start the calibration.

Parameter	Multiplicative Range	Absolute Range	Initial Dummy Value
<b>ESCO</b>	[0.5, 1.5]	[0.01, 1.0]	1
<b>EPCO</b>	[0.2, 2.0]	[0.01, 1.0]	1
<b>CN2</b>	[0.5, 1.5]	[30, 100]	1
<b>CANMX</b>	[0.1, 1.5]	[0, 10]	5

For each Monte Carlo iteration, SWAT input files (.hru, .mgt) were programmatically updated using a custom Python function. The model was then executed, and monthly ET outputs were extracted per subbasin. These outputs were compared against monthly averages remote sensing-based ET data (from sources such as WaPOR or MODIS), aggregated to the subbasin scale. Goodness-of-fit was quantified using multiple statistical indicators, including the R<sup>2</sup> score, root mean square error (RMSE), and Pearson's correlation coefficient. The results of each run, along with the corresponding parameter values, were saved to allow post-analysis and ranking of model configurations. WaPOR data are available from February 2009 to July 2023. For calibration purposes, the overlapping period between the model data and WaPOR data spans from 2009 to 2018. Accordingly, the calibration period was defined as 2009–2015. No additional time series analysis was performed, as the data was already aggregated to monthly values and the focus was on long-term hydrological behavior.

Based on the calibration results, the best-performing parameter set per subbasin was identified using the highest R<sup>2</sup> value as the selection criterion. These optimal parameters were then reapplied to the SWAT model for validation over the leftover time period (2016–2018). The validation run served to assess the model's ability to simulate ET under independent conditions. The output statistics were again evaluated per subbasin and stored, ensuring that the final parameterization achieves reliable ET estimates across both the calibration and validation periods.

Two datasets are available that provide time series of actual ET data on a higher spatial resolution and with daily records. These are the MODIS16A2GF (Running et al., 2021) and the WaPOR datasets (FAO, 2020). However, the accuracy of the evapotranspiration values are not always consistent with precipitation data, being either too high or in some cases

too low. In addition, both datasets can yield significantly different ET values for the same areas and time frames due to differences in methodology and resolution. MODIS relies on a Penman–Monteith approach using meteorological and vegetation data, while WaPOR uses an energy balance model tailored for agricultural monitoring, which leads to the different values for the same area and timeframe. As such calibration against these values may either yield too much runoff or recharge when the ET estimates are too low, or vice versa if ET values are too high. Hence, after calibration an assessment needs to be done by to see if the predicted runoff is in correspondence with observations of the river discharge and its annual pattern.

### 4.3 HAWQS cloud-based interface

The Hydrologic And Water Quality System (HAWQS) is a web-based decision support tool developed by the U.S. Environmental Protection Agency (EPA) that provides users with easy access to the powerful simulation capabilities of the SWAT (Soil and Water Assessment Tool) model (Figure 5). HAWQS offers a user-friendly graphical interface that allows for the setup, execution, and analysis of hydrological and water quality simulations without requiring extensive modelling expertise (HAWQS, 2020).

Users can select predefined watersheds or define custom study areas, and this tool supports a variety of scenario analyses, enabling users to evaluate the potential impacts of land management changes, agricultural practices, and climate variability on water flow, sediment yield, nutrient transport, and other key hydrologic processes. HAWQS also includes visualization features for interpreting model outputs such as streamflow, nitrogen and phosphorus loads, and sediment concentrations across spatial and temporal scales. By combining the robust simulation engine of SWAT with an accessible online platform, HAWQS facilitates watershed-scale assessments for researchers, policymakers, and water resource managers interested in evaluating environmental outcomes and supporting sustainable water management strategies.

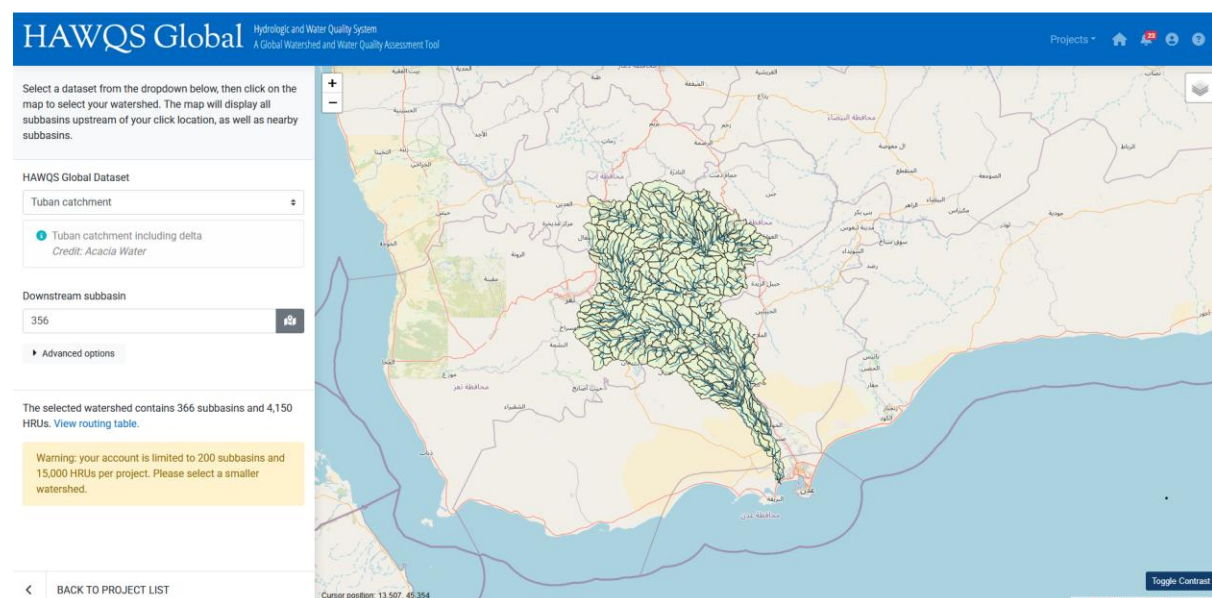


Figure 5. HAWQS cloud-based interface.

# 5. Data sources

## 5.1 Field data collection

A 14-day intensive field survey was conducted to collect detailed data for developing a hydrological model for the Wadi Tuban Basin, covering areas in Lahj and Taiz governorates. The collected data included surface and groundwater resources, water infrastructure, soil information, and agricultural use. The surveyed areas were selected based on their hydrological and geological diversity across four targeted districts. This section presents only a summary of the main findings from the field survey. Full details of the data collection campaign—including methodologies, tools used, site-specific observations, and results—are provided in a separate report.

The field team included 19 experts from the National Water Resources Authority and the Ministry of Agriculture, Irrigation and Fisheries. These experts were organized into four technical teams focusing on:

1. Hydrological monitoring
2. Groundwater
3. Soil and agriculture
4. Laboratory analysis

Fieldwork was preceded by a detailed planning phase, which included the development of tools and forms, training sessions, team deployment, and quality assurance protocols. Custom field data collection tools/forms were designed to gather relevant information on wells, springs, monitoring stations, water structures, soil and agricultural patterns, and potential water harvesting interventions. The field teams used instruments such as GPS units, EC and pH meters, dip meters, and followed standardized protocols for calibration and documentation.

In Taiz (Al-Mawaset and Al-Selw districts):

- 39 wells, 10 springs, and 3 monitoring stations were documented.
- During the field work and along with the representatives from MoAIF and NWRA a new water harvesting sites were proposed, and erosion-prone areas were identified.

In Lahj (Tuban Delta and Al-Mosaymer districts):

- 79 wells, 6 monitoring stations, and 32 water structures were recorded.
- Al-Musaymir, in particular, showed critical needs for rainwater harvesting and flood protection projects.

Field surveys were also carried out across selected locations within the entire catchment to validate satellite-derived data, based on hydrological modelling requirements and site accessibility. The data collected were:

- Crop types observed during the growing season
- Vegetation cover analysis for land use classification
- Soil characteristics, including type and depth profiles
- Irrigation methods used at farm and basin scales
- Water table measurements from selected boreholes for groundwater assessment

A spatial database was developed (in Shapefile and Geodatabase formats), with data cards linked to each site. These included images as well as both quantitative and qualitative attributes. Software tools such as ArcGIS, Google Earth, and ERDAS Imagine were used to generate maps and analyse topography, drainage networks, and watershed boundaries. Digital Elevation Models (DEMs) supported detailed analyses of slope, contour lines, and terrain features.

The collected data revealed spatial disparities in water availability and infrastructure across the basin (Figure 6 and Figure 7). Based on these findings, key recommendations include:

- Expanding the monitoring network
- Implementing soil erosion protection measures
- Prioritizing the rehabilitation of existing rainwater harvesting projects before initiating new construction activities, given the complexities of local water rights systems.

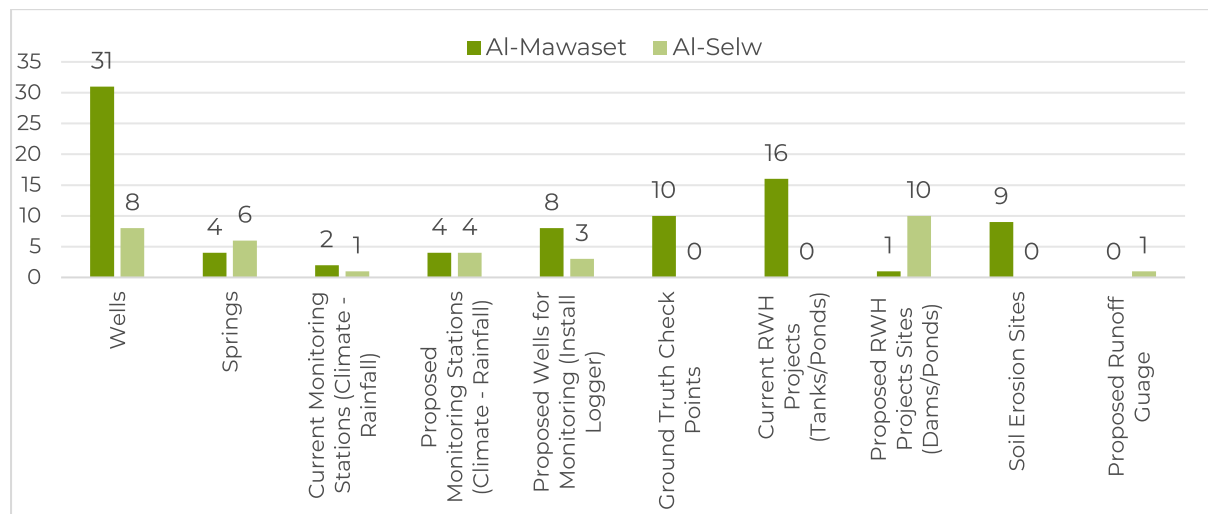


Figure 6. Field data collected from Al-Mawaset and Al-Selw Districts

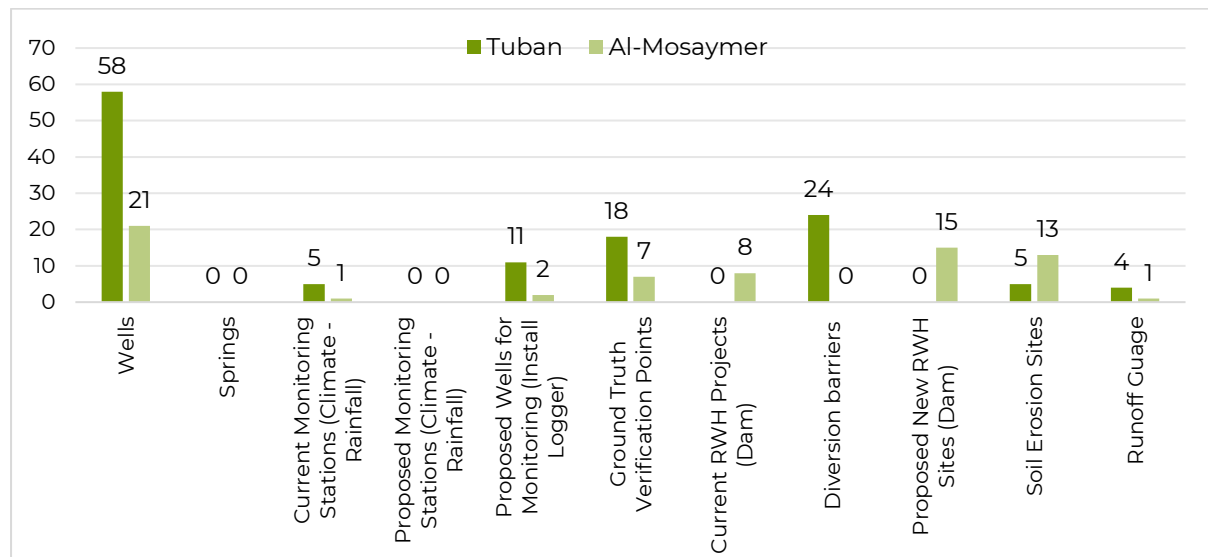


Figure 7. Field data collected from Tuban and Al-Al-Mosaymer Districts

Justifications for the absence of storage dams in the targeted sites in Al-Selw district:

**Limited coverage of the study area:** The sites assessed during the fieldwork are located within the areas under the control of the internationally recognized government (IRG), which cover only about 30% of the total area of Al-Silw District. Approximately 60% of the district is under the control of the de facto authority (Houthis), while around 29% of the district lies outside the Wadi Tuban catchment area.

**Small-scale nature of existing water harvesting projects:** Most of the water harvesting projects in the areas assessed are small-scale interventions, such as ponds, small reservoirs, and diversion structures, with storage capacities ranging from 40 to 2,400 cubic meters. The stored water is typically consumed rapidly for domestic use and does not contribute to groundwater recharge, as these structures are lined with cement. Consequently, they have no significant impact on the hydrological model or the overall water balance

The follow table present the information on Existing Water Harvesting and Diversion Structures in Al-Selw.

Project Name	Type	Location (Area/Sub-area/Village)	Coordinates (°)		Storage Capacity (m³)
			N	E	
Al-Dhanib cistern	Storage Weir	Al-Du'ah Sub-area / Al-Dhanib Village / Dhi Eil. Stream	13.346704	44.184946	2,400
Al-'Uzar Pond	Storage Weir	Al-Du'ah Sub-area / Al-'Uzar Village / Al-Shoubain. Stream	13.346124	44.181239	2,000
Al-Saeed Weir	Storage Weir	Al-Qabilah Sub-area / Al-Saeed Village	13.326848	44.207266	2,200
Al-Mudah Pond	Pond	Al-Akeeshah Sub-area / Al-Salahiif Village	13.324094	44.188537	75
Al-Safaa Pond	Pond	Al-Akeeshah Sub-area / Al-Salahiif Village	13.323773	44.186531	41
Ain Al-Jarf Pond	Pond	Al-Du'ah Sub-area / Sa'arah Village	13.332109	44.186531	96
Aqmat Na'ous	Reservoir	Al-Qabilah Sub-area / Al-Saeed Village	13.325845	44.208097	200
Hameed Reservoir	Reservoir	Al-Qabilah Sub-area / Al-Saeed Village	13.328211	44.212307	1,400



Figure 8. Photos taken during field work in the targeted districts.

## 5.2 Input data for SWAT modelling

To simulate water resources in the Tuban Basin using the SWAT model, several datasets were collected and prepared to reflect the physical and environmental characteristics of the area as accurately as possible. These datasets include topography, land use and land cover, geology, soil, and climate variables. Given the complexity of the landscape and data limitations, the input data were processed through a combination of global sources, remote sensing, field observations, and expert adjustments. The integration of these sources ensures that the model reflects local conditions as accurately as possible. Table 3 summarizes the global datasets used and their respective sources.

This section presents only the final input datasets used in the model; all processing steps, data sources, adjustment methods, and resulting maps are described in detail in Annex 2: Input Data Preparation and Processing for the SWAT Model.

Table 3. Global datasets used for the input data for the SWAT model.

Data	Spatial Resolution	Temporal Resolution	Source
<b>Land use map</b>	300 m	-	Land Cover- GlobCover 2009: <a href="http://due.esrin.esa.int/page_globcover.php">http://due.esrin.esa.int/page_globcover.php</a>
	10 m		ESA Worldcover <a href="https://esa-worldcover.org/en">https://esa-worldcover.org/en</a>
<b>Soil map</b>	250 m	-	Soilgrids (Hengl et al., 2017) World Reference Base for Soil Resources (WRB) <a href="https://soilgrids.org/">https://soilgrids.org/</a>
<b>Elevation</b>	30 m	-	SRTM: <a href="https://lpdaac.usgs.gov/products/srtmgl1v003/">https://lpdaac.usgs.gov/products/srtmgl1v003/</a>
<b>Precipitation</b>	5566 m 11132 m	Daily	CHIRPS v2.0: <a href="https://chc.ucsb.edu/data/chirps">https://chc.ucsb.edu/data/chirps</a> ERA5: <a href="https://cds.climate.copernicus.eu/">https://cds.climate.copernicus.eu/</a>
<b>Temperature 2m max</b>	11132 m	Daily	ERA5: <a href="https://cds.climate.copernicus.eu/">https://cds.climate.copernicus.eu/</a>
<b>Temperature 2m min</b>	11132 m	Daily	ERA5: <a href="https://cds.climate.copernicus.eu/">https://cds.climate.copernicus.eu/</a>
<b>Dewpoint temperature 2m</b>	11132 m	Daily	ERA5: <a href="https://cds.climate.copernicus.eu/">https://cds.climate.copernicus.eu/</a>
<b>Temperature 2m</b>	11132 m	Daily	ERA5: <a href="https://cds.climate.copernicus.eu/">https://cds.climate.copernicus.eu/</a>
<b>Surface net solar radiation sum</b>	11132 m	Daily	ERA5: <a href="https://cds.climate.copernicus.eu/">https://cds.climate.copernicus.eu/</a>
<b>U wind component</b>	11132 m	Daily	ERA5: <a href="https://cds.climate.copernicus.eu/">https://cds.climate.copernicus.eu/</a>
<b>V wind component</b>	11132 m	Daily	ERA5: <a href="https://cds.climate.copernicus.eu/">https://cds.climate.copernicus.eu/</a>
<b>Evapotranspiration</b>	500m	Monthly	MOD16: <a href="https://www.ntsg.umt.edu/project/modis/mod16.php">https://www.ntsg.umt.edu/project/modis/mod16.php</a>
<b>Stream discharge</b>		Monthly	GRDC: <a href="https://www.bafg.de/GRDC/EN/Home/homepage_node.html">https://www.bafg.de/GRDC/EN/Home/homepage_node.html</a>
<b>Dams</b>			GRanD v1.3: <a href="https://globaldamwatch.org/grand/">https://globaldamwatch.org/grand/</a>

Data from the field study were used to better parameterise the SWAT model. As these are point measurements, generalisation and translation to the scales of the input maps was needed.

- **Soil Data:** The soil input data were based on the information collected in the area such as soil depths.
- **Land use validation:** The irrigated area in the land use map was validated against observations of irrigated areas made in the field, whereas crop data were used to design rotation schemes. To implement all different observed land use practises in the model is impossible as this would lead to a prohibiting complexity. In collaboration with the SWAT model developers efforts were also made to enter new plant species in the database such as mango, guava and qat that are grown used in Yemen.
- **Terraces:** The terrace map made for the field study allowed for changes in the soil map inputs reflecting the specific terraced condition. The terrace mapping was not completed, however, and this needs more work to make a complete map of existing terrace locations in the Tuban Basin. A comparison with a global mapping database (Li et al., 2025) showed that this dataset is far from complete and lacks sufficient detail (Figure 9). Manual mapping is therefore required also because of the insufficiently high resolution of topographic data (10 m) used to do the global mapping.

- **Groundwater data:** Information on well and spring information were used to determine groundwater level and abstraction status, although time restrictions did not allow for incorporating these data in the 1 km resolution of the groundwater model. These field data did also give a background against which model input decisions could be made.

In some cases generalisation was needed to account for the impossibility to represent the landscape in the model. The field information collected will also be useful in the future to allow, for instance, quantification of the impact of water abstraction on groundwater levels in different areas and for making decisions on monitoring locations and criteria.

Field data collection is required and should continue as this is a path forward to improving the developed models and to validate modelling results. The current field studies add to data collected in previous studies and should form a basis for continuous monitoring of agricultural practices and environmental status indicators.

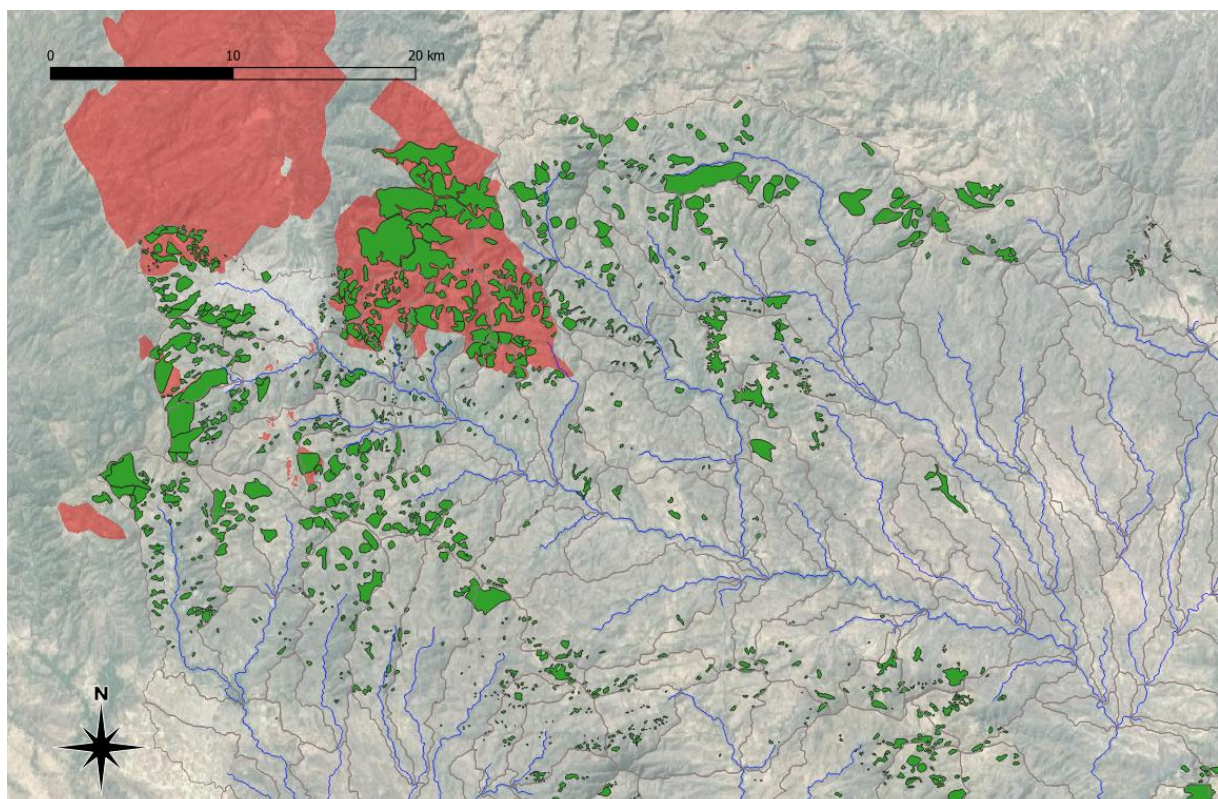


Figure 9. Comparison between a global terrace mapping database shown as red areas (Li et al., 2025) and the terrace mapping done in this study (green polygons) for the northern part of the Tuban Basin. The global database does not include many terrace areas and lumps distinct terrace areas together.

### 5.2.1 Topography

A 30-m resolution Digital Elevation Model (DEM) from the ALOS satellite was used to define the topography of the Tuban basin (Takaku et al., 2014). The DEM provides elevation data critical for hydrological modelling and was used to delineate the watershed boundary, define drainage networks, and extract slope, aspect, and flow length characteristics. Figure 10 shows the elevation distribution across the basin, which ranges

from approximately -7 m near the coastal delta to over 3,190 m in the upstream highlands. This topographic variation significantly influences precipitation, runoff and erosion processes in the basin.

To capture the landscape variability across the basin, three slope classes were defined (Table 4). These classes allow the model to more accurately represent land surface dynamics and improve the differentiation of hydrological response units (HRUs) based on topographic conditions for the main Tuban Basin model:

- **0–8%**: Representing 30% of the watershed, mostly located in the flat delta regions.
- **8–32%**: Covering 31%, these are moderate slopes.
- **>32%**: Steep terrain, accounting for 39% of the basin, mainly in the upstream mountainous zones.

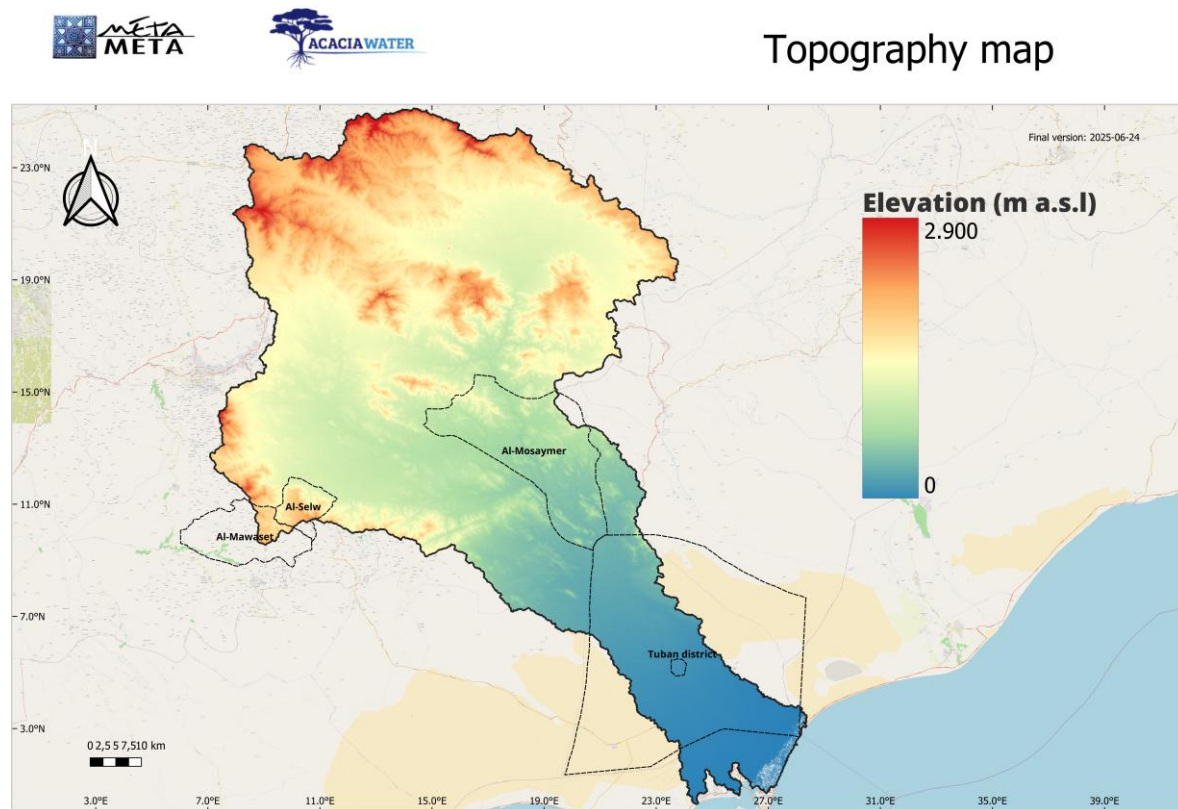


Figure 10. Digital Elevation map of the Tuban basin, Yemen.

Table 4. Slope classes defined for the SWAT model of the Tuban Basin and associated areas.

Slope class	Area (Ha)	% Watershed
0 – 8	221582	30
8 – 32	224258	31
> 32	288524	39

For the detailed models only two slope classes were define, being 0-8 or 0-10%and > 8 or 10%. This was necessary to limit the number of HRUs to avoid high complexity and extended run times.

## 5.2.2 Land Use and Irrigation

Land use and land cover information for the Tuban basin was derived from the high-resolution ESA WorldCover dataset (Zanaga et al., 2022) and refined to distinguish irrigated cropland using NDVI (Normalized Difference Vegetation Index) derived from Landsat imagery for the dry month of February over a period of five years. Areas irrigated through spate irrigation and groundwater abstraction were further identified and validated through field observations and comparison with satellite-based estimates. The full methodology for dataset selection, correction, and preparation is detailed in Annex 2: Input Data Preparation and Processing for the SWAT Model.

As illustrated in Figure 11, shrubland (33%) and bare or sparsely vegetated areas (31%) dominate the landscape, particularly in the upstream and central mountainous regions. Grassland (17%) and cropland (8%) are distributed across the middle and lower reaches, while irrigated cropland accounts for 10% of the basin, mainly located in the delta and lowland areas. Built-up areas are limited (0.7%), with small portions of tree cover represented by mango and guava orchards (0.5%) and wetlands (<0.0%).

This LULC classification plays a crucial role in defining the hydrological behaviour of different zones in the basin and was essential for generating accurate Hydrological Response Units (HRUs) in the SWAT model (

Table 5).

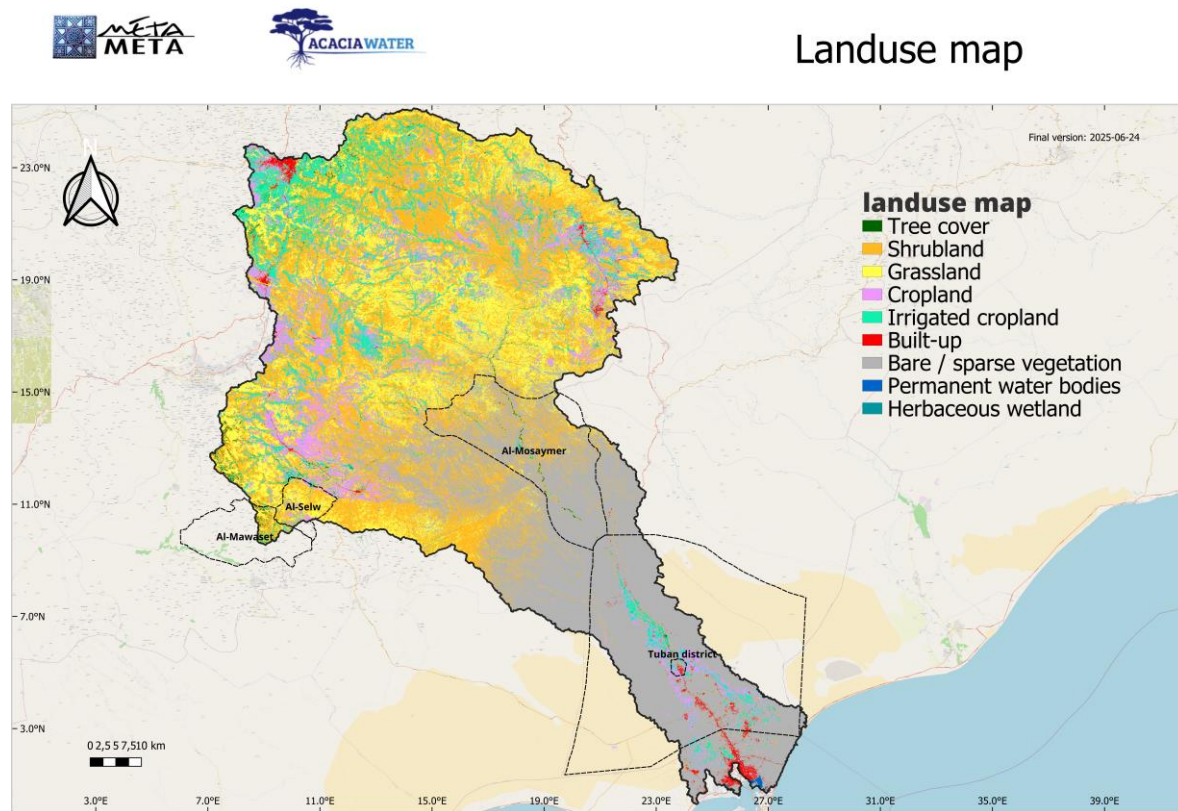


Figure 11. Land use land cover (LULC) map of the Tuban basin, Yemen.

Table 5. Land use codes, types and corresponding SWAT land use code.

SWAT Code	Description	Area (ha)	% Watershed
DWHT	Cropland	59851	8
RNGB	Grassland	128014	17
AGRL	Irrigated cropland	69951	10
SHRB	Shrubland	239068	33
BARR	Bare / spare vegetation	228686	31
URBN	Built-up	5422	0.7
WATR	Permanent water bodies	90	0.0
ORCD	Tree cover- representing mango and guava orchards	3280	0.5

### 5.2.3 Crop rotation schedules

Two different crop rotations were defined for the irrigated crop lands, based on field data about common crop types. An overview of the rotations and crop characteristics is given in Table 6. The areas classified as forest in the land use map were mango and guava orchards, but both species do not appear in the SWAT model plant database. As such the default orchard was used and the SWAT model developers are working to include these species into the plant database. The orchards were irrigated, as the trees cannot survive in the low precipitation regime in most of the basin, with a maximum irrigation of 7 mm d<sup>-1</sup> and an efficiency of 0.6. The harvesting indices and target biomass were obtained from literature data. For mango and guava species these were not available as the indices relate to fruit maturity rather than mango - orchard biomass proportions.

Table 6. Overview of the crop rotation operations schedules used for the upland and delta target areas. Auto irrigation is the start of irrigation at a certain soil moisture level, HI is harvesting index, Target BMS is the biomass attained for harvesting, Max. irr and Irr. Eff. Are the maximum irrigation quantity and the efficiency, respectively.

Crop	Year	Planting	Harvesting	Auto Irr.	HI	Target BMS	Max. irr.	Irr. Eff.
		[month]	[month]	[ $\cdot$ ]	[ $\cdot$ ]			
<b>Schedule WMEL Upland</b>								
Water melon	1	3	6	0.9	0.75	1	6	0.5
Tomato	1	8	11	0.9	0.6	6	5	0.5
Sorghum	2	4	6	0.8	0.5	15	5	0.6
Onion	2	8	11	0.9	0.85	7	10	0.5
<b>Schedule COTS Delta</b>								
Corn	1	5	10	0.9	0.46	28	7	0.5
Green beans	1	11			0.5	6	7	0.5
	2		3	0.9				
Cotton	2	11			0.45	6	7	0.5
Cotton	3		4	0.9				

## 5.2.4 Soils

Soil properties play a critical role in hydrological processes such as infiltration, runoff, and evapotranspiration within a catchment. In the SWAT model, soil input data must include a range of physical and chemical attributes—such as texture, depth, bulk density, organic carbon content, hydraulic conductivity, and available water capacity—typically specified per soil layer. These classifications are essential for defining Hydrological Response Units (HRUs) and accurately simulating land–atmosphere interactions.

For the Tuban Basin, soil data were sourced from a modified version of the World Reference Base for Soil Resources (WRB) most probable soil type from the global SoilGrids dataset (Hengl et al., 2017), which was further enhanced using local field measurements, interpretation of land use/land cover, and expert knowledge. This refinement included adjustments for specific conditions in the basin, such as rock outcrops, shallow soils, and the presence of agricultural terraces, particularly in the steep upland zones—features that significantly affect soil depth and infiltration capacity. The complete methodology and processing steps used to generate the final soil map are provided in Annex 2.

To ensure compatibility with SWAT's internal soil database, global WRB (World Reference Base) soil classifications were translated into SWAT soil classes using expert judgment and literature sources (**Error! Reference source not found.**).

Table 7. WRB soil codes and SWAT Name code associated to the Soil map, in the Tuban Basin.

WRB Code	Type / phase	SWAT SNAM	Depth [m]	Area [Ha]	% Watershed
6	Cambisols	Be73-2c-3673	0.3	73139.61	9.96
1006	Cambisols_fault	Be73-2c-3673_f	0.3	12114.95	1.65
2006	Cambisols_terraced	Be73-2c-3673_t	1.5	538.72	0.07
16	Leptosols	I-Y-bc-3515	0.55	192322.3	26.19
1016	Leptosols_fault	I-Y-bc-3515_f	0.55	35393.99	4.82
200	Leptosols_shallow	I-Y-bc-3515_s	0.2	92283.62	12.57
1200	Leptosols_shallow_fault	I-Y-bc-3515_s_f	0.2	13848.33	1.89
2200	Leptosols_shallow_terraced	I-Y-bc-3515_s_t	1.5	1675.93	0.23
2016	Leptosols_terraced	I-Y-bc-3515_t	1.5	13339.21	1.82
11	Fluvisols	Je61-2a-3530	1	76631.66	10.44
1011	Fluvisols_fault	Je61-2a-3530_f	1	714.87	0.1
5	Calcisols	Lk5-3ab-3534	0.74	10418.52	1.42
1005	Calcisols_fault	Lk5-3ab-3534_f	0.74	829.97	0.11
2005	Calcisols_terraced	Lk5-3ab-3534_t	1.5	7.81	0
1024	Regosols_fault	Rc30-1ab-3546_f	1	5561.18	0.76
2024	Regosols_terraced	Rc30-1ab-3546_t	1	58.84	0.01
24	Regosols	Rc34-3b-4033	1	33511.12	4.56
100	Rock outcrop	Rock_Tuban	0.1	145768	19.85
1100	Rock_outcrop_fault	Rock_Tuban_f	0.1	17190.91	2.34
2100	Rock_outcrop_terraced	Rock_Tuban_t	0.1	100.67	0.01
29	Vertisols	Vp39-3b-3563	1	6871.95	0.94
1029	Vertisols_fault	Vp39-3b-3563_f	1	2007.25	0.27
2029	Vertisols_terraced	Vp39-3b-3563_t	1	34.47	0

As shown in Figure 12, the most dominant soil types in the Tuban basin are:

- Lithosols and Leptosols, covering much of the upland and mountainous areas, characterized by shallow depth and limited water-holding capacity.
- Cambisols, common in moderately sloping zones, with moderate depth and structure suitable for agriculture.
- Fluvisols, concentrated in the lower delta areas, represent fertile, deeper alluvial soils used extensively for irrigated agriculture.

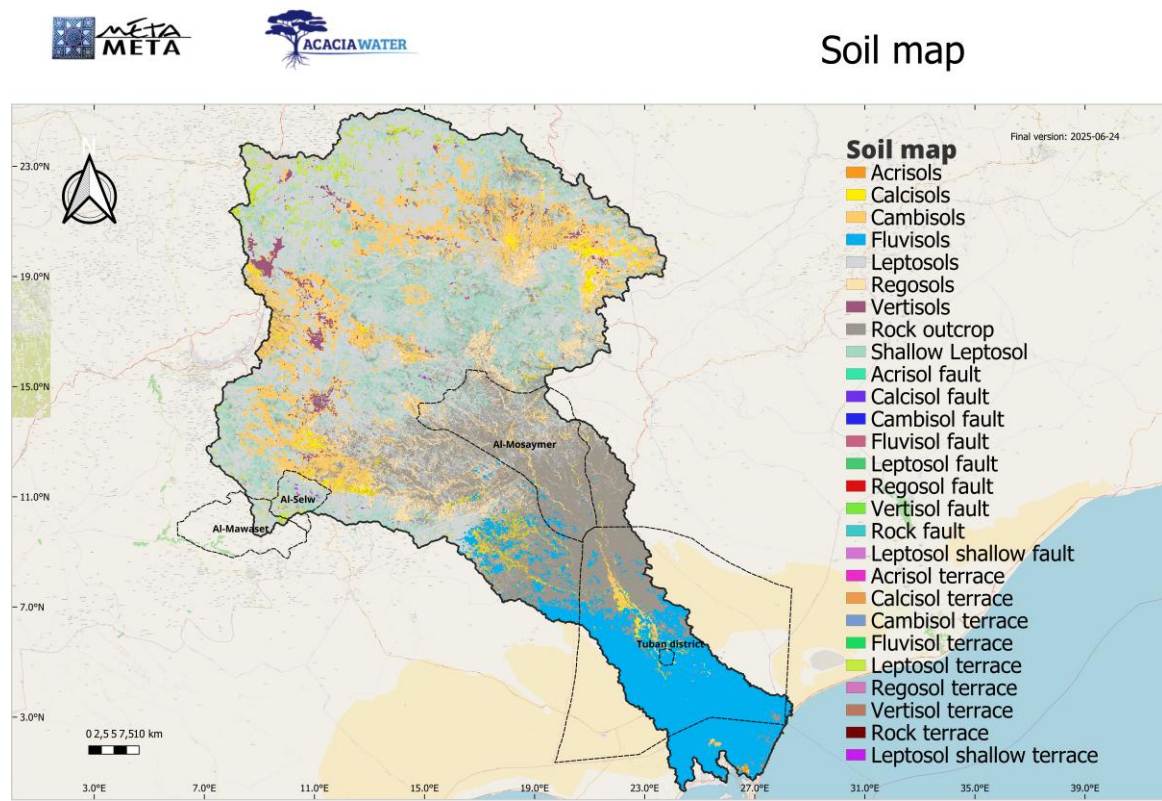


Figure 12. Soil map of the Tuban Basin, Yemen.

Following a test run with this soil input configuration the model proved too complex for practical application and the fault soils did not yield significant changes with respect to their non-fault equivalent in relation to groundwater recharge. These were therefore removed from the final model for the basin.

### 5.2.5 Climate Data

Daily weather data are fundamental inputs for hydrological modelling in SWAT, which requires five key meteorological variables: daily precipitation, minimum and maximum temperature, wind speed, solar radiation, and relative humidity. In the case of the Tuban Basin, the scarcity of reliable and continuous in-situ weather station records required the use of publicly available global datasets.

Daily precipitation data were obtained from the CHIRPS dataset (Climate Hazards Centre, n.d.), which combines satellite imagery with in-situ data for improved spatial coverage. Temperature and other meteorological variables (wind speed, solar radiation, and relative humidity) were sourced from the ERA5-Land reanalysis dataset, which offers high-resolution global climate information (Hersbach et al., 2020). To improve the representativeness of these datasets over the diverse topography of the basin, a correction

method was applied to the raw data, taking into account elevation gradients and available point measurements. The full methodology for dataset selection, correction, and preparation is detailed in Annex 2: Input Data Preparation and Processing for the SWAT Model.

Figure 13 presents both annual averages (top) and monthly mean values (bottom) for temperature and precipitation across the Tuban Basin, where are the final inputs for the SWAT model.

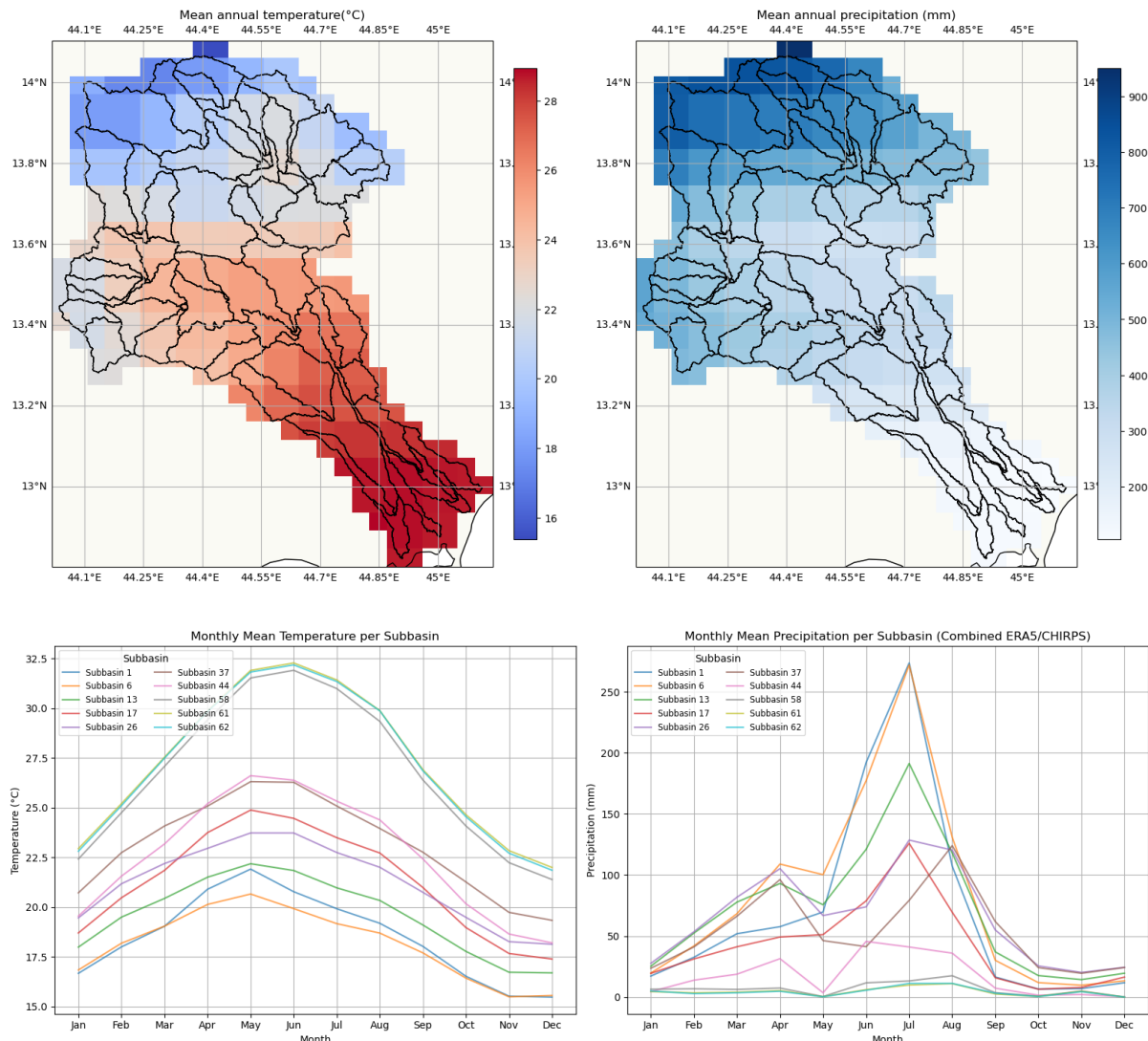


Figure 13. Annual average maps (top) and monthly mean values graphs (bottom) for precipitation (right) and temperature (left) across the Tuban Basin, Yemen. Sources CHIRPS (Climate Hazards Centre, n.d.) and ERA5 (Hersbach et al., 2020) datasets.

The final spatial distribution of precipitation and temperature inputs for the Tuban Basin presented the following patterns:

- Top left: The mean annual temperature map shows a clear north-south gradient, with cooler temperatures (as low as ~18°C) in the higher-elevation northern parts of the basin, and significantly warmer conditions (over 28°C) in the southern lowlands.

- Top right: The mean annual precipitation distribution highlights a similar spatial trend, with the northern highlands receiving the highest rainfall (>800 mm/year), while the southern and eastern lowland areas receive less than 300 mm annually.
- Bottom left: The monthly mean temperature per subbasin plot shows strong seasonality, with peak temperatures occurring between June and August. Subbasins in the south (e.g., Subbasin 2, 6, and 13) exhibit notably higher average temperatures compared to the northern ones.
- Bottom right: The monthly mean precipitation per subbasin indicates a marked concentration of rainfall between May and August, typical of the seasonal monsoon influence. The northern subbasins receive the bulk of the rainfall, while the southern subbasins remain relatively dry.

These spatial and temporal patterns were used to inform the climatic input parameters for the SWAT model. The representation of variability between subbasins is particularly important for simulating runoff generation, evapotranspiration, and water availability across different zones of the catchment.

# 6. Hydrological modelling at reconnaissance level

## 6.1 Methods

### 6.1.1 Model setup Tuban Basin

The hydrological modelling for this study was conducted using the most recent version of the SWAT+ 2012 model Version 2022/Rev 687. Model setup and parameterization were carried out through its QGIS-based interface, which streamlines tasks such as watershed delineation, stream network definition, and the spatial integration of soil, land use, and slope datasets. Although the official area of the Tuban catchment, shown in Figure 1, is approximately 7,169 km<sup>2</sup>, the area used for modelling differs slightly in the delta region, with some coastal zones not fully included. This is because, in SWAT, sub-basin delineation is based on the digital elevation model (DEM). In low-lying coastal areas, the model identifies the final drainage outlet based on topography, which does not always match the official administrative catchment boundary (Figure 14). The delineated modelling area was divided into 93 subbasins and further into 8,586 Hydrologic Response Units (HRUs), based on unique combinations of land use, soil type, and slope class (Figure 14). In the initial setup, several very large HRUs were generated in the Tuban Delta due to the uniformity of soil, slope, and land use—especially in areas away from the wadis. However, it became clear during the analysis that a more detailed delineation was needed to better represent spatial variability, particularly in precipitation patterns.

Daily rainfall records were incorporated into the model, and potential evapotranspiration was estimated using the Penman–Monteith method. Surface runoff was calculated with the Curve Number (CN) method, while the variable storage coefficient method was applied for channel flow routing. The model simulation period spanned from 1981 to 2018 (38 koens simulation length), due to the lack of ERA-5 re-analysis data after May 2019. The first 18 years (1981–1999) were used as a warm-up period to reduce the impact of initial condition uncertainty.

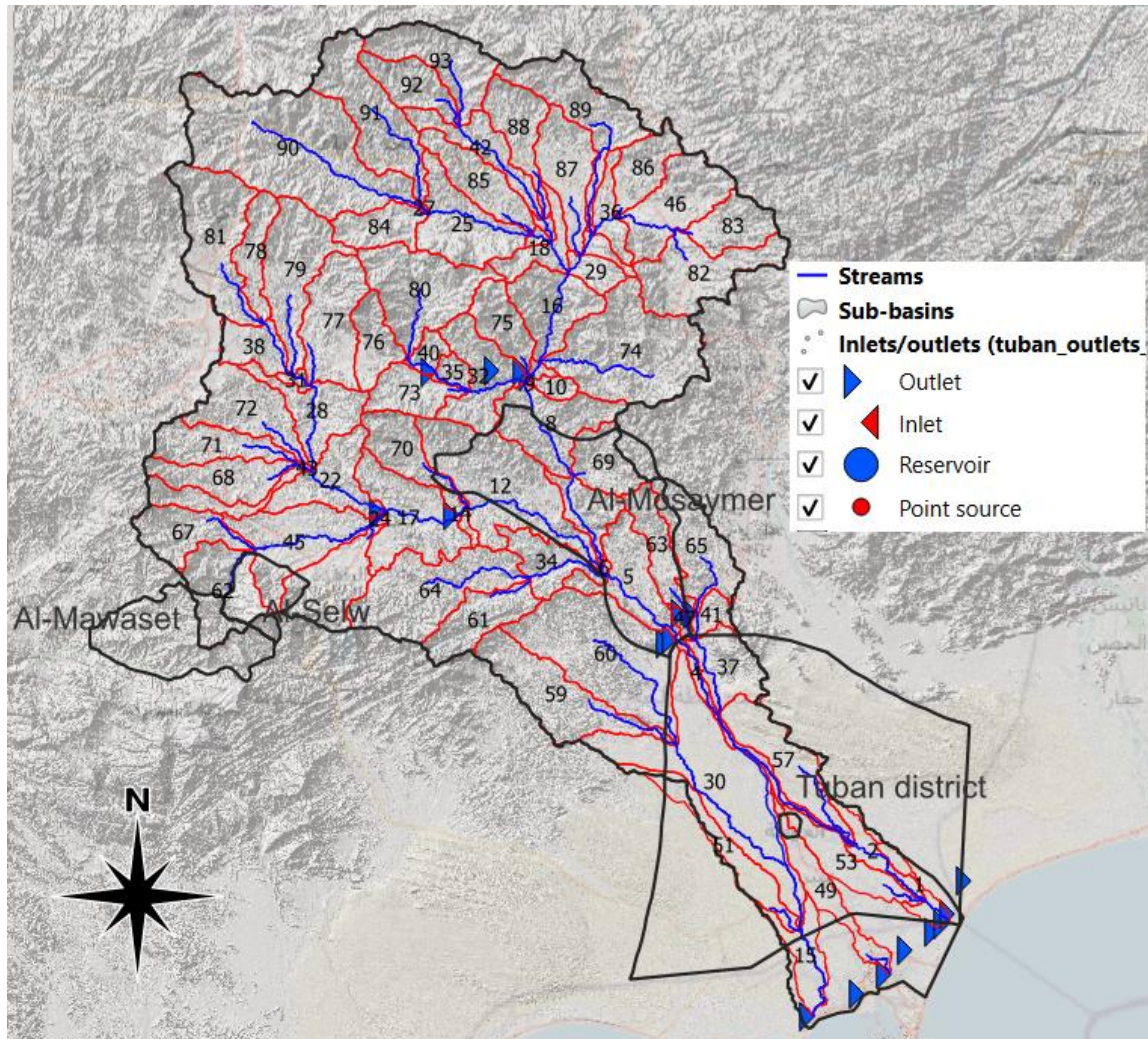


Figure 14. SWAT model setup map of the Tuban basin, Yemen.

### 6.1.2 Modelling assumptions, limitations, and uncertainty analysis

The SWAT model developed for the Tuban catchment aims to provide a reconnaissance-level understanding of hydrological processes across a large and complex basin in southern Yemen. Given the size of the catchment, its diverse hydroclimatic zones, and significant data limitations, several key assumptions were made during model setup, parameterization, and calibration. These assumptions influence the reliability and intended use of the model outputs.

#### Assumptions

1. Spatial Representativeness of Global Data  
Due to limited access to long-term, continuous in-situ measurements (e.g. precipitation, climate, greenness data), the model relies on global climate datasets (e.g. CHIRPS, ERA5, and Landsat-derived NDVI). These datasets were assumed to sufficiently represent spatial and temporal variability in climate inputs across the basin.
2. ET-Based Calibration as Proxy for Streamflow  
Continuous streamflow records were not available for calibration at sub-basin level. As a proxy, the model was calibrated using reference evapotranspiration ( $ET_0$ ) data derived from global datasets. This approach assumes that matching ET-based water

balance dynamics provides a reasonable surrogate for discharge calibration in data-poor basins.

### 3. Uniform Soil and Land Use Characteristics in Data-Scarce Zones

Where field observations were unavailable—particularly in remote or insecure areas—the model assumes that soil and land use types mapped from global datasets (e.g. SoilGrids, ESA WorldCover) are accurate and homogenous within delineated HRUs. This includes assumptions about rooting depth, permeability, and vegetation cover, especially in mountainous and rocky terrain.

### 4. Terrace soils

The terrace soils were assumed to be of the same type as those for the non-terrace areas in the surroundings, but with deeper rooting depth, soil layering and higher permeability.

### 5. Channel bed roughness and transmission loss

The channel permeability was set to  $50 \text{ mm h}^{-1}$  for the upland part of the Tuban Basin and detailed models and to  $100 \text{ mm h}^{-1}$  for the Delta area to simulate infiltration of river water into the channel bed that would contribute to groundwater recharge. Channel Manning's n was increased from the default value of 0.014 to 0.045 to reflect river bed morphology in all models.

### 6. Simplified Groundwater Representation

The Tuban basin is heavily dependent on groundwater abstraction, especially for agriculture. However, the absence of reliable data on extraction volumes, recharge rates, and aquifer parameters led to a simplified groundwater module setup. Groundwater-surface water interactions and depletion trends were not explicitly simulated but instead embedded indirectly via adjusted soil and percolation parameters.

### 7. Water Infrastructure

Only those with a storage capacity above approximately  $10,000 \text{ m}^3$  were simulated, as this is the minimum threshold required by SWAT. The remaining reservoirs, which have lower storage capacities, are currently inactive in the simulation but remain part of the model setup. These can be activated in future scenarios to evaluate the potential impact of upgrading or constructing new infrastructure. The locations of water infrastructure identified during fieldwork are shown in Figure 22.

### 8. Irrigation

The locations and areas of irrigated crop lands were estimated based on NDVI time-series, which represents the greenness of the land surface. NDVI should be low in dry periods where crops are not being irrigated. The threshold for classification of irrigated crop was taken as the average NDVI in the dry month of January 2020-2025  $>0.20$ , Landsat 8 imagery courtesy of the U.S. Geological Survey) to classify irrigated vs. non-irrigated croplands. Estimates for the irrigation water use of crops were from Gevaert et al. (2024). Irrigation sources in the wet period were taken as surface water (spate irrigation), whereas those in the Tuban Delta were taken as deep groundwater. The locations of boreholes in the Tuban Delta matched the areas classified as irrigated cropland well.

### 9. Warm-up and Validation Periods

A 5-year warm-up period (2008–2012) was applied to stabilize model conditions.

## **Limitations**

The hydrological model developed for the Tuban catchment (~734,000 ha) provides valuable insights at a regional level. However, several limitations affect the accuracy and resolution of the model, largely due to data gaps and the complex hydrological setting of the area.

### *Data Availability and Quality*

A major constraint in this study is the limited availability of local measured data. Continuous climate records—especially rainfall and temperature—are scarce or fragmented across the basin. Due to this, global datasets were used to estimate evapotranspiration ( $ET_0$ ) and precipitation inputs. While useful for large-scale modelling, these datasets lack the resolution and accuracy of on-the-ground measurements, which introduces uncertainty into model calibration and outputs. Similarly, data on groundwater abstraction—despite its importance in Tuban—is largely unavailable, which prevents realistic representation of aquifer depletion in the model.

### *Hydrological and Topographic Complexity*

The Tuban basin spans a highly variable landscape, from steep mountainous terrain to flat coastal plains. Rainfall distribution is uneven, and water management practices such as terracing, spate irrigation, and seasonal flood control further complicate runoff dynamics. These small-scale features are difficult to capture with global datasets, and cannot be fully represented in the model structure. As a result, key processes like localized infiltration, runoff retention, and seasonal variability may be oversimplified.

### *Lack of Discharge and Groundwater Flow Data*

Reliable streamflow data, critical for model calibration and validation, is not available for most sub-basins. This meant that the model had to be calibrated using indirect methods—primarily focusing on aligning modelled evapotranspiration with expected hydrological behaviour, rather than using actual flow observations. This limits the ability to verify whether modelled river discharge reflects reality. Furthermore, while the basin contains around 3,600 wells, data on abstraction volumes, recharge rates, and well productivity is insufficient. This limits the model's capacity to simulate groundwater levels or depletion trends accurately.

### *Catchment-Scale Generalization*

Due to the large size of the Tuban basin, the model applies generalizations to simulate hydrological processes across sub-basins. While this is appropriate for strategic planning and regional assessments, the model is not designed for field-level water management decisions. Local variations in land use, soil conditions, and infrastructure (such as check dams or irrigation systems) are not fully resolved at the model scale, and should be addressed in follow-up site-specific studies.

### *Vegetation characteristics*

The SWAT models knows many vegetation types that are common in the USA. However, some common crops for Yemen such as Mango, Guave, Qat are not in the plant database and had been substituted for other crops with possibly different growth and water use characteristics.

### **6.1.3 Model calibration**

After setting up the SWAT model, calibration was done using monthly evapotranspiration data from WaPOR. A total of 2,000 simulations were performed to ensure a robust calibration. The period from 2010 to 2016 was used for calibration, while data from 2016 to 2018 was used for validation.

For each simulation, R-squared scores were calculated at the subbasin level to evaluate model performance. After the Monte Carlo simulations, the parameter set yielding the best statistical performance for each subbasin was selected. These optimal parameter values were then used in a final calibration run to produce the final calibrated model. See annex 3 for the best fit statistics per subbasin. The time required for calibration depends on the size and complexity of the model. In this case, a relatively large model covering 7.3 km<sup>2</sup> took approximately 30 seconds of runtime per simulated year, resulting in a total of around 15 minutes per Monte Carlo run. In total the process took about 12 days. However by processing in parallel over four machines reduced the runtime to three days.

## **6.2 Results**

### **6.2.1 Evapotranspiration calibration**

The SWAT model was calibrated using monthly ET data from WaPOR between 2010 and 2016. The validation period was 2016–2018. A total of 2,000 Monte Carlo simulations were run with varying parameter sets (ESCO, EPCO, CN2, CANMX), and model performance was assessed at the subbasin level using R<sup>2</sup>, RMSE, and Pearson's r. For each subbasin, the best-performing parameter combination was selected for the final SWAT run (Annex 3).

Annex 3 shows the distribution of R<sup>2</sup> and r values across all subbasins. The results vary to quite some the extent, with some subbasins showing moderate to strong correlation (e.g., subbasin 11, 9, and 27), while others performed poorly in terms of R<sup>2</sup>. In several cases, R<sup>2</sup> scores were negative, which indicates the model underperformed compared to the mean of the observations (just a straight line through the mean). Despite this, many subbasins show reasonably strong seasonal trends.

Figure 15 shows the actual calibration time series for six upstream subbasins. Most plots show clear seasonal alignment between WaPOR and SWAT, especially during the April–September period when ET typically peaks. The match between modelled and observed ET differs per subbasin. For instance, subbasins 8 and 27 show overall lower ET values, while others align better. SWAT generally simulates lower ET than WaPOR, which is expected as WaPOR tends to overestimate ET, especially in areas with sparse vegetation or limited water availability (Blatchford et al., 2020).

Figure 16 shows the land use distribution across the catchment. Most subbasins are dominated by range shrubland (RNGB), followed by (SHRB). These land use types influence the ET patterns: irrigated cropland generally shows higher ET due to additional water input, while RNGB shows lower but more variable ET linked to rainfall dynamics. Urban areas show the lowest ET, as expected due to impervious surfaces.

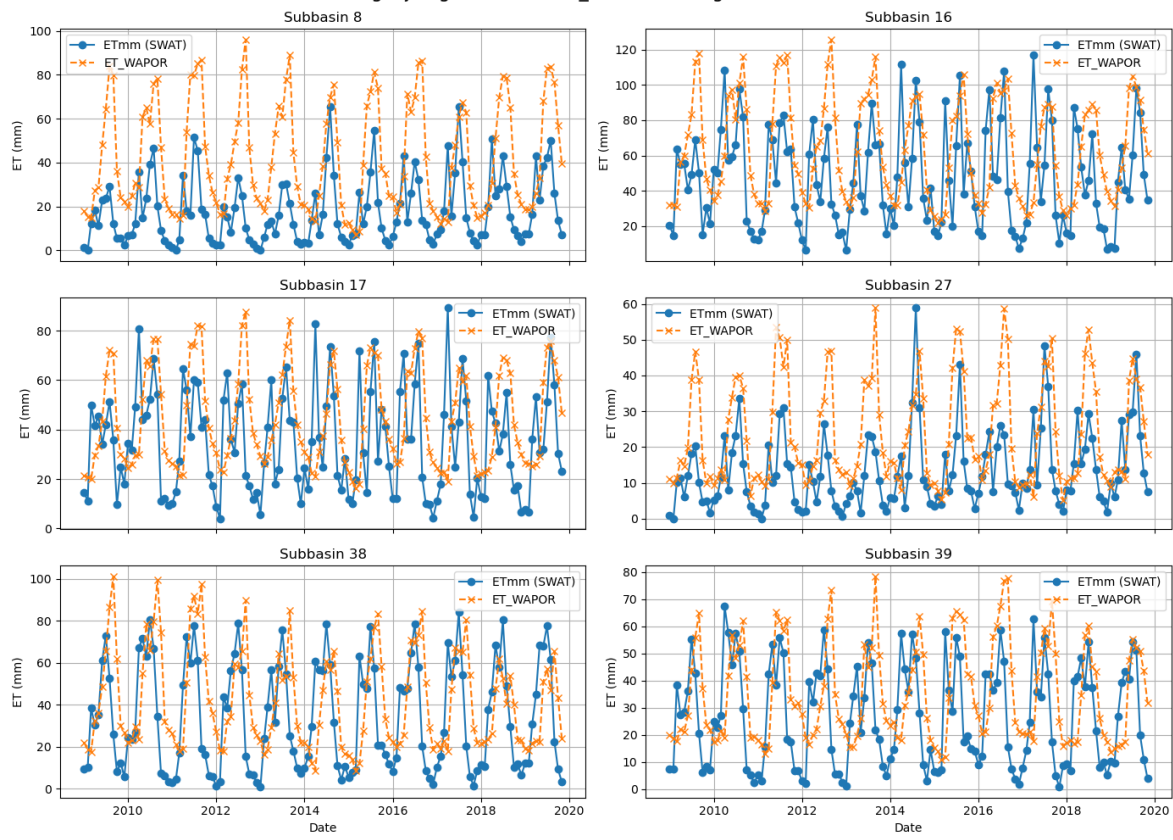


Figure 15. Monthly ET time series for six subbasins comparing SWAT simulations and WaPOR estimates.



Figure 16. Portions of land use types per subbasin

### 6.2.2 Water balance estimation

The SWAT model was used to estimate the water balance of the Tuban basin at a reconnaissance level, relying mainly on global datasets due to limited local data. The results give a first overview of how water moves through the basin and help to identify key dynamics and pressure points, especially in relation to seasonal availability and evapotranspiration.

The model shows that the basin receives an average of 420 mm of rainfall per year over the period 1999–2018, of which the majority (around 81%) is lost to actual evapotranspiration (342 mm  $a^{-1}$ ). This is expected, considering the arid to semi-arid conditions in the area, where the annual potential evapotranspiration exceeds 1,500 mm (Figure 17). In terms of runoff, the model estimates about 21 mm  $a^{-1}$  of surface runoff, and 22 mm  $a^{-1}$  of lateral flow. Recharge to groundwater is likely included in the percolation and lateral components, but we can't separate it clearly given the scale and input data (Figure 17). Because of the low precipitation amounts, surface runoff is low at 21 mm  $a^{-1}$ , as well as shallow groundwater recharge (54 mm  $a^{-1}$ ) of which part is re-evaporated and 7 mm  $a^{-1}$  contributes to baseflow. Deep groundwater recharge was taken as 10% of shallow groundwater recharge and amounted to 5 mm  $a^{-1}$  (Figure 17).

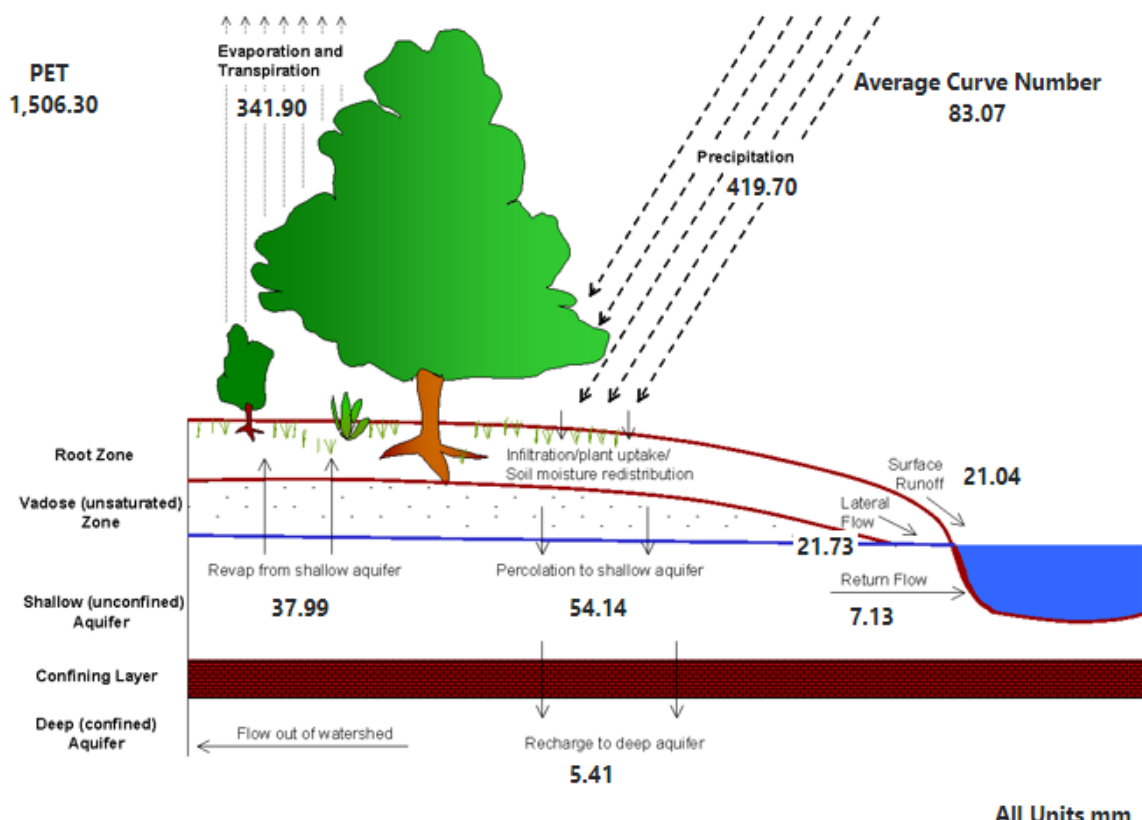


Figure 17. Annual average water balance component schematic for Tuban catchment model over the 20-year period 1999-2018.

Average monthly water balance component values for Tuban Basin are given in Table 8. The seasonal patterns show that rainfall peaks between June and August, with July showing the highest monthly rainfall (98 mm). During this period, we also see the highest runoff and water yield values—surface runoff reaches 7 mm in July, and water yield peaks in August at 12 mm. This confirms that most of the basin's surface water availability is concentrated in just a few months during the wet season.

Evapotranspiration stays high throughout the year, especially from March to September, reaching its maximum in July (57.8 mm). In the dry months (roughly October to March), water yield drops significantly or becomes negligible, reinforcing the need to capture and store water during the wet season.

Sediment yield remains low overall (estimated at 2.9 tonnes  $\text{ha}^{-1} \text{a}^{-1}$ ), with minor increases during the rainy season, suggesting a moderate erosion risk under current land cover.

There is a substantial gap between rainfall and PET, confirming the climatic water deficit typical of this region. While rainfall is highly seasonal and variable, PET remains consistently high, creating challenges for water availability, particularly during dry months (e.g., January–March, and October–December) when water yield is minimal or near zero. Crop that needs to be irrigated throughout the year (Tuban District) includes mango and guava orchards and may need well over 1000 mm  $\text{a}^{-1}$  irrigation water to maintain production.

Table 8. Average monthly water balance component values for Tuban Basin. SURF Q is surface runoff, LATQ is lateral flow, EY is actual evapotranspiration, PET is potential evapotranspiration.

<b>Month</b>	<b>Rainfall [mm]</b>	<b>SURF Q [mm]</b>	<b>LAT Q [mm]</b>	<b>Water Yield [mm]</b>	<b>ET [mm]</b>	<b>Sed.Yield [t ha<sup>-1</sup>]</b>	<b>PET [mm]</b>
<b>1</b>	8.9	0.2	0.3	0.5	10.4	0.1	97.9
<b>2</b>	16.5	0.3	0.5	0.7	13.8	0.0	107.2
<b>3</b>	35.9	1.8	1.4	2.7	31.6	0.6	144.4
<b>4</b>	48.9	1.8	2.1	3.4	42.8	0.5	153.0
<b>5</b>	34.3	0.7	1.5	2.2	36.1	0.1	139.2
<b>6</b>	58.4	2.7	2.1	4.0	37.9	0.3	130.2
<b>7</b>	98.0	7.3	5.2	11.0	53.6	0.7	146.1
<b>8</b>	69.7	4.6	5.4	12.4	47.5	0.4	129.8
<b>9</b>	23.9	1.3	2.0	6.9	27.3	0.2	113.8
<b>10</b>	9.3	0.2	0.7	2.3	17.5	0.0	128.2
<b>11</b>	6.8	0.0	0.3	0.7	12.4	0.0	115.5
<b>12</b>	8.9	0.1	0.3	0.5	10.8	0.0	100.1
<b>Annual</b>	419.5	21.0	21.7	47.3	341.8	2.9	1505.3

Before presenting the spatial outputs of the model, it is important to note that due to the lack of streamflow records in the Tuban basin, the SWAT model was calibrated using global evapotranspiration (ET) datasets. As a result, some quantitative outputs — particularly ET — may be overestimated. However, the spatial distribution patterns remain consistent and reliable, offering valuable insights into where key hydrological processes are more or less active across the basin. The following maps should therefore be interpreted with a focus on spatial trends rather than exact values.

#### Precipitation and actual evaporation patterns

The precipitation map (Figure 18) shows the spatial distribution of average annual rainfall across the Tuban basin. Rainfall is clearly concentrated in the central and upstream areas, particularly around the highland zones, while coastal and downstream areas receive significantly less precipitation. This aligns with regional climate trends, where orographic effects enhance rainfall in elevated zones, while the coastal plain remains much drier. The spatial contrast helps explain differences in runoff generation and water availability across sub-basins. Actual evaporation shows the influence of the spatial variation in precipitation, with minor differences caused by irrigated cropland and orchards in some of the subbasins. This is illustrated by the higher ET in subbasin 4 in the Tuban district.

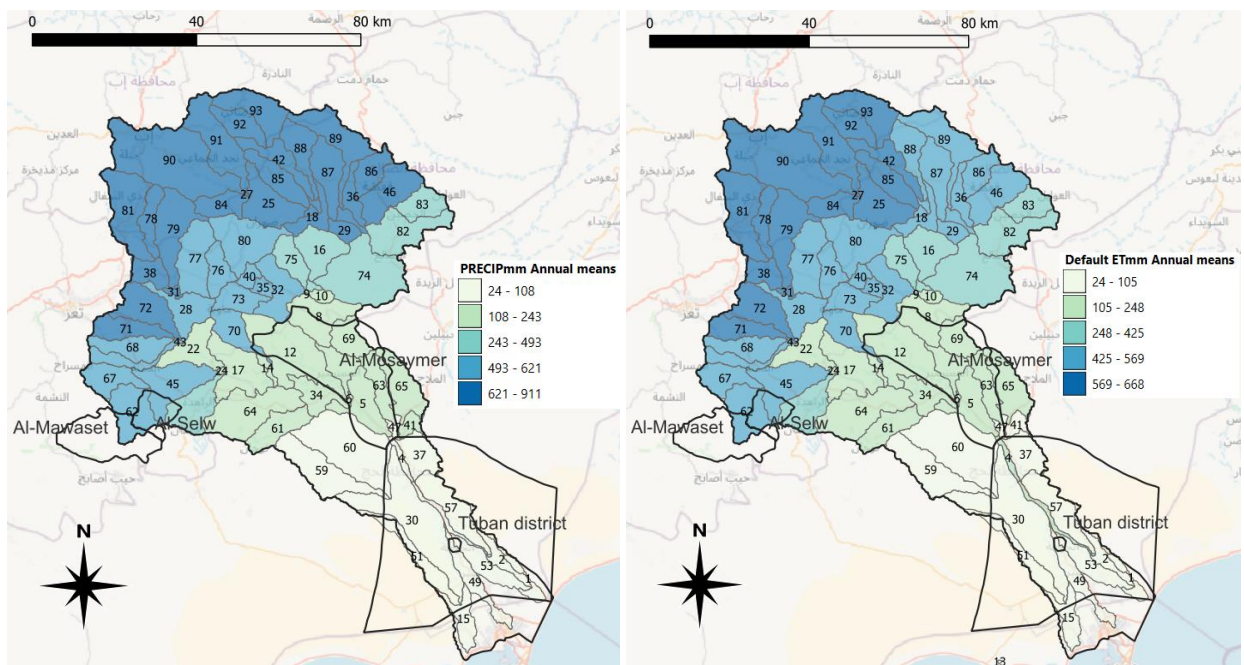


Figure 18. Average annual precipitation (left) and actual evapotranspiration-ET (right) spatial distribution over the Tuban Basin as simulated by SWAT for the period 1999 - 2018.

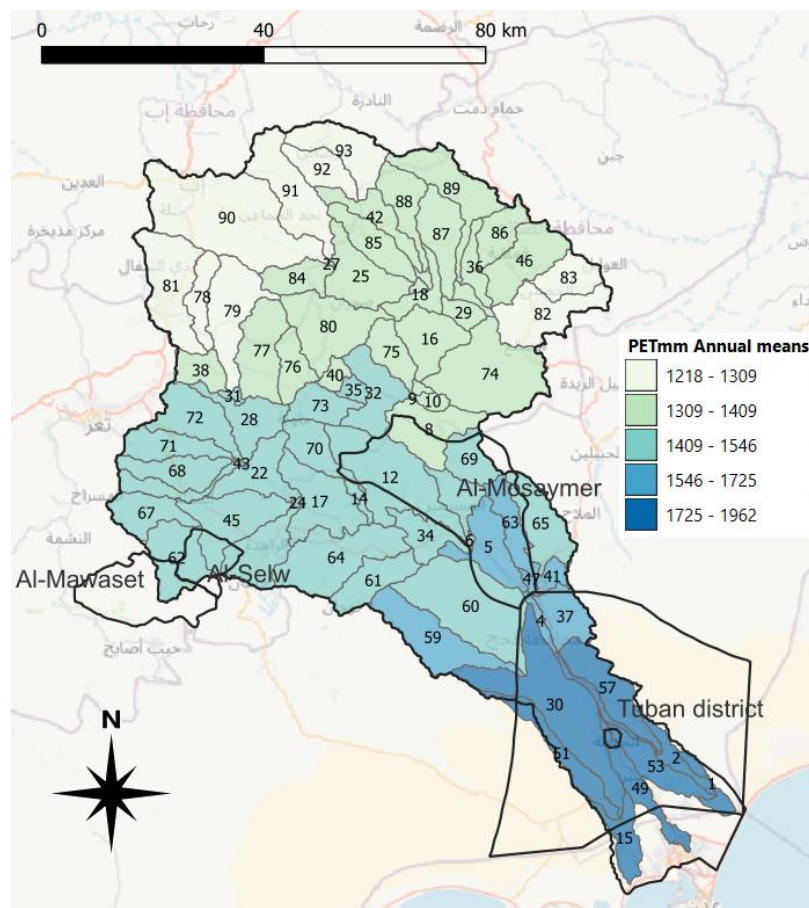


Figure 19. Average annual potential evaporation (PET) as modelled with SWAT for the Tuban basin for the period 1999-2018.

In contrast to the actual evaporation, which is related to the precipitation input, the potential evaporation increases from North to South and reaches its maximum of over 1700 mm  $y^{-1}$  in the Tuban District in the coastal area (Figure 19).

## Water yield

The water yield map highlights the areas contributing most to streamflow, including both surface runoff and lateral flow. The highest water yield values are concentrated in the upper catchment, where rainfall and slope gradients are greater. In contrast, the lower basin and delta zones show minimal yield, due to flat terrain and higher evapotranspiration losses (

Figure 20). This pattern underscores the importance of upstream areas for basin-wide water availability and suggests priority zones for water harvesting and recharge interventions.

The construction of terraces in the landscape increases water yield, and lowers surface runoff. However, because of higher continued evapotranspiration by crop on these terraces, deep aquifer recharge may not increase. The gain is then in the green water (used for crop) rather than in blue water.

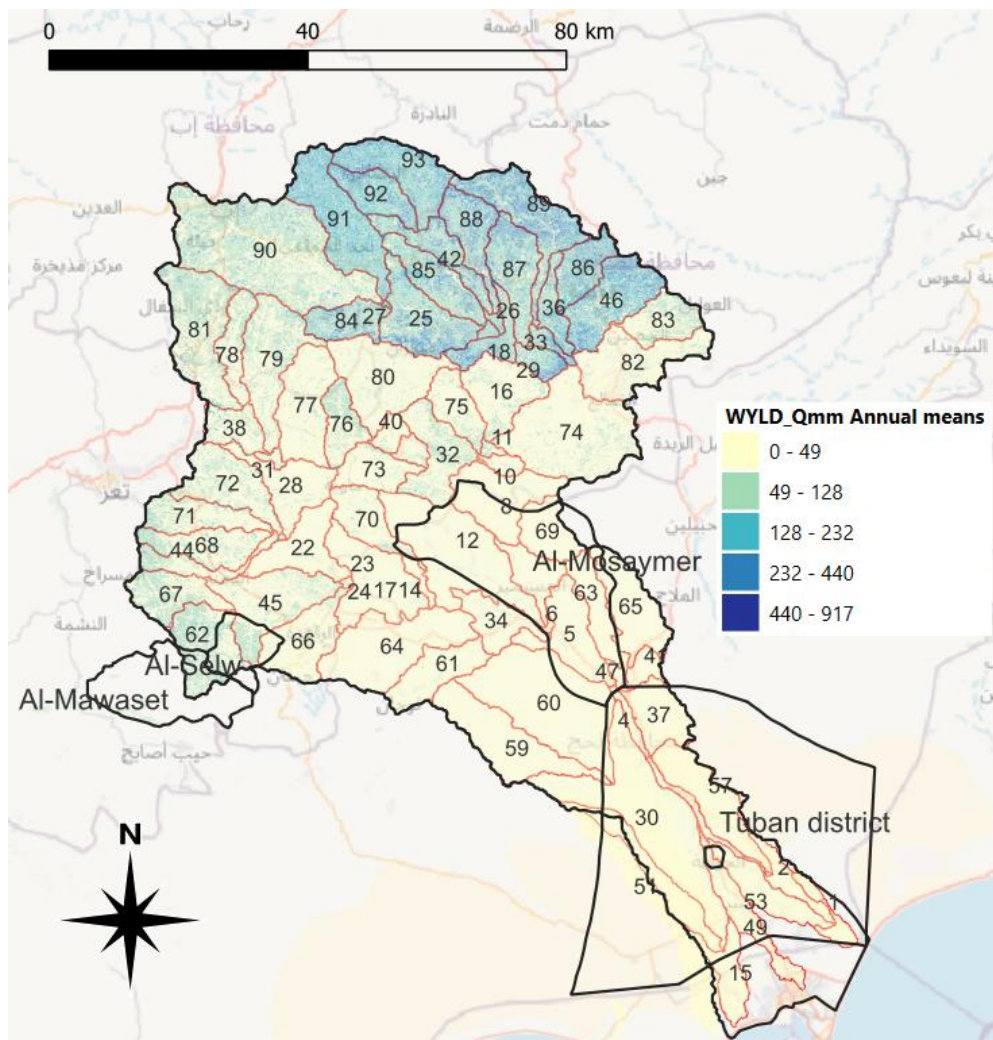


Figure 20. Average annual water yield over the Tuban catchment as simulated by SWAT for the period 1999 - 2018.

### Runoff generation

The surface and river runoff map (Figure 21) shows clear hotspots in steep-sloped areas with high rainfall, mainly in the upstream northern subbasins and somewhat less in the central basin zone. These areas are responsible for most of the quick flow response during rainfall events. In contrast, runoff generation is minimal in the flat, lower basin, where water is more likely to infiltrate or be lost through ET (Figure 21). These patterns also suggest erosion-prone areas and indicate where small-scale retention structures or check dams could be most effective. The northern subbasins also contribute most water to the flow in the main stem in the basin that feeds the Tuban District, with flow from western subbasins with lower rainfall into the Al-Mosaymer District being much lower. Very little flow is generated in the subbasins in the Tuban Delta.

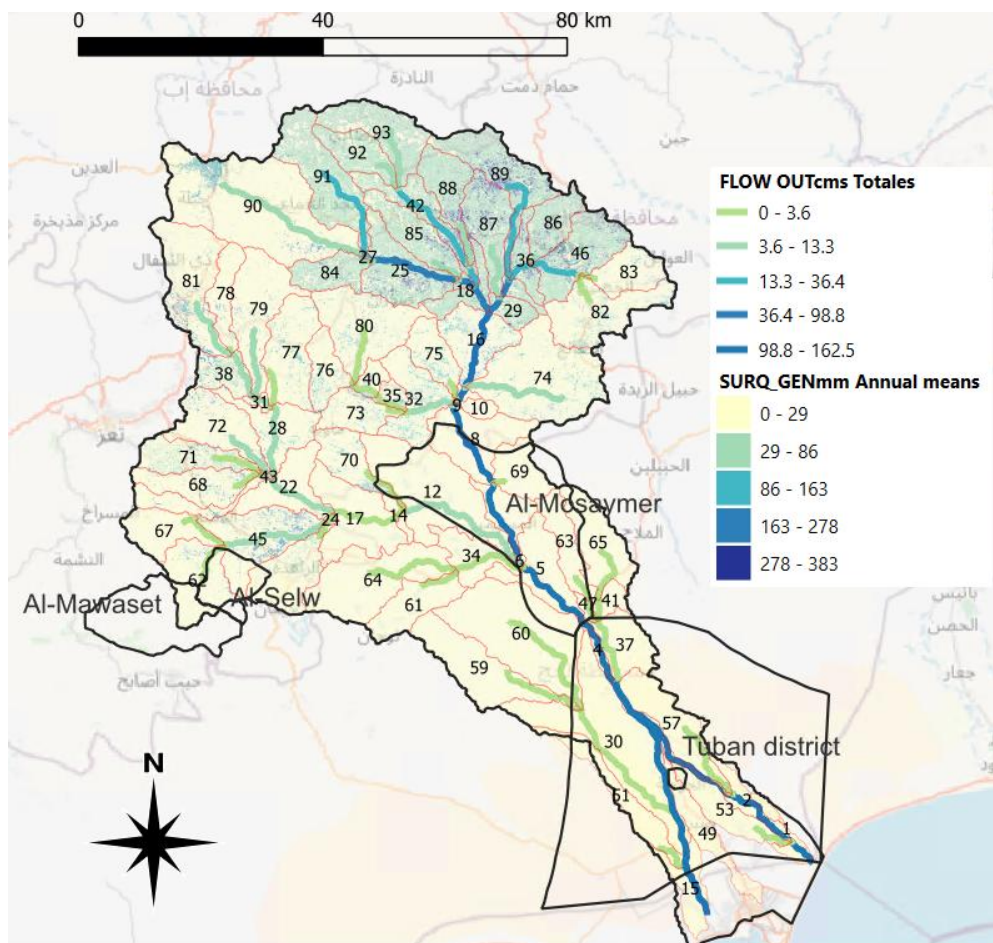


Figure 21. Average monthly surface runoff generation and subbasin stream outflow over the Tuban Basin as simulated by SWAT for the period 1999 - 2018.

### Reservoirs

The dataset provided by MetaMeta contained reservoirs, ponds, tanks and diversion structures in the catchment. These are shown in Figure 22. Reservoir capacity is up to 970,000 m<sup>3</sup> storage capacity for the Al Damoum Dam Park and 670,000 m<sup>3</sup> and 556,000 m<sup>3</sup> for the Al Khalaf Mawiya and Al Saqia dam reservoirs. The combined storage capacity for the Tuban basin is about 6.9 Mm<sup>3</sup>. This represents a 0.9 mm surface water storage over the whole basin. Total reservoir surface area was very limited, amounting to 46 ha for reservoirs filled to capacity.

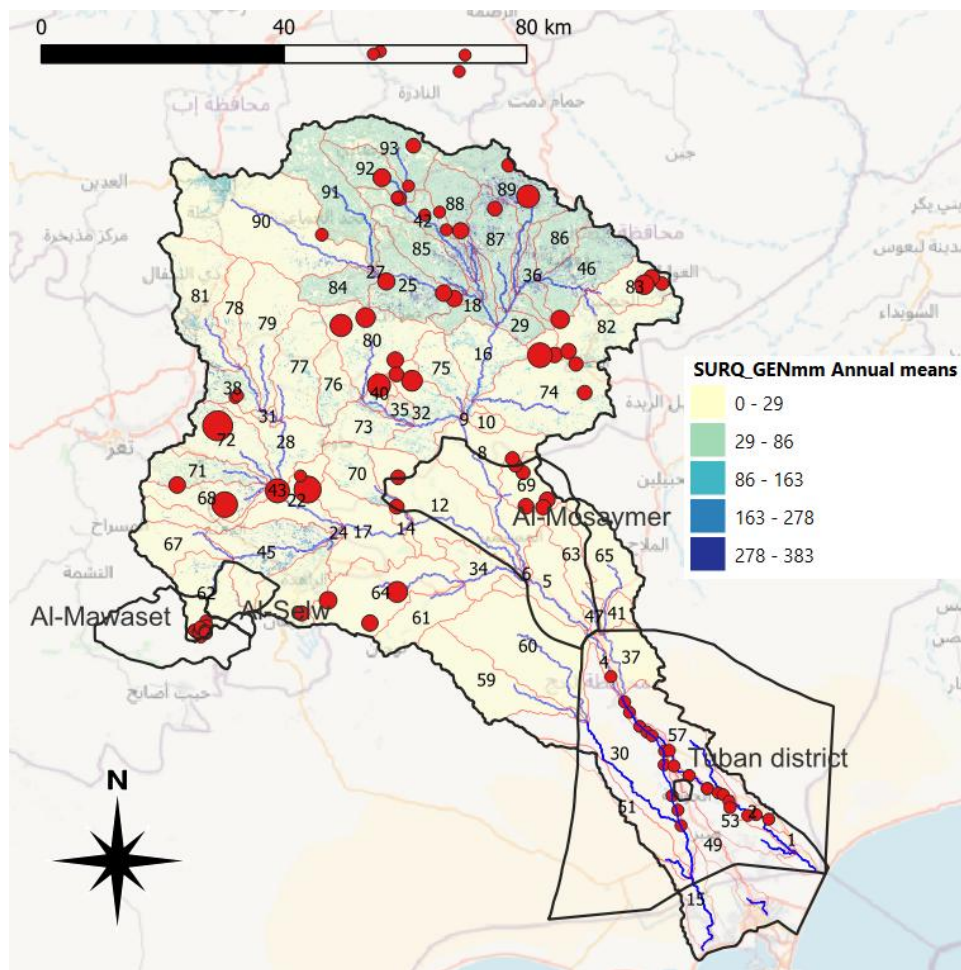


Figure 22. Map of the Tuban Basin showing water harvesting infrastructure (dam reservoirs, ponds, tanks, diversions) as red dots, of which the size indicates the storage capacity (0-900,000 m<sup>3</sup>). The reservoirs implemented in the SWAT model are shown as large blue dots. These have not been activated.

The Al-Selw and Al Mawaset Districts seem not to have large reservoirs, and water storage is limited to ponds and tanks. The Al Mosaymer District has two dam reservoirs with a capacity of 60,000 m<sup>3</sup> each (Al Humrah and Wadi Al-Wu'ayrah dams) and five smaller dam reservoirs, with a total combined capacity of 273,000 m<sup>3</sup>. These districts receive relatively low precipitation and produce less flow than the areas towards the North. In the Tuban District water storage dams, barriers and diversions structures are in or along the main Wadi and have limited storage capacities. It is uncertain if all structures could be identified, and some of the structures have collected sediment such that the initial storage capacity may have been reduced to some extent.

#### Groundwater recharge

The groundwater recharge map, interpreted from lateral flow and percolation estimates, indicates that recharge is relatively modest across the basin. The most favorable recharge conditions appear in the high-precipitation zones, where infiltration may allow infiltration. Recharge potential decreases toward the lower basin, likely due to compacted soils and reduced precipitation (Figure 23). While the model offers only a broad estimate, these results help identify target areas for managed aquifer recharge and further investigation.

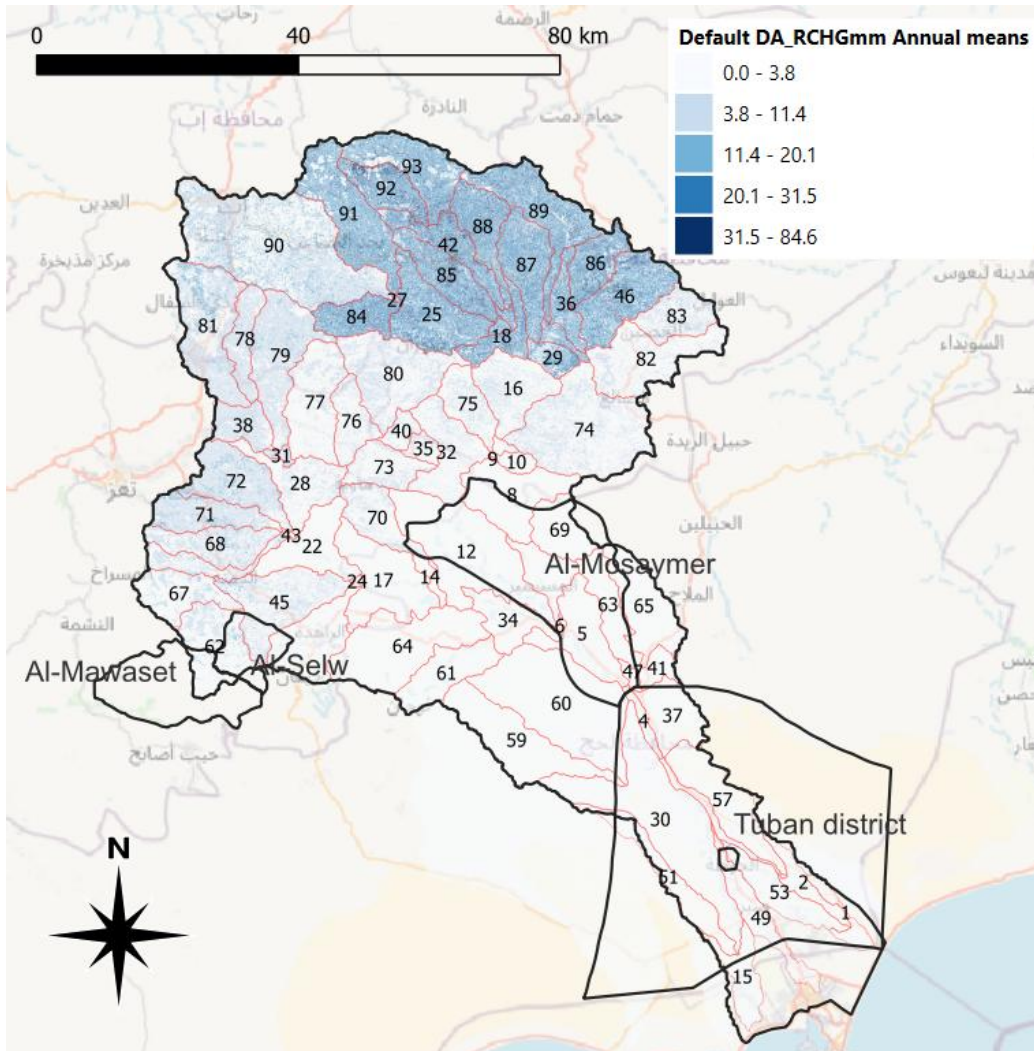


Figure 23. Average annual dep aquifer recharge estimates for the Tuban Basin as simulated by SWAT for the period 1999 - 2018.

#### Irrigation water use

The water use form irrigation is shown in Figure 24. Irrigation consumes up to  $1415 \text{ mm a}^{-1}$  of water at certain orchards in the Tuban District, with an average of  $402 \text{ mm a}^{-1}$  consumed by orchards (33 ha) in the basin. While irrigation is scattered in the upland parts of the basin with higher precipitation, consuming  $109 \text{ mm a}^{-1}$  for crop rotations (624 ha), concentration occurs along the main wadi in the Tuban district where precipitation is very low. This places considerable stress on the groundwater resources.

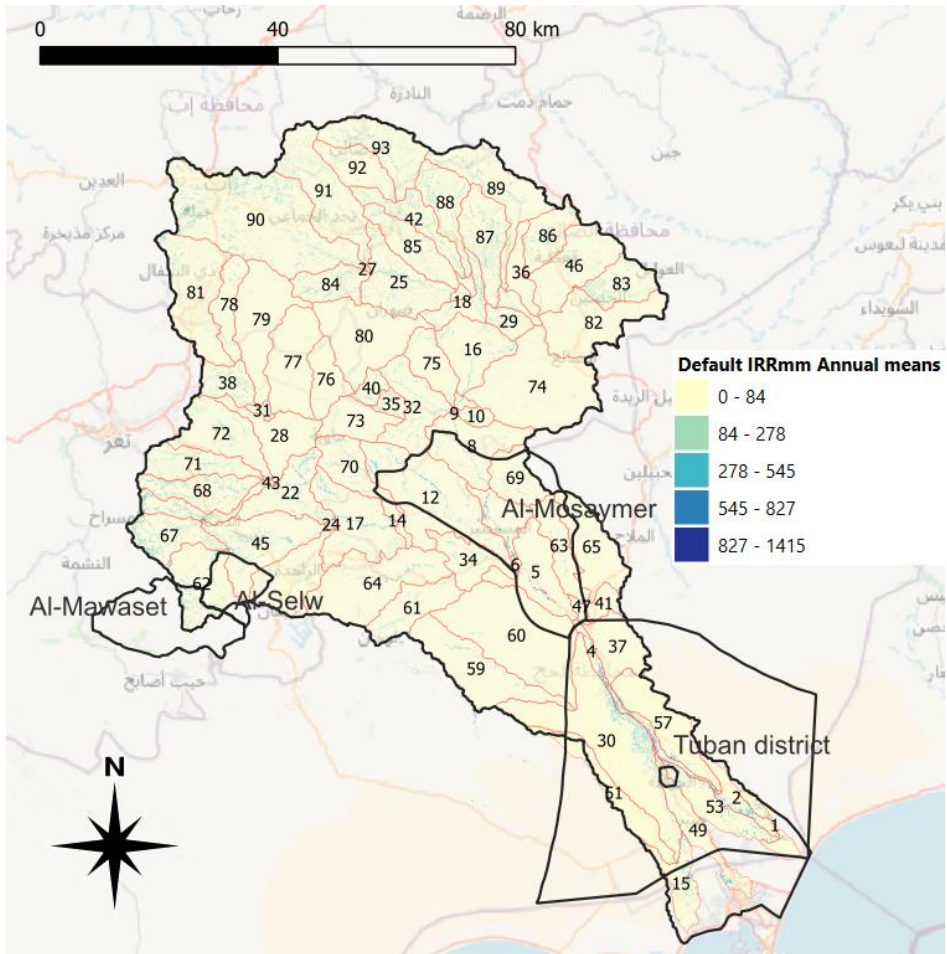


Figure 24. Annual average irrigation water use in the Tuban Basin for the period 1999-2018.

### 6.3 General conclusions of the Hydrological modelling at reconnaissance level

The significant gap between rainfall and potential evapotranspiration (PET) confirms the basin's high evaporative losses and seasonal water deficit. Most rainfall is quickly lost to ET, highlighting the urgent need for water storage solutions (e.g., harvesting during wet months) and improved irrigation efficiency to make better use of limited water resources.

To address these challenges in more detail, three detailed models were developed using the field data collected on land use, crop types, irrigation methods, and water use. Among these, only the Tuban District model includes a dedicated groundwater component, allowing for a more in-depth analysis of aquifer dynamics. These detailed models build directly on the findings of the general reconnaissance-level model and help refine water management strategies at the local level.

Despite its limitations, the reconnaissance model provides a valuable first estimate of the water balance and the spatial distribution of key hydrological processes across the basin. It also serves as a critical input for the more detailed models, helping to guide where deeper analysis and data collection are needed. While groundwater contributions appear low in this initial model, actual abstraction is likely much higher. Additional field data and

monitoring will be essential to better capture groundwater dynamics and support long-term water planning.

In summary, the current model offers a strategic overview of water availability and distribution, but it should not be used for site-specific planning or management decisions until further calibration and data refinement are completed. Field validation of the model outcomes remains necessary before implementation can be undertaken.

# 7. Detailed sub-catchment hydrological assessment

## 7.1 Description study area

Detailed description of the biophysical characteristics of the four target districts has been presented by Gevaert et al. (2024). To perform a detailed hydrological assessment of the four districts of interest within the catchment, we developed separate models based on their geographic proximity. Ultimately, three models were created because the two northern districts, Al-Mawaset and Al-Selw, are located close to each other and could be combined into a single model. The first model thus covers both Al-Mawaset and Al-Selw Districts, the second covers the district of Al-Mosaymer, and the third covers the District of Tuban in the delta area. This approach allowed us to incorporate detailed, area-specific field data for a more accurate assessment. Figure 25 shows the boundaries of the three developed models within the model of the Tuban Basin. And, The general information for the four models is summarised in Table 9. Note that the Al-Mosaymer District is located in a crystalline rock area and that the main soil type is therefore rock outcrop with very limited soil formation. Agriculture in this area is therefore practised on sedimentary deposits in the wadis.

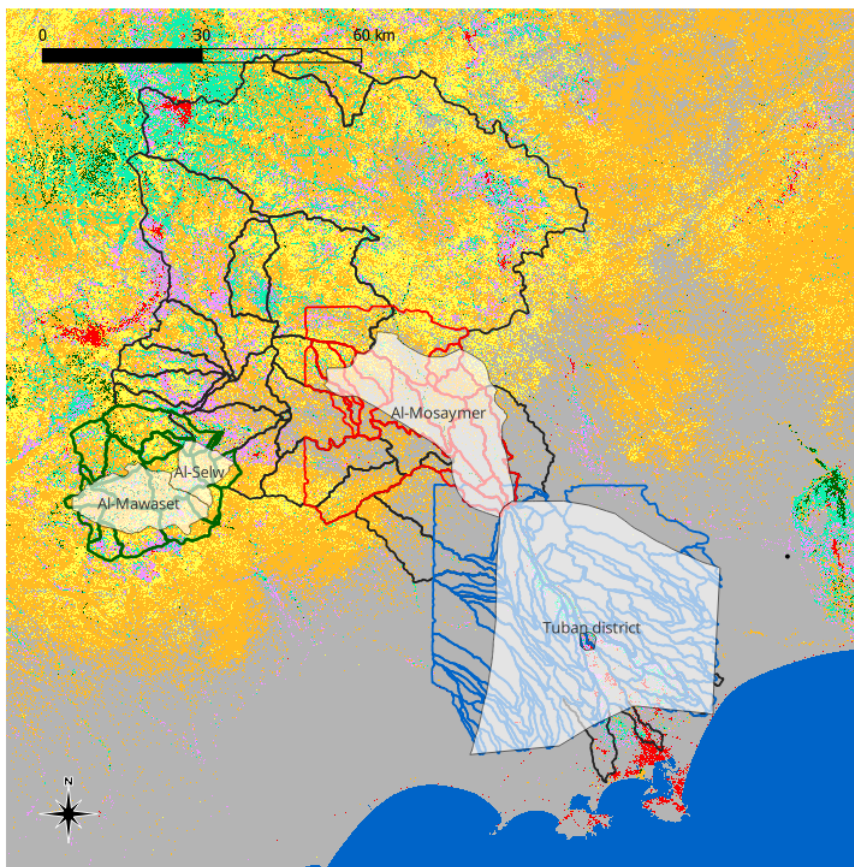


Figure 25. Location in the Tuban Basin of detailed hydrological models covering the districts of interest. The blue, red and green lines indicate the sub-catchments in the detailed models, whereas the black lines are from the Tuban Basin model. The base map is the land use map. District are indicated in white.

Table 9. Information on the three sub-models developed for the districts in the Tuban Basin and for the entire Tuban Basin.

District	Area [ha]	Sub-basins	HRUs	Slope bands	Dominant land use	Dominant soil
Al Selw / Al Mawaset	69,751	18	1210	0, 8, 9999	Shrub (47%)	I-Y-bc-3515 (51%)
Al Mosaymer	117,984	18	1110	0, 10, 9999	Bare (50%)	Rock outcrop (50%)
Tuban District	226,944	70	1402	0, 8, 9999	Bare (93%)	Je61-2a-3530 (59%)
Tuban Basin (v.6)	830,440	93	8586	0, 8, 32, 9999	Bare (38%)	I-Y-bc-3515 (28%)

## 7.2 Materials and Methods

### 7.2.1 Input data and setup

The input data for the three sub-models consisted of soil, land use and slope band classifications. The soil and land use maps were identical for all models. The detailed models were all run with the 2-year WMEL crop rotation schedule (rotations of water melon, tomato, sorghum and onions). However, the resolution of the models was much finer resulting in more detailed and smaller sub-catchments, especially for the Tuban District model. Reservoirs were included in most of the larger sub-catchments but only those with a storage capacity above approximately 10,000 m<sup>3</sup> were simulated, as this is the minimum threshold required by SWAT. The remaining reservoirs, which have lower storage capacities, are currently inactive in the simulation but remain part of the model setup. However, the reservoirs may be activated to model the impact of future construction of reservoirs in the subbasins. For the Tuban District, NWRA emphasized the importance of representing the diversion dam in the delta, with a flow allocation of 70% to the west wadi and 30% to the east wadi. Figure 26 shows the representation of the reservoirs, inlet and outlets configuration in SWAT model.

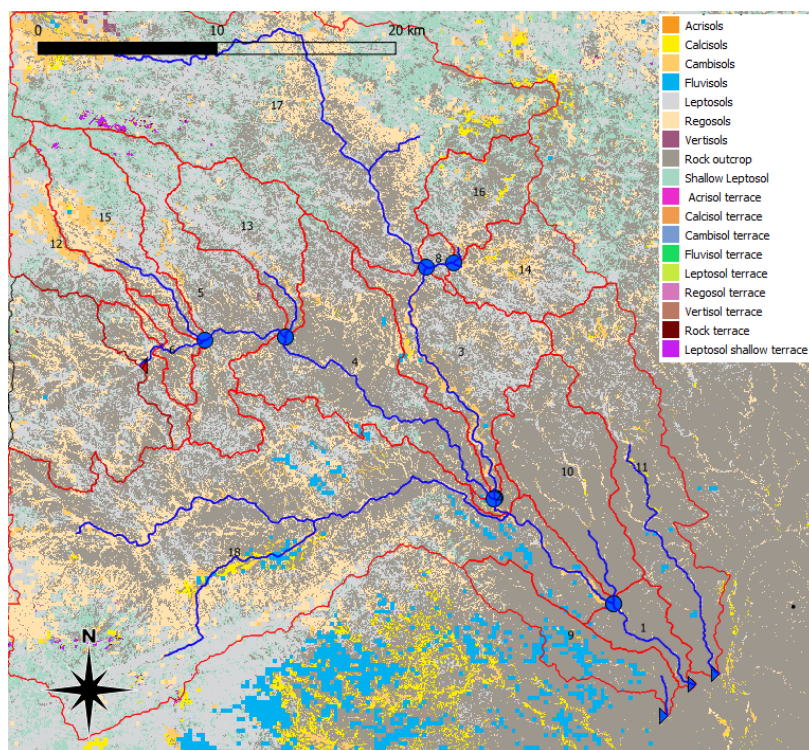


Figure 26. Subbasin (red lines), reservoir (blue circles), inlet (red triangle) and outlets (blue triangles) of Al-Mosaymer district catchment model, as overlain on the soil map.

## 7.2.2 Model calibration

Due to time constraints in the modelling it was not possible to fully calibrate and validate the three sub-models. Note that each calibration requires several hundred or runs of the models to obtain the best fit. With a single run lasting between 10 and 20 minutes of time, calibration requires several days. After consultation with stakeholders and receiving their feedback, we will proceed with continuing the calibration process to improve model accuracy. The tests with calibration on actual evaporation datasets (WaPOR, MODIS16A2) did not result in sufficiently good fits. The Tuban Basin model was therefore calibrated such that the annual discharge was comparable to the estimates published (average 125 Mm<sup>3</sup> a<sup>-1</sup>). The final calibration provided a discharge at Dukeim of less than 200 Mm<sup>3</sup> a<sup>-1</sup>. The calibration difficulties show the need for daily discharge data at at least one station (Dukeim), and preferably at more stations. The locations of these stations depends on the areas to be modelled but should include small as well as larger basins and cover the spatial variation in precipitation with the basin.

## 7.3 Results

### Al Selw / Al Mawaset model

#### Water balance overviews

The tuban\_al-selw\_ext\_v1 hydrological model was developed to include both Al Selw and Al Mawaset Districts and provides a detailed understanding of water balance dynamics in this upstream region of the Tuban catchment. These districts receive the highest precipitation, averaging approximately 620 mm a<sup>-1</sup> over the 1999–2018 period. Of this, Of this, the majority—about 555 mm a<sup>-1</sup>—is lost to actual evapotranspiration. The model estimates surface runoff at around 12 mm/year, and lateral flow at 39 mm a<sup>-1</sup> (Figure 27). A portion of the shallow groundwater is lost again through evaporation, while 39 mm a<sup>-1</sup> contributes to lateral flow. Additionally, deep groundwater recharge is estimated at 4 mm a<sup>-1</sup> (Figure 27).

The model simulates the main components of the water balance, including surface runoff, lateral flow, groundwater contribution, evapotranspiration, and sediment yield. The monthly water balance components are summarized in Table 10, showing that rainfall is concentrated in a few months (March, April, July, August, and September), which results in corresponding peaks in surface and lateral flow. Evapotranspiration (ET) closely follows rainfall patterns and represents the largest loss component across the year, with an annual total of 553 mm. The total annual water yield—defined as the water that contributes to streamflow—was estimated at 67 mm.

The land use and crop-specific results from the model are presented in Table 11. This includes key indicators such as Curve Number (CN), crop yield, biomass, and irrigation volumes. The results show clear differences in hydrological response between land uses: for example, orchards (ORCD) show the highest evapotranspiration rates, exceeding 1100 mm/year, due to high irrigation inputs. In contrast, rainfed crops such as wheat (DWHT) and shrublands (SHRB) show lower ET and water yields. Sediment yields also vary by land use, with bare areas (BARR) contributing the highest values.

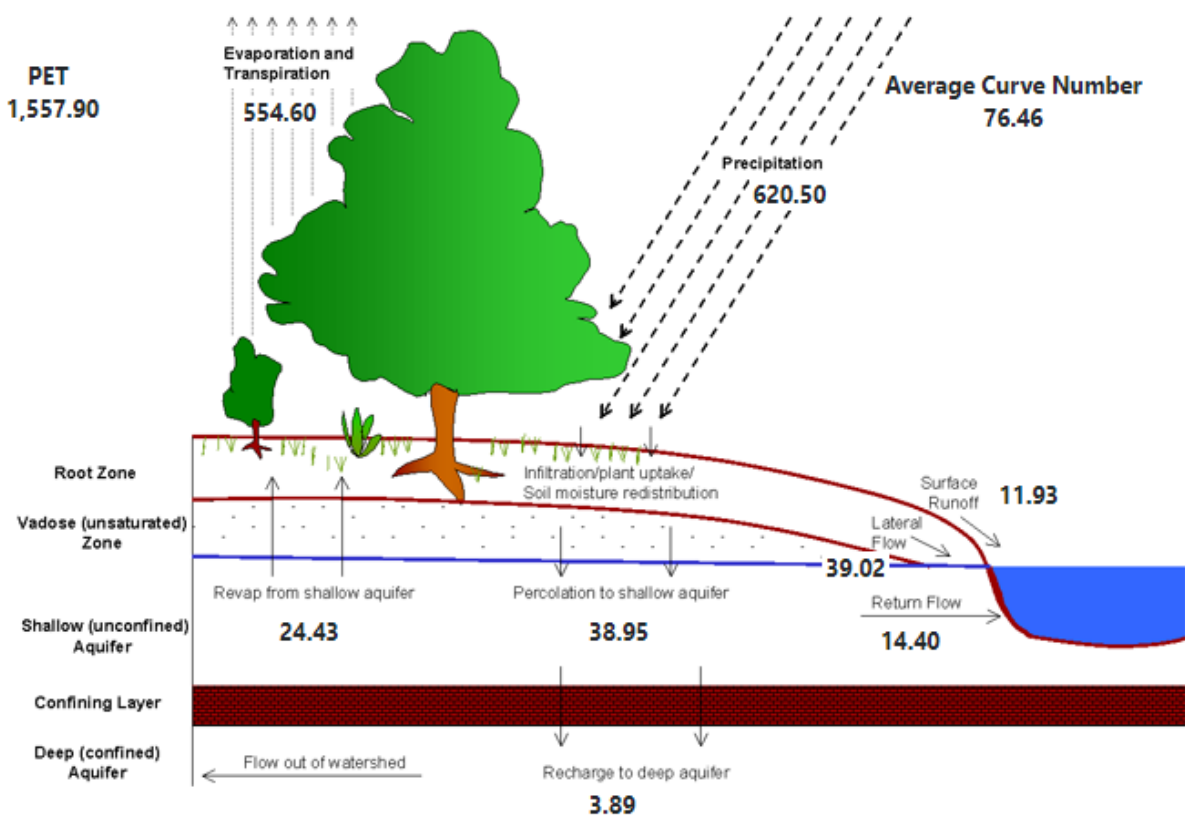


Figure 27. Annual average water balance schematic for the Al-Selw / Al Mawaset district model over the period 1999-2018.

Table 10. Monthly overview of water balance components for the Al Selw / Al Mawaset region for the period 1999-2018.

Month	Rainfall [mm]	SURF Q [mm]	LAT Q [mm]	Water Yield [mm]	ET [mm]	Sed.yield [t ha <sup>-1</sup> ]	PET [mm]
<b>1</b>	15.9	0.2	1.0	1.8	18.5	0.2	98.0
<b>2</b>	24.4	0.1	1.0	1.6	22.6	0.1	114.1
<b>3</b>	65.8	1.9	3.4	5.3	57.3	1.8	156.1
<b>4</b>	89.0	2.2	5.1	8.0	79.5	1.7	163.0
<b>5</b>	50.7	0.2	3.2	5.1	62.8	0.1	132.0
<b>6</b>	36.5	0.1	1.4	2.3	39.0	0.0	133.8
<b>7</b>	79.2	0.4	3.3	4.0	58.9	0.1	164.3
<b>8</b>	114.3	2.2	7.2	9.5	75.7	0.9	132.8
<b>9</b>	72.6	3.9	8.0	14.4	53.8	3.1	106.1
<b>10</b>	29.8	0.4	3.0	7.6	39.3	0.3	131.2
<b>11</b>	18.2	0.0	1.2	3.3	25.1	0.0	123.1
<b>12</b>	23.8	0.3	1.2	2.4	21.9	0.3	102.5
<b>Annual</b>	620.3	11.9	39.0	65.3	554.4	8.5	1556.9

Table 11. Overview of simulated outputs of SWAT for the Al Selw / Al Mawaset district catchment over the period 1999-2018 for each land use type (LULC). CN is the curve number, BIOM is the biomass of the vegetation, whereas YLD is the crop yield.

LULC	AREA [ha]	CN	IRR [mm]	PREC [mm]	SURQ [mm]	GWQ [mm]	ET [mm]	SED [t ha <sup>-1</sup> ]	BIOM [t ha <sup>-1</sup> ]	YLD [t ha <sup>-1</sup> ]
<b>BARR</b>	11.2	89.0	0.0	627.3	127.5	20.8	467.0	42.4	0.0	0.0
<b>BERM</b>	1.1	77.5	0.0	628.0	79.2	9.3	531.5	1.0	14.9	10.6
<b>DWHT</b>	65.6	77.4	0.0	627.9	15.4	12.3	573.2	1.3	7.5	2.0
<b>ONIO</b>	72.1	70.0	56.0	627.9	4.6	17.0	624.6	0.6	8.6	3.5
<b>ORCD</b>	16.8	70.0	524.8	627.5	0.8	34.4	1107.7	0.0	15.1	0.0
<b>RNGB</b>	200.4	77.0	0.0	627.7	12.3	90.0	495.1	19.0	0.5	0.4
<b>SHRB</b>	330.4	77.3	0.0	627.5	10.7	52.6	547.0	6.5	1.4	1.0
<b>WATR</b>	0.0	83.2	0.0	628.0	0.0	0.0	1593.8	0.0	0.0	0.0
<b>WETL</b>	0.0	70.0	0.0	628.0	3.6	8.5	581.3	0.2	1.8	1.2

The long-term monthly variation in several water balance components is shown in Figure 28. On totals range from close to zero to 200 mm. The monthly pattern of ET reflects precipitation inputs. The monthly average outflow of reach 5 is usually below 0.5 m s<sup>-1</sup>.

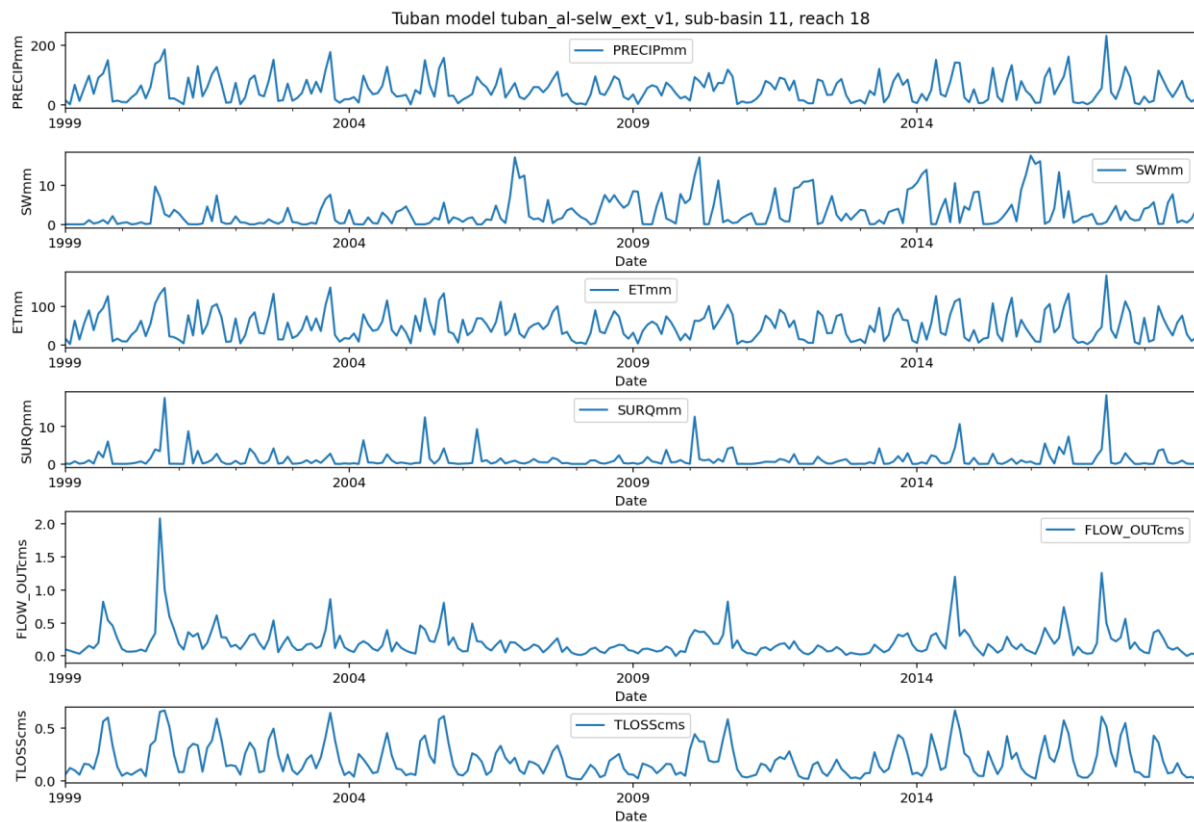


Figure 28. Monthly variation in precipitation (Precip [mm]), soil water content (SW [mm]), actual evapotranspiration (ET [mm]) and surface runoff (SURQ [mm]) for subbasin 11, and wadi outflow FLOW\_OUT [ $m^3 s^{-1}$ ] and wadi bed infiltration (TLOSS [ $m^3 s^{-1}$ ]) for reach 18 over the period 1999-2108.

The average monthly outflow in reach 18 is shown in Figure 29 and clearly shows a bi-modal pattern reflecting the rainfall inputs. The total outflow of this reach, which includes flow from the Al Selw District, is simulated at 6.5 Mm<sup>3</sup> a<sup>-1</sup>.

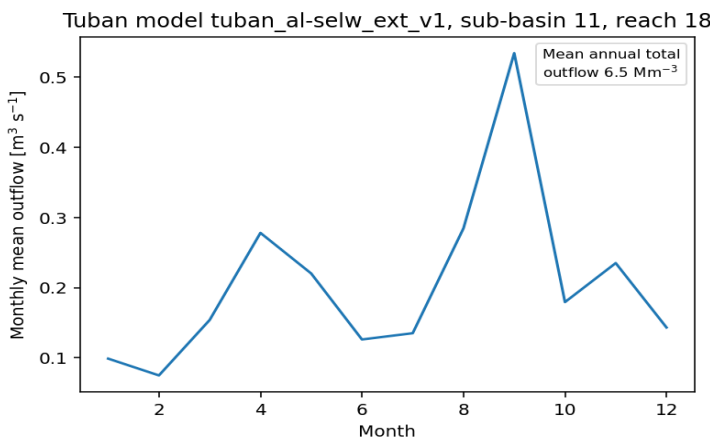


Figure 29. Average monthly outflow and total annual outflow of reach 18 in the Al Selw - Al Mawaset region over the period 1999-2018.

#### Precipitation and evapotranspiration patterns

Precipitation is highest in the Al Selw / Al Mawaset District and is uniform over the district between 419 to 621 mm a<sup>-1</sup>, for the period 1999-2018, as shown in Figure 30. The distribution of actual evapotranspiration (ET) across the modelled area is shown in Figure 31. The figure reveals a clear spatial pattern: higher ET values are found in areas with intensive vegetation or irrigated crops, especially orchards, while lower ET occurs on barren or sparsely vegetated slopes. This spatial variability reflects both land use and water availability, and helps identify where water is being used most intensively.

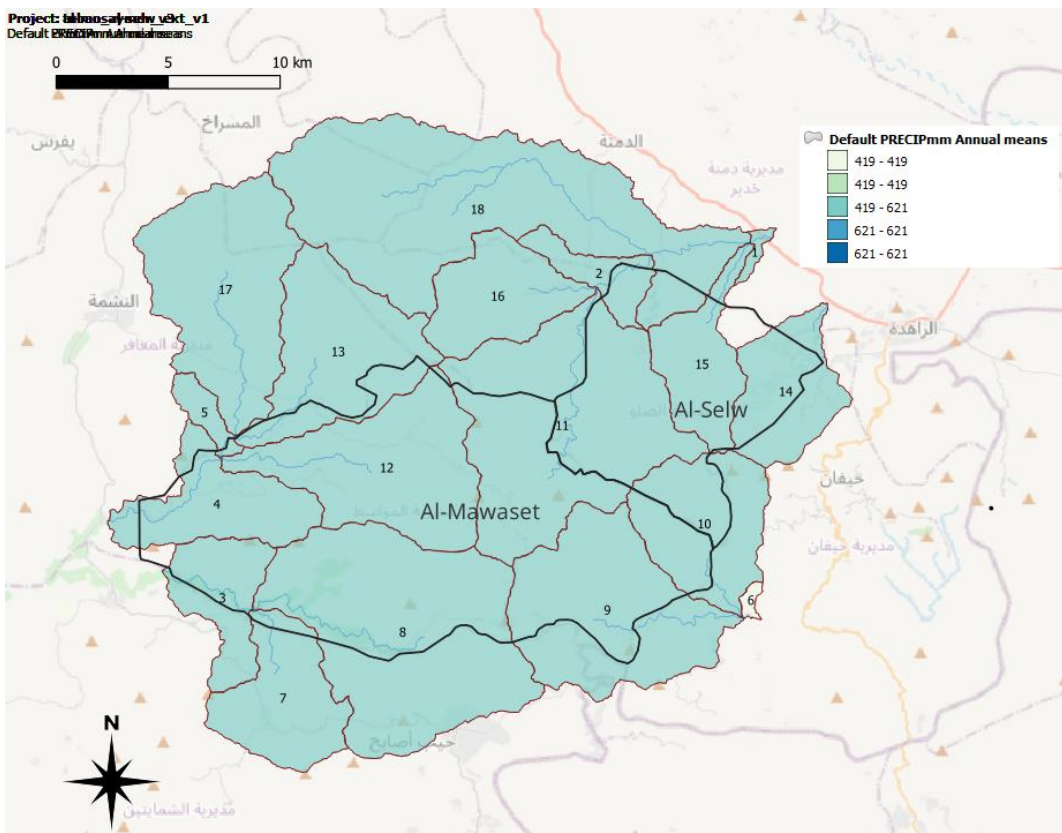


Figure 30. Average annual precipitation distribution over the Al Selw / Al Mawaset Districts (black line) for the period 1999 - 2018.

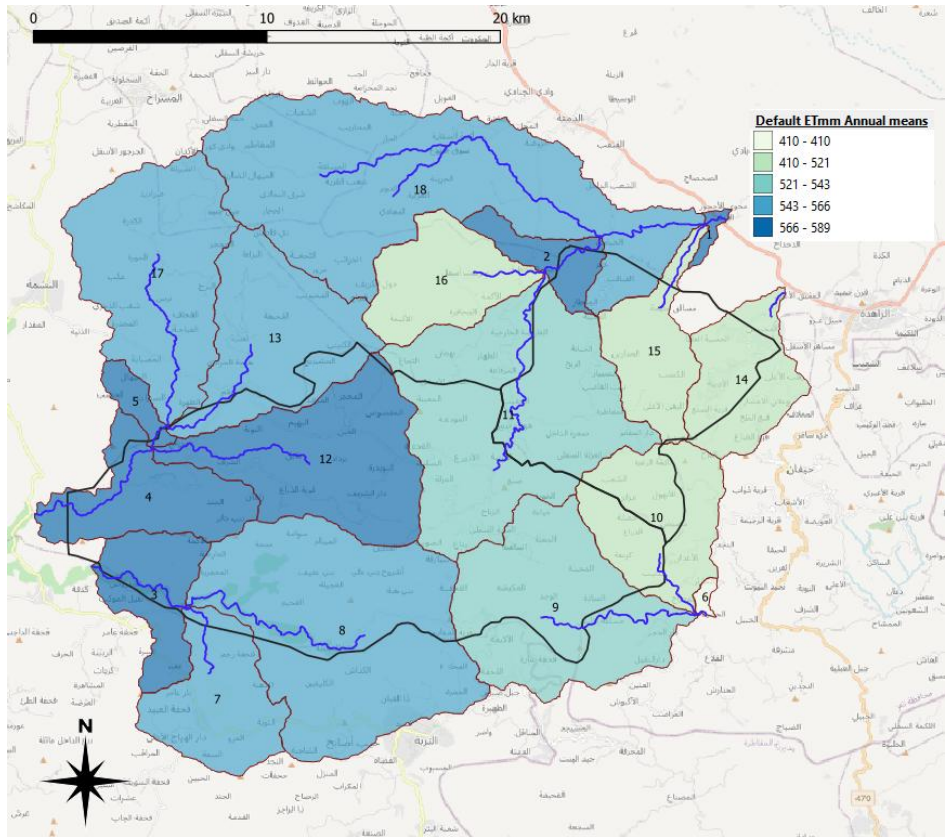


Figure 31. Average annual actual evapotranspiration distribution over the Al Selw / Al Mawaset Districts (black line) as simulated by SWAT for the period 1999 - 2018.

### Water yield

The water yield, defined as the net amount of water that leaves the subbasin and contributes to streamflow in the reach provides an indication of the availability of water accounting for losses by ET. The spatial distribution of water yield is shown in Figure 32, where clear differences can be observed between ridges and valley bottoms. Water yields are generally higher in valley areas, where soil moisture and lateral contributions accumulate.

Terrace and other water harvesting infrastructure maps are very useful for determining optimal locations for the implementation of water harvesting structures. There is a clear positive impact of some terraces construction on water yields as simulated by the SWAT model, as shown in Figure 32. It is important to note that part of the Al Mawaset District lies outside the Tuban Basin boundary, and terrace mapping was not completed for these outer areas. This highlights the importance of mapping existing water harvesting structures for integration into hydrological models.

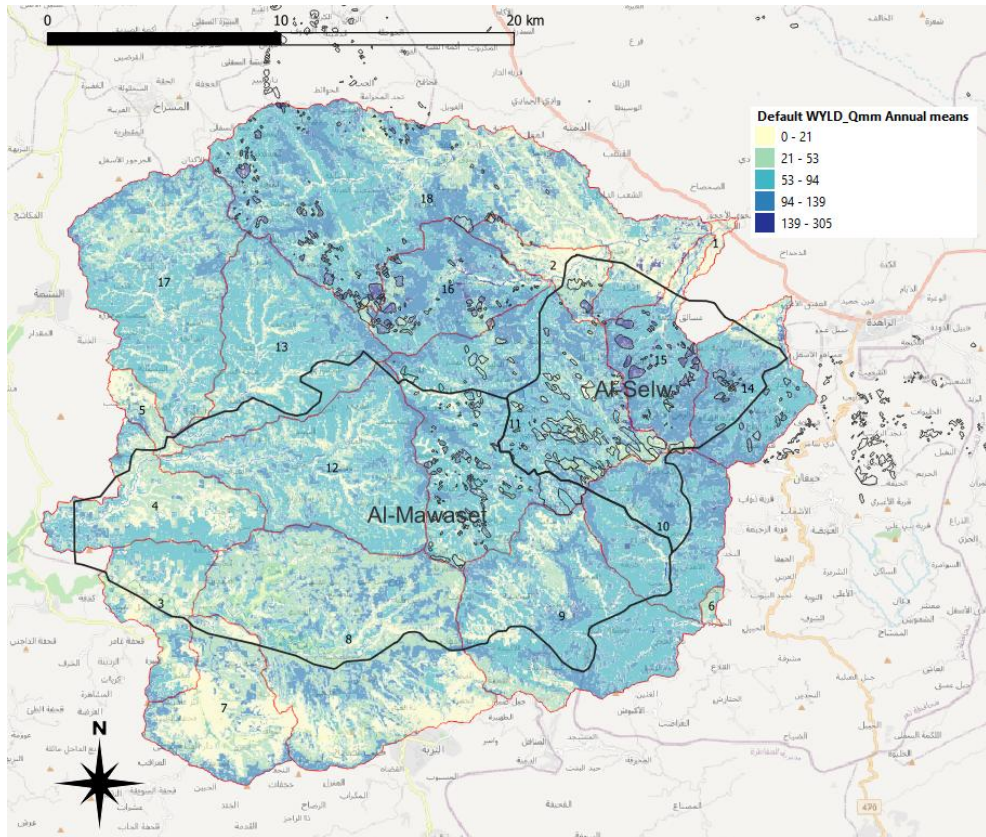


Figure 32. Average annual water yield distribution over the Al Selw / Al Mawaset Districts (black lines) as simulated by SWAT for the period 1999 - 2018. Terrace areas indicated by thin black lines.

### Runoff generation

SWAT provides estimates of surface runoff based on soil, land use and slope characteristics. The surface runoff is shown in Figure 33 and is limited remaining mostly below  $45 \text{ mm a}^{-1}$  in both districts. The eastern part of the Al Mawaset District had low surface runoff rates, mostly below  $12 \text{ mm a}^{-1}$  and most precipitation would therefore be infiltrating into the soil and subsequently evaporate. Subbasins 9, 11 and 12 in Al Mawaset and 11, 13 and 14 in Al Selw do have landscape features that cause surface runoff (Figure 33) with higher runoff in the valley areas in subbasin 12. The impact of terrace agriculture on reduction of surface runoff is also illustrated as terraced areas have lower surface runoff (and erosion) than the surrounding landscape.

The precipitation input is uniform and soil and land use therefore determine the generation of wadi flow. Most river flow is generated in subbasins 11 and 18, with main reaches along the border of the Al Selw District.

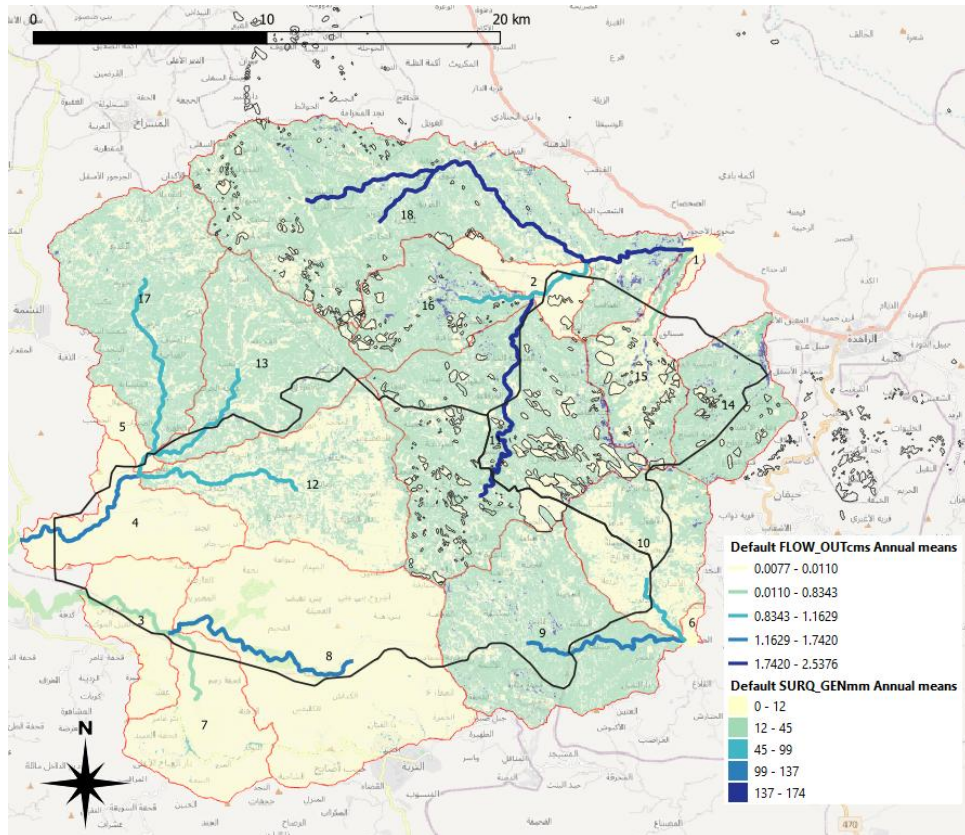


Figure 33. Average annual surface runoff generation and river runoff for the Al Selw / Al Mawaset Districts (black lines) as simulated by SWAT for the period 1999 - 2018. Thin black lined polygons represent terraced areas.

#### Groundwater recharge

Recharge is controlled by precipitation, land cover, and soil permeability. Groundwater recharge occurs in the HRUs, as well as through transmission losses in the river channels. The former HRU groundwater recharges are displayed Figure 34. The simulated recharge also includes short-term groundwater that may serve as a source for evaporation and for baseflow contributions towards rivers. The deep aquifer recharge contributing to regional flow is therefore often much lower.

As precipitation input is rather uniform in the Al Selw / Al Mawaset districts, the observed recharge pattern is caused by variations in the landscape rather than by precipitation. Recharge seems to be highest along subbasin boundaries (the higher parts in the landscape.) Recharge is generally low and ranges from close to zero to a high maximum of  $156 \text{ mm a}^{-1}$ . Moderate recharge also occurs in valleys as illustrated by the dendritic patterns in subbasins 12 and 13 (Figure 34).

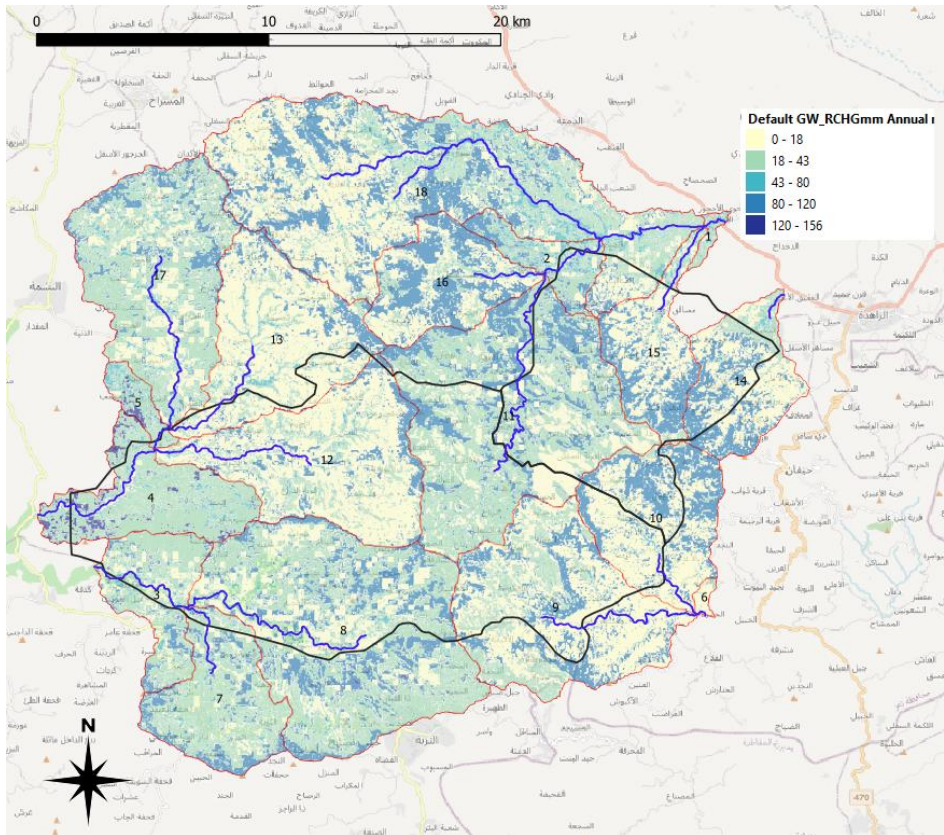


Figure 34. Average annual groundwater recharge in the Al Selw / Al Mawaset Districts (black lines) as simulated by SWAT for the period 1999 - 2018. Recharge is into the shallow and deep aquifers. The shallow aquifer recharge can contribute to evapotranspiration and baseflow.

## Al Mosaymer model

### Water balance overviews

Al Mosaymer hydrological model provides insight into the water balance and spatial hydrological variability in this mid-catchment district of the Tuban Basin. The annual water balance schematic in Figure 35 summarizes the key hydrological components simulated over the period 1999–2018. Rainfall in the district averages about  $166 \text{ mm a}^{-1}$ , of which the majority ( $158 \text{ mm a}^{-1}$ ) is lost through actual evapotranspiration (ET). The remaining water contributes to surface runoff ( $4.8 \text{ mm a}^{-1}$ ), lateral flow ( $8.4 \text{ mm a}^{-1}$ ), and a total water yield of  $11.1 \text{ mm a}^{-1}$ . Recharge to deep groundwater is very limited, at just  $4 \text{ mm a}^{-1}$ , and sediment yield is low, about  $0.5 \text{ t ha a}^{-1}$ , due to low rainfall and relatively stable land cover.

Table 12 shows the monthly average water balance components over the simulation period. The highest rainfall months are April to August, which correspond to the highest surface runoff and water yield. Even during these months, runoff remains low (monthly max  $\sim 1.5 \text{ mm}$ ) due to limited rainfall intensity and high infiltration. ET is highest between March and August, peaking around  $27 \text{ mm mo}^{-1}$  in July. Potential evapotranspiration (PET) remains high year-round ( $\sim 130\text{--}150 \text{ mm mo}^{-1}$ ), which indicates strong evaporative demand compared to the available rainfall. This imbalance results in water stress conditions for most land cover types. Sediment yields are negligible across all months, further confirming limited surface erosion.

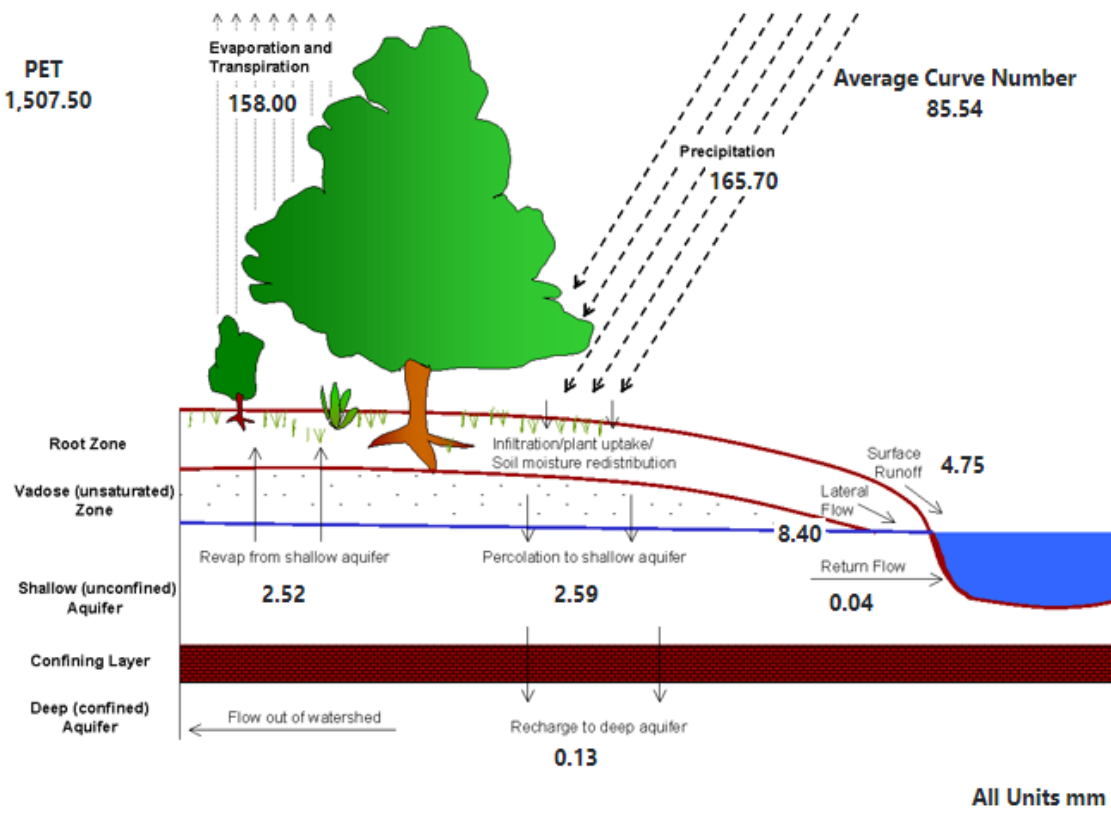


Figure 35. Annual average water balance schematic for the Al Mosaymer district model over the period 1999-2018.

Table 12. Monthly overview of water balance components for the Al Mosaymer catchment for the period 1999-2018.

Mon	Rainfall [mm]	SURF Q [mm]	LAT Q [mm]	Water Yield[mm]	ET [mm]	Sed.yield [t ha <sup>-1</sup> ]	PET [mm]
<b>1</b>	3.3	0.0	0.1	0.2	4.5	0.0	94.3
<b>2</b>	7.2	0.1	0.3	0.3	6.3	0.0	104.9
<b>3</b>	14.8	0.1	0.6	0.7	13.3	0.0	142.5
<b>4</b>	23.5	0.3	1.0	1.1	20.7	0.0	152.3
<b>5</b>	5.7	0.1	0.4	0.5	10.4	0.0	141.5
<b>6</b>	29.9	0.9	1.1	1.5	17.0	0.1	131.2
<b>7</b>	39.1	1.5	2.0	2.8	27.6	0.2	151.8
<b>8</b>	28.7	1.5	1.8	2.7	24.1	0.1	132.7
<b>9</b>	8.4	0.2	0.7	0.9	14.7	0.0	113.7
<b>10</b>	2.1	0.0	0.2	0.3	9.5	0.0	128.4
<b>11</b>	2.4	0.0	0.1	0.2	6.1	0.0	114.9
<b>12</b>	0.5	0.0	0.1	0.1	3.9	0.0	98.4
<b>Annual</b>	165.7	4.8	8.4	11.1	158.0	0.5	1506.5

Table 13 presents the SWAT-simulated hydrological outputs per land use type. Orchards (ORCD) and onion fields (ONIO) show high evapotranspiration rates (960 mm and 308 mm/year) and receive significant irrigation (808 mm a<sup>-1</sup> and 133 mm a<sup>-1</sup>, respectively),

which sustains productivity despite low rainfall. Bare land (BARR) has the highest surface runoff ( $9.3 \text{ mm a}^{-1}$ ) and sediment yield, though still low ( $\sim 0.9 \text{ t ha a}^{-1}$ ). Rainfed agriculture and natural vegetation (e.g., DWHT, SHRB, RNGB) have low water yields and minimal runoff, with most rainfall lost to ET. Crop yield and biomass are notably higher for irrigated crops (e.g., ONIO:  $3.7 \text{ t ha}^{-1}$ ) compared to rainfed land uses. These results highlight the dependence of agricultural productivity on irrigation in this low-rainfall environment and the relatively low erosion risk under current land use. Few terraces were mapped in the district in the northwestern part in subbasins 5 and 13 (Figure 39).

Table 13. Overview of simulated outputs of SWAT for the Al Mosaymer district catchment over the period 1999-2018 for each land use (LULC). CN is the curve number, BIOM is the biomass of the vegetation, whereas YLD is the crop yield.

LULC	AREA [ha]	CN	IRR [mm]	PREC [mm]	SURQ [mm]	GWQ [mm]	ET [mm]	SED [t ha $^{-1}$ ]	BIOM [t ha $^{-1}$ ]	YLD [t ha $^{-1}$ ]
<b>BARR</b>	595.0	91.8	0.0	157.9	9.3	6.6	143.2	0.9	0.0	0.0
<b>BERM</b>	0.2	85.9	0.0	143.3	13.7	2.4	128.1	0.7	1.5	1.1
<b>DWHT</b>	21.4	83.6	0.0	177.6	0.3	1.2	176.7	0.0	1.0	0.2
<b>ONIO</b>	19.9	70.0	133.3	176.9	0.0	2.7	307.7	0.0	8.9	3.7
<b>ORCD</b>	4.0	66.7	808.3	165.4	0.0	14.0	959.9	0.0	14.3	0.0
<b>RNGB</b>	149.4	79.7	0.0	185.7	0.2	13.2	170.6	0.2	0.3	0.2
<b>SHRB</b>	390.3	79.3	0.0	168.9	0.1	10.2	158.9	0.0	0.5	0.4
<b>WATR</b>	0.0	90.0	0.0	155.3	0.0	0.0	1647.4	0.0	0.0	0.0

#### Precipitation and evapotranspiration patterns

As shown in Figure 36, average annual precipitation in Al Mosaymer varies spatially, ranging from approximately  $200 \text{ mm a}^{-1}$  in the northeast (sub-basin 15) to below  $150 \text{ mm a}^{-1}$  in the southern parts of the district. This spatial variability influences hydrological processes such as runoff and recharge. Figure 37 presents the distribution of actual ET, which is highest in cultivated and irrigated areas and lowest in barren or sparsely vegetated zones. ET patterns closely follow the rainfall gradient and land use.

Monthly water balance data time series are shown in Figure 38 for subbasin 3, located in the center of the district, and for reach 18, which drains most of the area. Precipitation remains low peaking at about  $50 \text{ mm}$  in the wet months and actual ET remains below  $50 \text{ mm mo}^{-1}$ . Surface runoff in the area is very low and only occurs sporadically when precipitation peaks. The average monthly outflow from subbasin/reach 18 remains below  $0.3 \text{ m}^3 \text{ s}^{-1}$ .

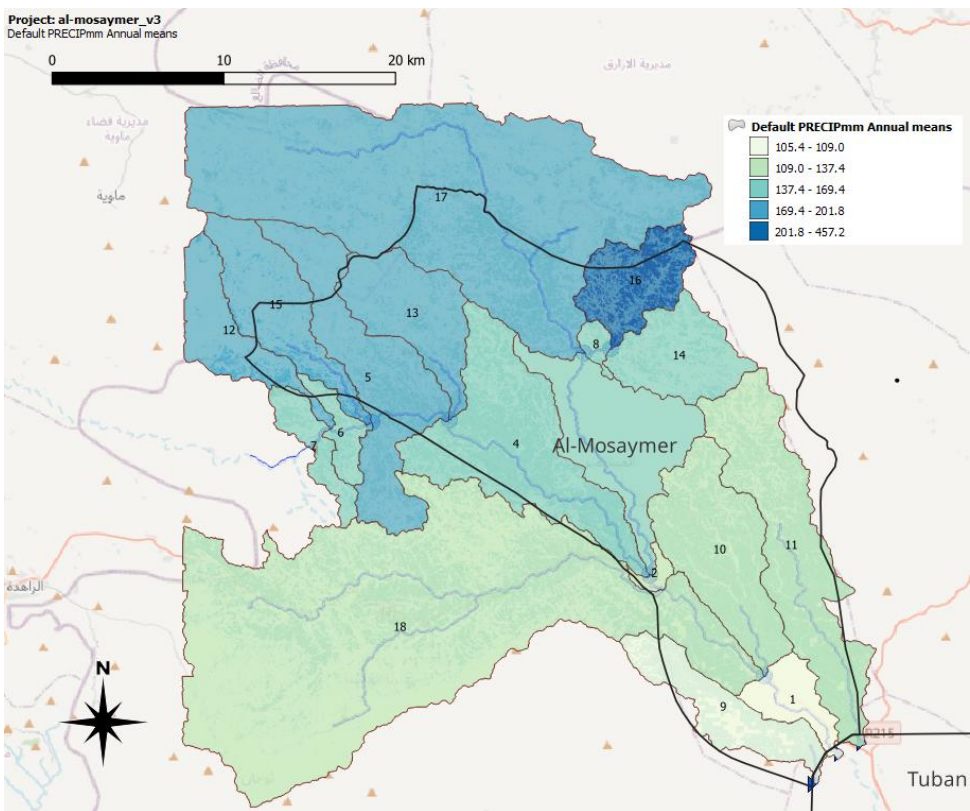


Figure 36. Average annual precipitation distribution over the Al Mosaymer District (black line) for the period 1999 - 2018.

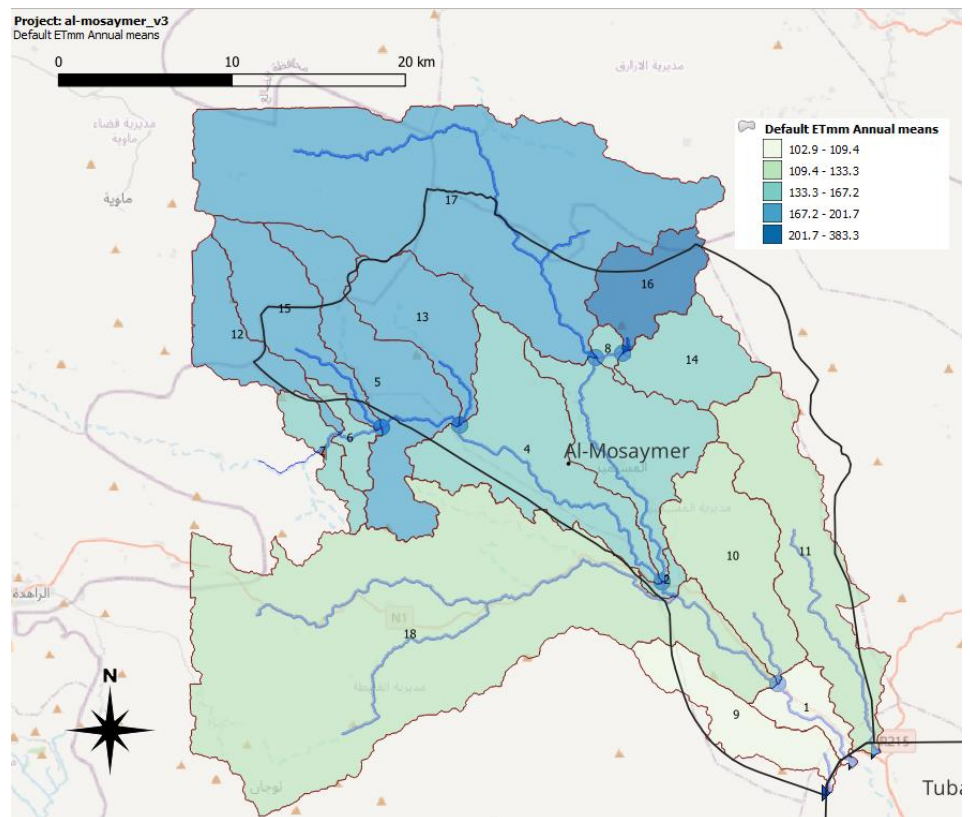


Figure 37. Average annual actual evapotranspiration distribution over the Al Mosaymer District (black line) as simulated by SWAT for the period 1999 - 2018.

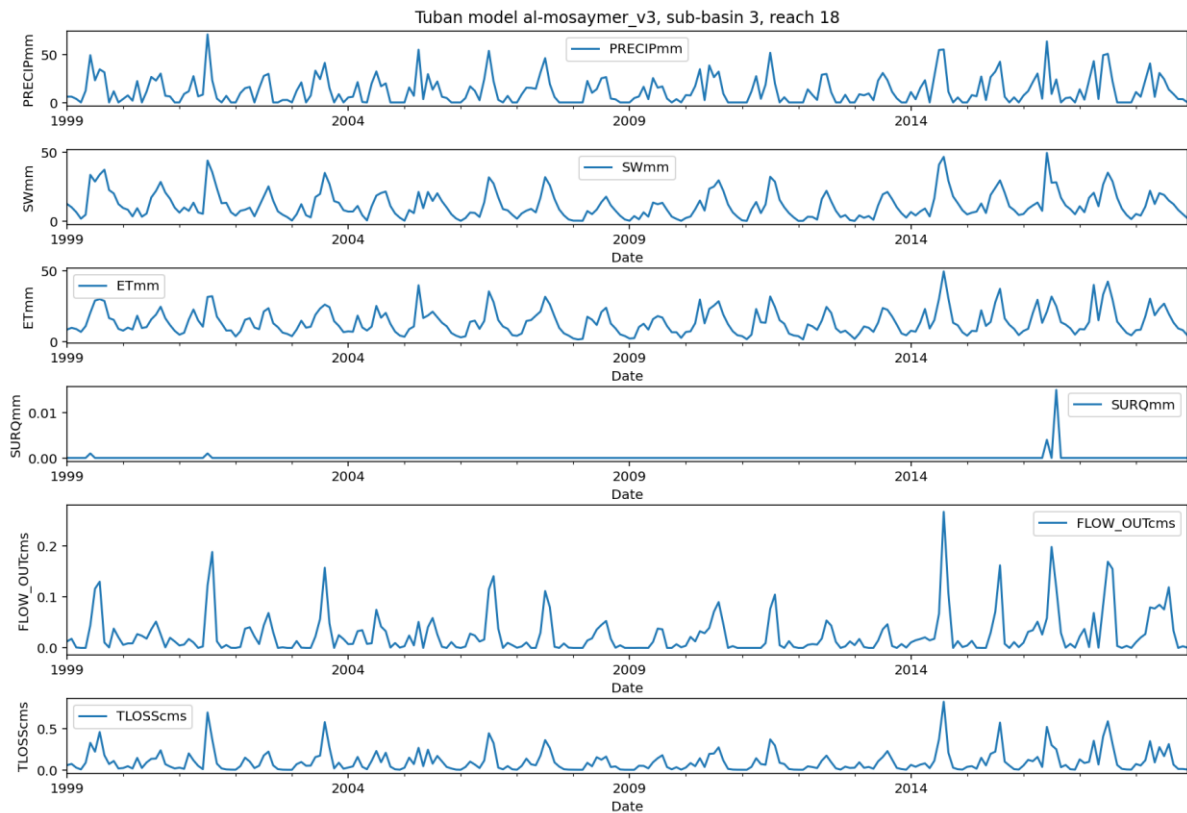


Figure 38. Monthly variation in precipitation (Precip [mm]), soil water content (SW [mm]), actual evapotranspiration (ET [mm]) and surface runoff (SURQ [mm]) for subbasin 11, and wadi outflow FLOW\_OUT [ $\text{m}^3 \text{s}^{-1}$ ] and wadi bed infiltration (TLOSS [ $\text{m}^3 \text{s}^{-1}$ ]) for reach 18 over the period 1999-2108.

### Water yield

Figure 39 displays the spatial distribution of water yield, which is the portion of water that contributes to streamflow after ET and losses. The highest water yields are seen in the northern part of the district and especially in Subbasin 15, corresponding to higher rainfall and more favourable land conditions. Most other areas show very limited yield, underlining the overall dryness of the district. Figure 39 illustrates the impact of terraces on water yield. Terraced zones demonstrate notably higher water yields due to improved soil moisture retention and reduced surface runoff, confirming the benefit of these traditional land management practices for increasing local water availability (Figure 40).

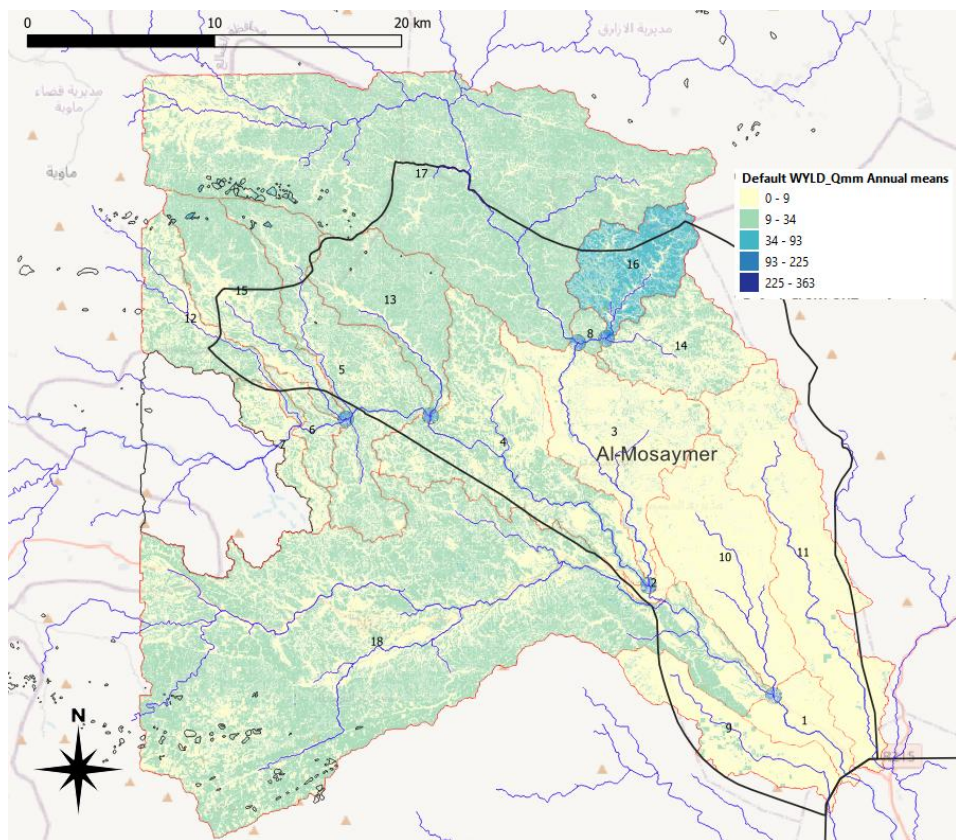


Figure 39. Average annual water yield distribution over the Al Mosaymer District (black line) as simulated by SWAT for the period 1999 - 2018.

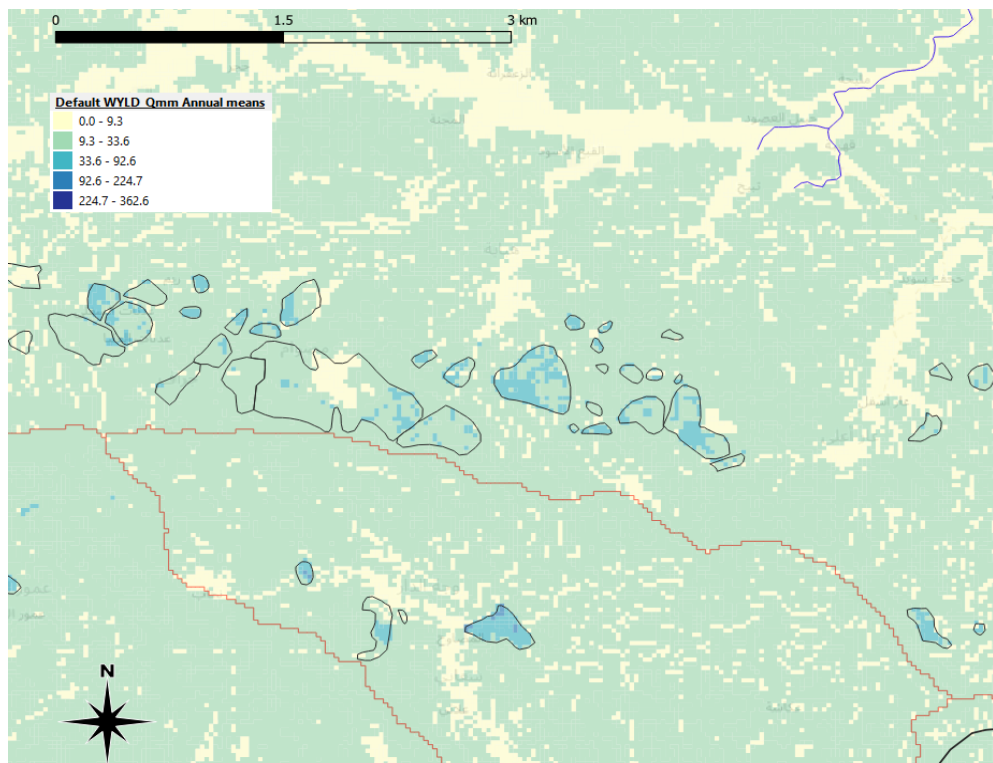


Figure 40. Impact of terraces (black-lined polygons) on the water yield in the north of the Al Mosaymer District region. Higher water yields are observed where terrace agriculture is being practiced due to soil infiltration and depth amelioration.

## Runoff generation

Al Mosaymer district shows a higher variation in surface runoff, most likely due to the larger variation in precipitation in that district. Subbasin 15 again shows the highest values (Figure 41), but even there, runoff peaks at less than  $9 \text{ mm mo}^{-1}$ , indicating the limited generation of overland flow under current conditions. This map may help identify areas suitable for water harvesting interventions, particularly where localized runoff accumulates. Average monthly runoff generation is unimodal with the peak in August (Figure 41), but discharge is low at about  $0.1 \text{ m}^3 \text{ s}^{-1}$ .

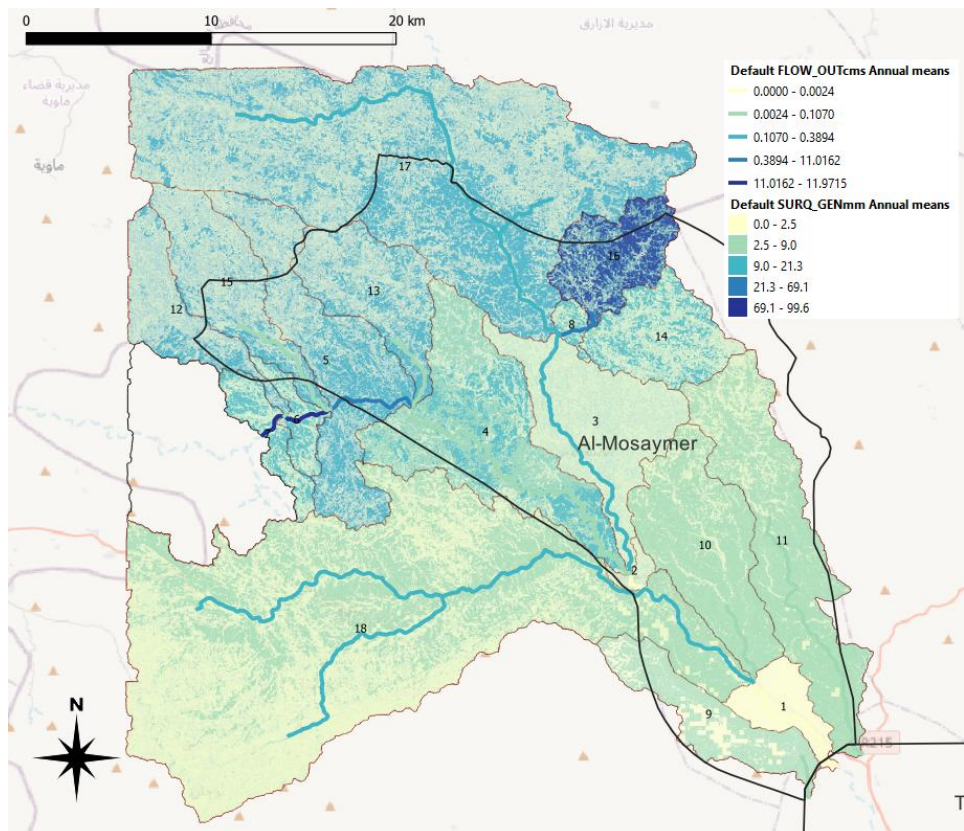


Figure 41. Average annual surface runoff generation and river runoff for the Al Mosaymer District (black line) as simulated by SWAT for the period 1999 - 2018.

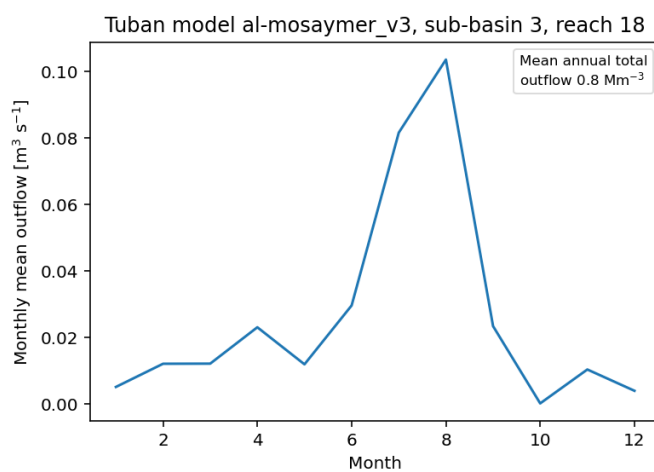


Figure 42. Average monthly outflow and total annual outflow of reach 18 in the Al Mosaymer region over the period 1999-2018.

## Groundwater recharge

Recharge is controlled by precipitation, land cover, and soil permeability. Groundwater recharge occurs in the HRUs, as well as through transmission losses in the river channels. The former HRU average annual groundwater recharges are displayed in Figure 43. The simulated recharge also includes short-term groundwater that may serve as baseflow contribution towards rivers and the deep aquifer recharge is therefore often much lower.

In Al Mosaymer district, groundwater recharge is generally modest and in most of the area below 0.4 mm a<sup>-1</sup> (Figure 43) but follows a similar pattern to runoff and water yield—higher in the wetter sub-basin 15, and very limited in the drier areas, reflecting limited infiltration due to low precipitation and high ET.

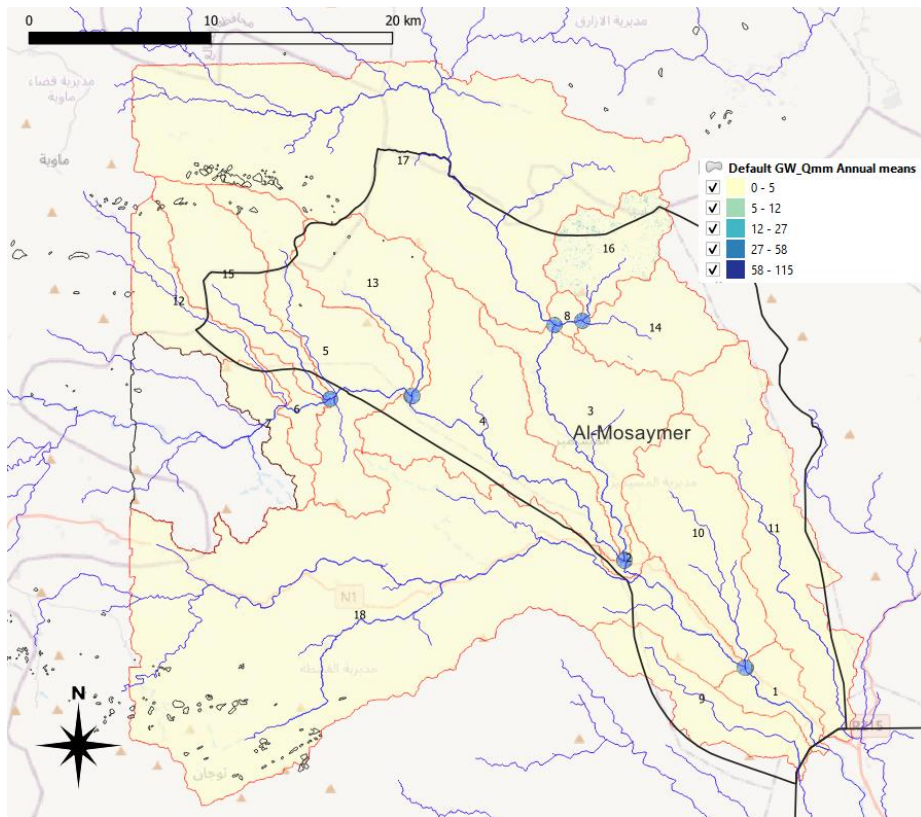


Figure 43. Average annual groundwater recharge over the Al Mosaymer District (black line) as simulated by SWAT for the period 1999 - 2018.

## Tuban District Model

### Water balance overviews

Tuban District model represents the hydrological behavior of the most downstream part of the Tuban Basin, including the delta region. This area is characterized by very low rainfall, high evapotranspiration, and a limited water balance. The model simulations cover the period 1999–2018 and provide a detailed look into monthly and annual water flows, land use responses, and recharge patterns. The annual water balance schematic is shown in Figure 44, summarizing the average hydrological components for the district. Rainfall is extremely low, averaging only 51.6 mm a<sup>-1</sup>. Almost all precipitation is lost to actual evapotranspiration (55.9 mm a<sup>-1</sup>), with very little runoff or lateral flow. The model estimates surface runoff at 0.5 mm a<sup>-1</sup>, and lateral flow 0.7 mm a<sup>-1</sup> at the lowest of all districts.

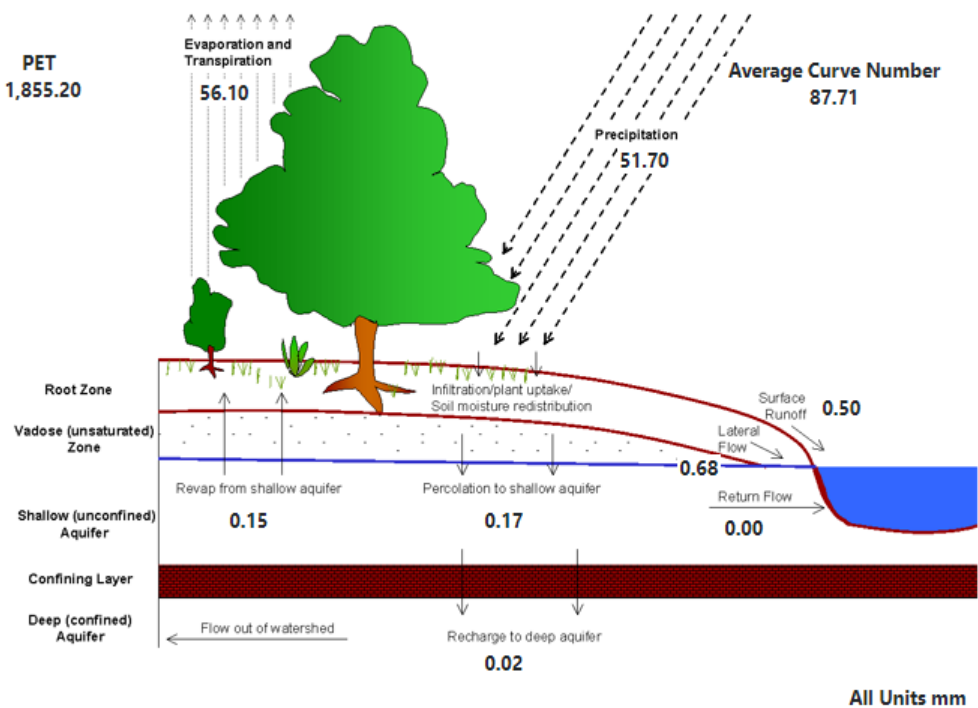


Figure 44. Annual average water balance schematic for the Tuban District model over the period 1999-2018, wadi flow 70/30%.

Table 14 presents the monthly average water balance for the Tuban District. Rainfall is minimal throughout the year, with slightly higher values in July and August (11.5 mm and 10.0 mm), corresponding to the minor peaks in water yield (max 0.42 mm in August). ET remains high year-round, ranging from 3 to 9 mm  $\text{mo}^{-1}$ , despite limited precipitation. Potential evapotranspiration (PET) values are consistently high (up to 187 mm  $\text{mo}^{-1}$  in April), indicating strong evaporative demand. As with the annual summary, sediment yields remain negligible throughout the year.

Table 14. Monthly overview of water balance components for the Tuban District catchment for the period 1999-2018.

Mon	Rainfall [mm]	SURF Q [mm]	LAT Q [mm]	Water Yield [mm]	ET [mm]	Sed.yield [t $\text{ha}^{-1}$ ]	PET [mm]
<b>1</b>	3.87	0.00	0.04	0.04	3.12	0.00	119.47
<b>2</b>	2.88	0.00	0.04	0.04	3.11	0.00	123.84
<b>3</b>	3.43	0.00	0.04	0.04	4.08	0.00	169.93
<b>4</b>	4.98	0.01	0.05	0.05	5.70	0.00	186.89
<b>5</b>	0.63	0.00	0.02	0.02	2.16	0.00	175.31
<b>6</b>	5.91	0.03	0.06	0.07	4.05	0.00	159.18
<b>7</b>	11.49	0.09	0.14	0.19	8.56	0.00	173.98
<b>8</b>	9.99	0.35	0.16	0.42	9.36	0.00	166.47
<b>9</b>	3.57	0.02	0.07	0.08	7.03	0.00	147.78
<b>10</b>	0.84	0.00	0.02	0.03	3.64	0.00	160.94
<b>11</b>	3.37	0.00	0.03	0.04	3.39	0.00	145.87
<b>12</b>	0.68	0.00	0.01	0.02	1.71	0.00	124.44
<b>Annual</b>	51.6	0.5	0.7	1.0	55.9	0.0	1854

Table 15 provides simulated SWAT outputs by land use (LULC). Bare land (BARR) covers the largest area and contributes the most to total runoff, although values are still low. Orchards (ORCD) and onions (ONIO) receive significant irrigation (1043 mm a<sup>-1</sup> and 238 mm a<sup>-1</sup>, respectively), resulting in high ET rates far exceeding local precipitation. For example, orchards show ET of 1093 mm a<sup>-1</sup>, clearly sustained by irrigation. Crop yields are only meaningful for irrigated crops, with onions reaching 3.8 t ha a<sup>-1</sup>, while rainfed crops and natural vegetation contribute little to yield or biomass. Runoff and sediment production are negligible across all land use types, reinforcing the conclusion that this is a very dry, evaporation-dominated system.

Table 15. Overview of simulated outputs of SWAT for the Tuban District catchment in the delta over the period 1999-2018 for each land use (LULC). CN is the curve number, BIOM is the biomass of the vegetation, whereas YLD is the crop yield.

LULC	AREA [ha]	CN	IRR [mm]	PREC [mm]	SURQ [mm]	GWQ [mm]	ET [mm]	SED [t ha <sup>-1</sup> ]	BIOM [t ha <sup>-1</sup> ]	YLD [t ha <sup>-1</sup> ]
<b>BARR</b>	2123.6	88.8	0.0	51.9	0.5	0.7	50.8	0.0	0.0	0.0
<b>BERM</b>	11.0	74.7	0.0	39.7	3.6	0.2	35.9	0.1	0.1	0.0
<b>DWHT</b>	57.1	74.7	0.0	45.1	0.0	0.1	45.0	0.0	0.0	0.0
<b>ONIO</b>	44.8	70.0	238.3	46.9	0.0	0.6	284.6	0.0	8.8	3.8
<b>ORCD</b>	1.2	70.0	1042.7	53.8	0.0	3.7	1092.8	0.0	11.5	0.0
<b>RNGB</b>	1.1	67.5	0.0	47.9	0.0	0.6	47.4	0.0	0.0	0.0
<b>SHRB</b>	29.9	73.7	0.0	64.0	0.0	1.1	63.0	0.0	0.1	0.1
<b>WATR</b>	0.0	89.8	0.0	66.8	0.0	0.0	1603.2	0.0	0.0	0.0

#### Precipitation and evapotranspiration patterns

In Tuban District, annual rainfall is very low overall, but it does show spatial variation. Precipitation ranges from less than 100 mm a<sup>-1</sup> in the northern upland parts of the district to under 30 mm a<sup>-1</sup> along the coastal areas (Figure 45). The central and eastern areas tend to receive slightly more rainfall than the coastal zones, though still much less than the upstream highland catchments.

This gradient is clearly visible within the black boundary line on the map, and it helps explain the limited runoff and groundwater recharge potential in the delta. Actual evapotranspiration (ET) is highest in areas with slightly more rainfall and vegetation mostly in the central parts of the district. However, high potential evapotranspiration (PET) across the entire region means that much of the rainfall is quickly lost to the atmosphere. These spatial patterns help identify areas where interventions such as drip irrigation could be effective in reducing water loss and improving water use efficiency.

Subbasin annual evaporation rates are strongly influenced by the annual precipitation, as well as by the irrigation of crops in the case of the Tuban district. Figure 46 shows the spatial distribution of actual evapotranspiration (ET). ET is highest where there is more vegetation and irrigation (central areas and along the wadi channel). In some subbasins (e.g., Subbasin 8, 13 and 15), ET even exceeds local rainfall, highlighting the impact of irrigation. These areas experience elevated water losses and could benefit from water-saving practices such as mulching or drip irrigation.

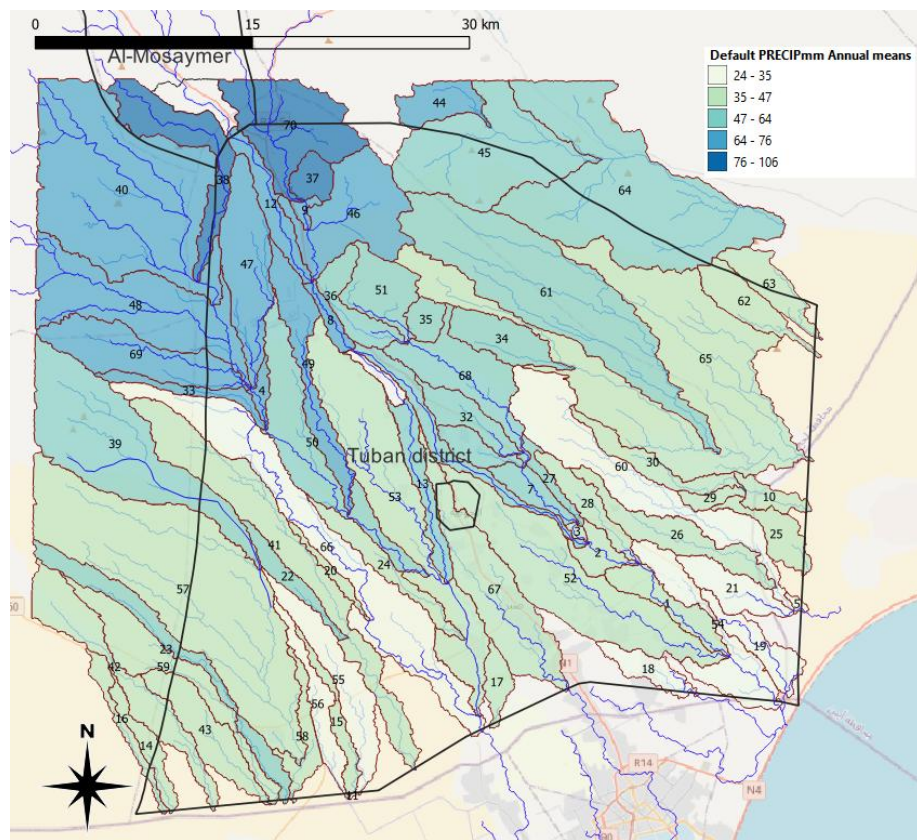


Figure 45. Average annual precipitation distribution over the Tuban District (black line) for the period 1999 - 2018.

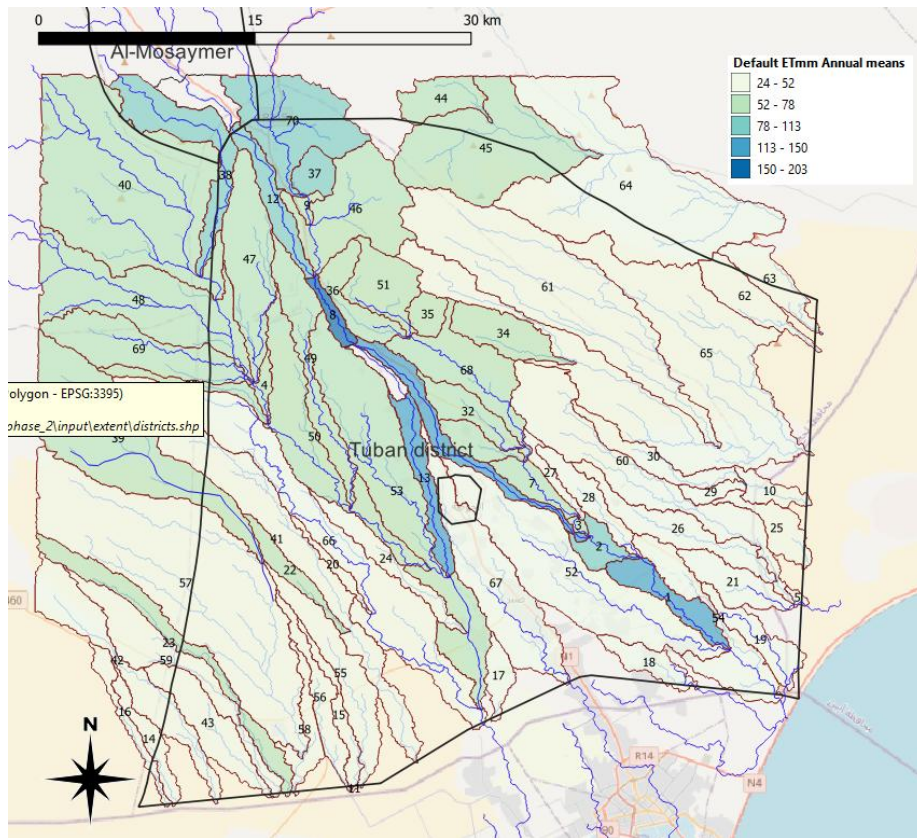


Figure 46. Average annual actual evapotranspiration distribution over the Tuban District (black line) as simulated by SWAT for the period 1999 - 2018.

Time series of the water balance components for the centrally located subbasin 6 in the Tuban District are shown in Figure 47. Monthly average precipitation is usually less than 20 mm and is similar to the actual evapotranspiration. The irrigated areas are relatively small and do not cause a higher ET than rainfall on this subbasin scale. The flow out of this basin is derived from the upstream Tuban Basin and shows a monthly maximum average of about  $40 \text{ m}^3 \text{s}^{-1}$  in 2003 and 2010, but usually peaks at about  $20 \text{ m}^3 \text{s}^{-1}$ . Bed infiltration with current infiltration value of 5 mm h is at maximum  $2 \text{ m}^3 \text{s}^{-1}$ .

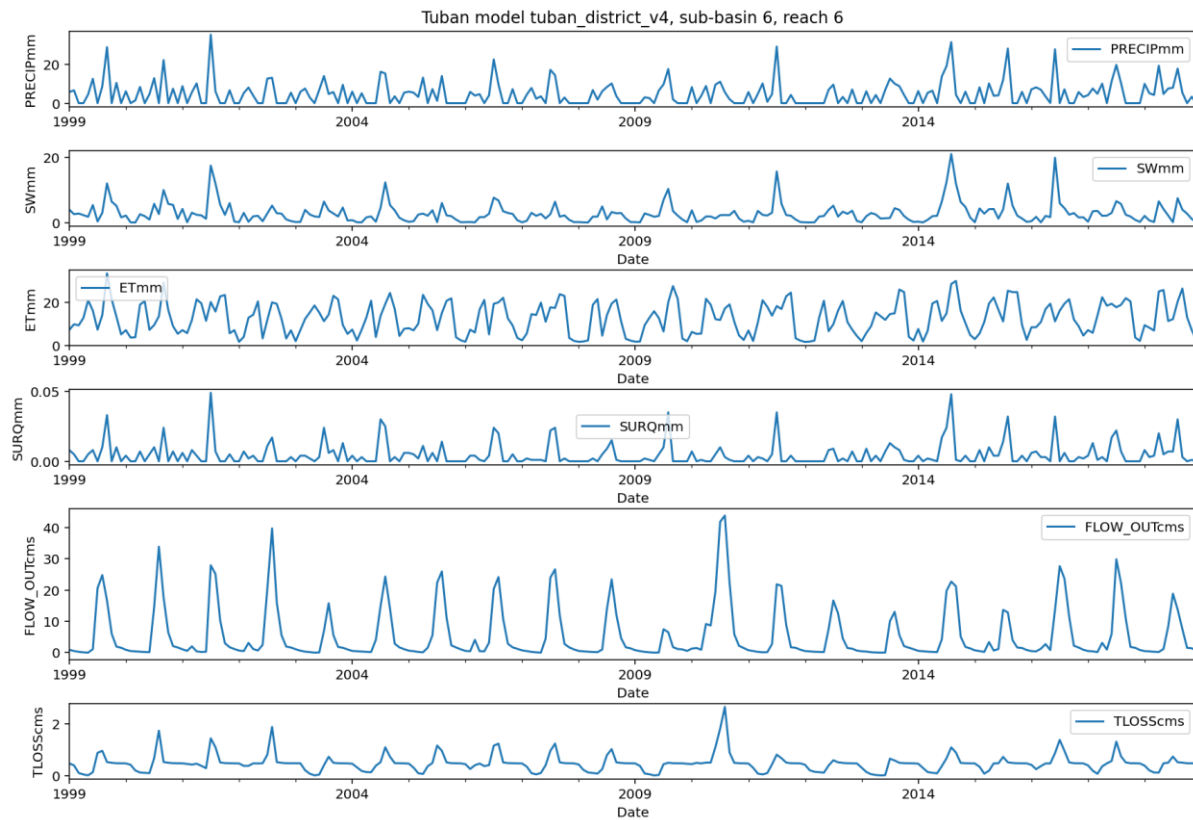


Figure 47. Monthly variation in precipitation (Precip [mm]), soil water content (SW [mm]), actual evapotranspiration (ET [mm]) and surface runoff (SURQ [mm]) for subbasin 6, and wadi outflow FLOW\_OUT [ $\text{m}^3 \text{s}^{-1}$ ] and wadi bed infiltration (TLOSS [ $\text{m}^3 \text{s}^{-1}$ ]) for reach 6 over the period 1999-2108.

### Water yield

The water yield, defined as the net amount of water that leaves the subbasin and contributes to streamflow in the reach provides an indication of the availability of water accounting for losses by ET. Figure 48 displays the spatial variation in water yield across the district. As expected, most of the district shows near-zero yields, except for a few irrigated areas along the main wadi (Figure 49). These results underline the extremely limited availability of surface water for downstream users, unless irrigation is externally sourced.

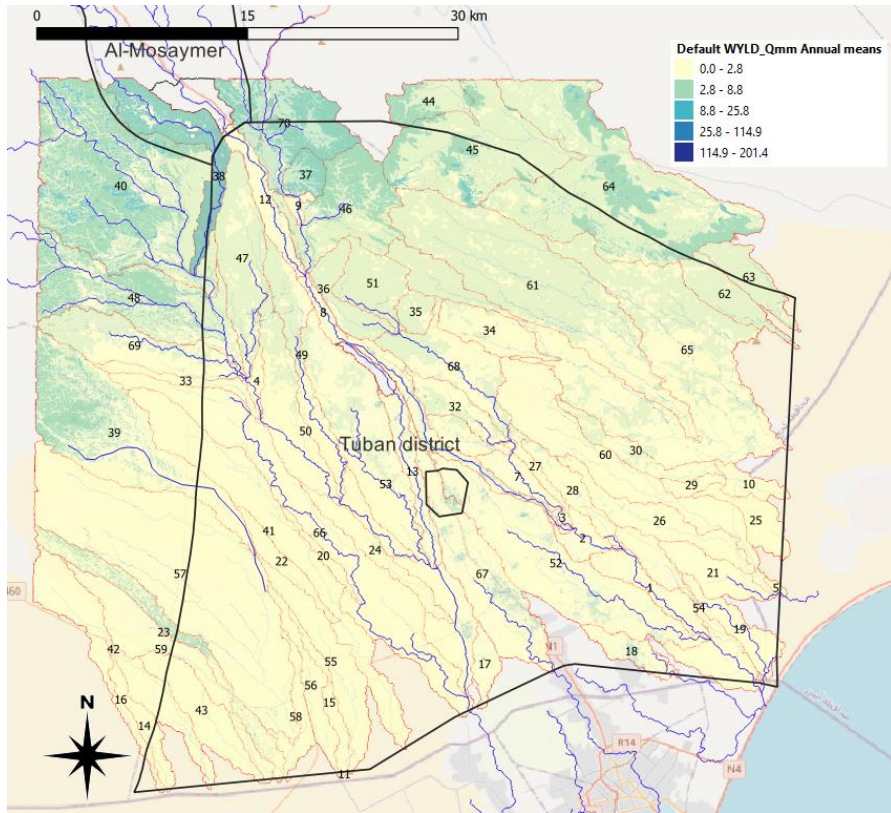


Figure 48. Average annual water yield distribution over the Tuban District (black line) as simulated by SWAT for the period 1999 - 2018.

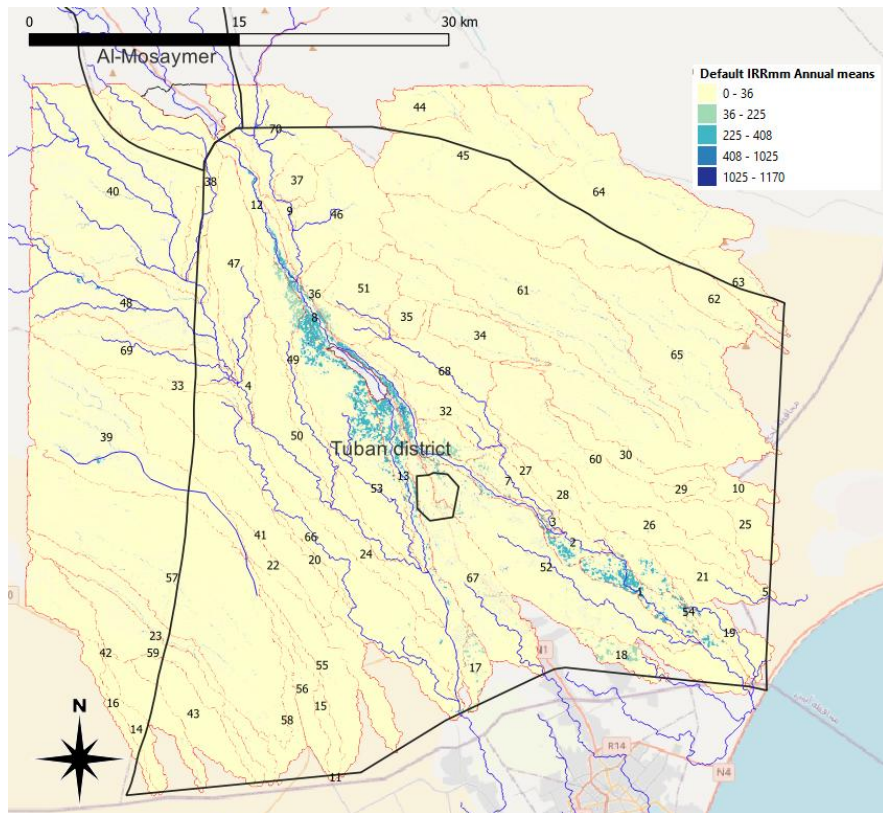


Figure 49. Average annual irrigation distribution over the Tuban District (black line) as simulated by SWAT for the period 1999 - 2018.

## Runoff generation

Surface runoff is negligible in the Tuban district with values well below  $1 \text{ mm mo}^{-1}$  on average (Figure 50), even in wetter areas. Despite this, the spatial pattern can help identify zones where local water harvesting interventions might be considered to capture scarce runoff. Wadi runoff is shown in Figure 51 and is unimodal with a peak of about  $20 \text{ m s}^{-1}$  in July and August.

In terms of streamflow, SWAT estimates FLOW\_OUT, which represents the water volume flowing out of each subbasin reach (typically expressed in cubic meters per second, cms). In the case of Tuban delta, FLOW\_OUT values are minimal, often less than 0.01 cms, especially in the delta region. This confirms that very little surface water is generated or passed downstream, and what does exist is likely dependent on localized runoff events or external irrigation return flows. Only a few subbasins, particularly those with slightly higher rainfall or near irrigated fields along the main wadi (dark blue line in Figure 50), show slightly elevated runoff and streamflow contributions, but these remain hydrologically insignificant for sustained flow.

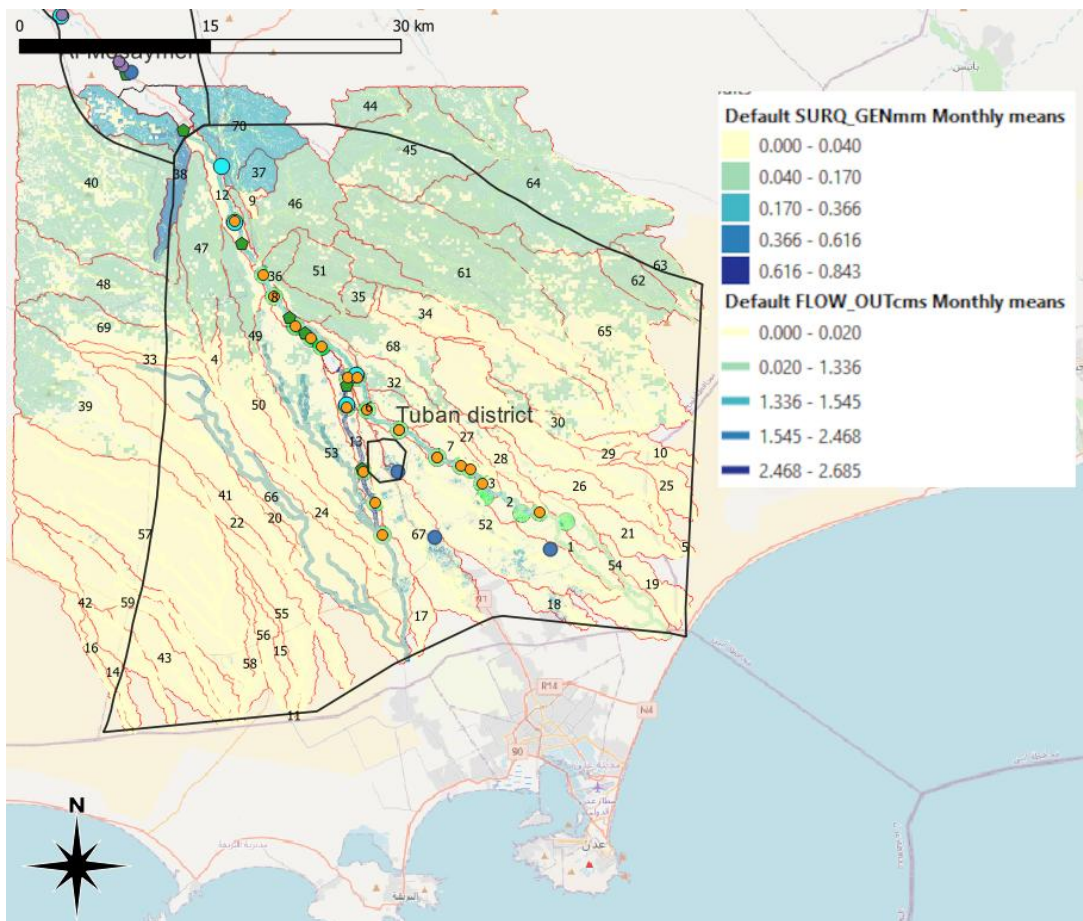


Figure 50. Average annual surface runoff generation over Tuban District (black line) as simulated by SWAT for the period 1999 - 2018. Main wadi diversion 70/30%.

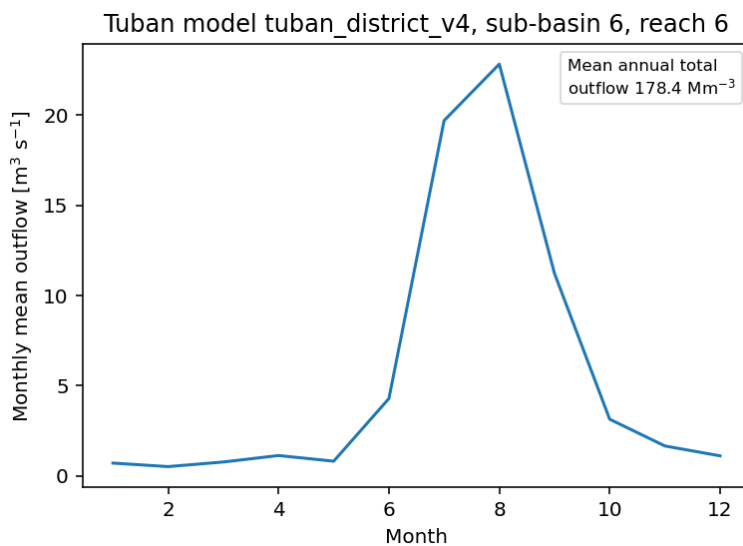


Figure 51. Average monthly outflow and total annual outflow of reach 6 in the Tuban District over the period 1999-2018.

#### Groundwater recharge

Recharge is controlled by precipitation, land cover, and soil permeability. Groundwater recharge occurs in the HRUs, as well as through transmission losses in the river channels. The former HRU groundwater recharges are displayed in Figure 52 . The simulated recharge also includes short-term groundwater that may serve as baseflow contribution towards rivers and the deep aquifer recharge is therefore often much lower.

Due to the low rainfall in the Tuban District no groundwater recharge was simulated (Figure 52). The model did not simulate significant recharge anywhere in the district due to the extremely low rainfall and high evaporative losses. While shallow recharge or transmission losses along the wadi channel may contribute to subsurface flows, these were not explicitly represented in this version of the SWAT model.

To address this limitation, an initial groundwater flow model was developed for the Tuban District and is described in more detail below. This involved the creation of a coupled SWAT-MODFLOW model using the QSWATMOD2 plugin for QGIS (Park et al., 2018). However, further model development will be needed to better represent wadi-aquifer interactions and improve understanding of groundwater availability in this low-rainfall environment.

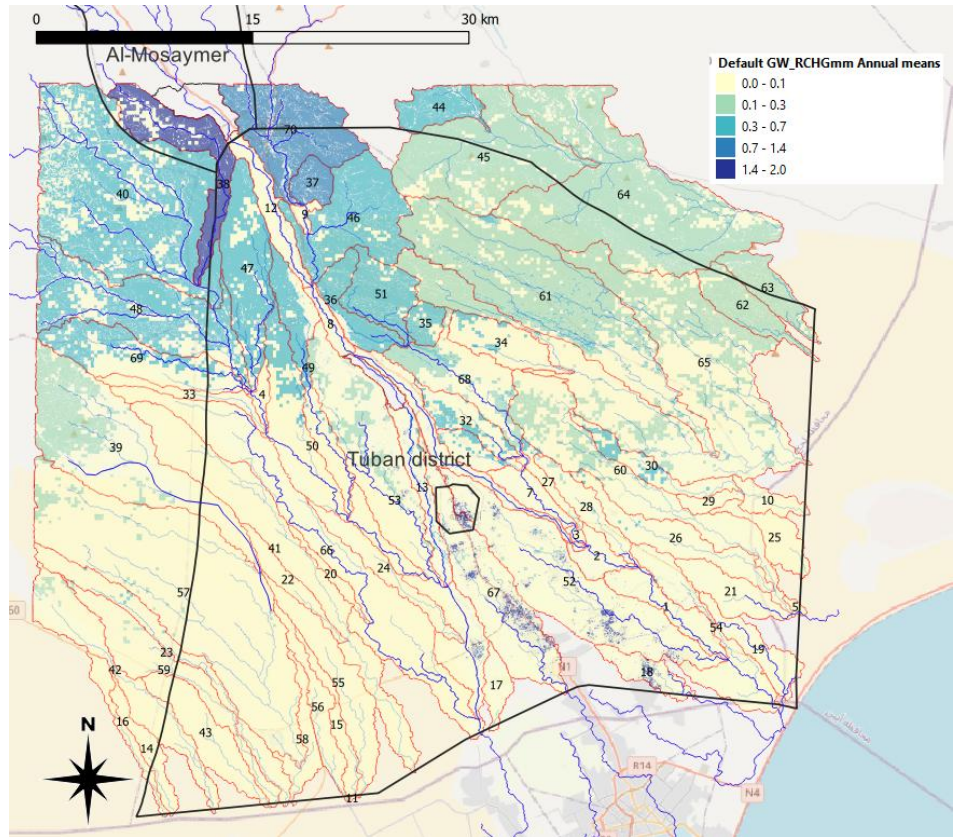


Figure 52. Average annual groundwater recharge over the Tuban District (black line) as simulated by SWAT for the period 1999 - 2018.

#### Groundwater flow model Tuban District

During the field reconnaissance mission in 2025 a selected number of boreholes were visited and groundwater level observations and EC analysis were done. The results of the water level and salinity measurements are given in Figure 53. The observations indicate negative hydraulic heads in the center of the Tuban district, indication freshwater groundwater flow occurring from the North towards the area, but also seawater intrusion from the coastal area in the South towards the center of the Tuban District. There is a large difference in groundwater heads between the upland boreholes and those in Tuban Delta. It is uncertain, however, if the upland area forms a source area for the Tuban Delta as geological and aquifer conditions are not well known. Some flow may occur along fractures that are buried below the sedimentary deposits, recharging the groundwater in the Delta.

The study of Al-Darwish (2023) in 2010 showed that there were slightly negative heads in the center of the Tuban District, but over the past 15 years the hydraulic head may have further dropped by  $1\text{-}2 \text{ m a}^{-1}$ , as already suggested by the comparison of water levels measured in May 2009 and 2010 (Al-Darwish, 2023). This clearly shows that the current recharge rates are well below the extraction rates required to irrigate crops in the Tuban Delta.

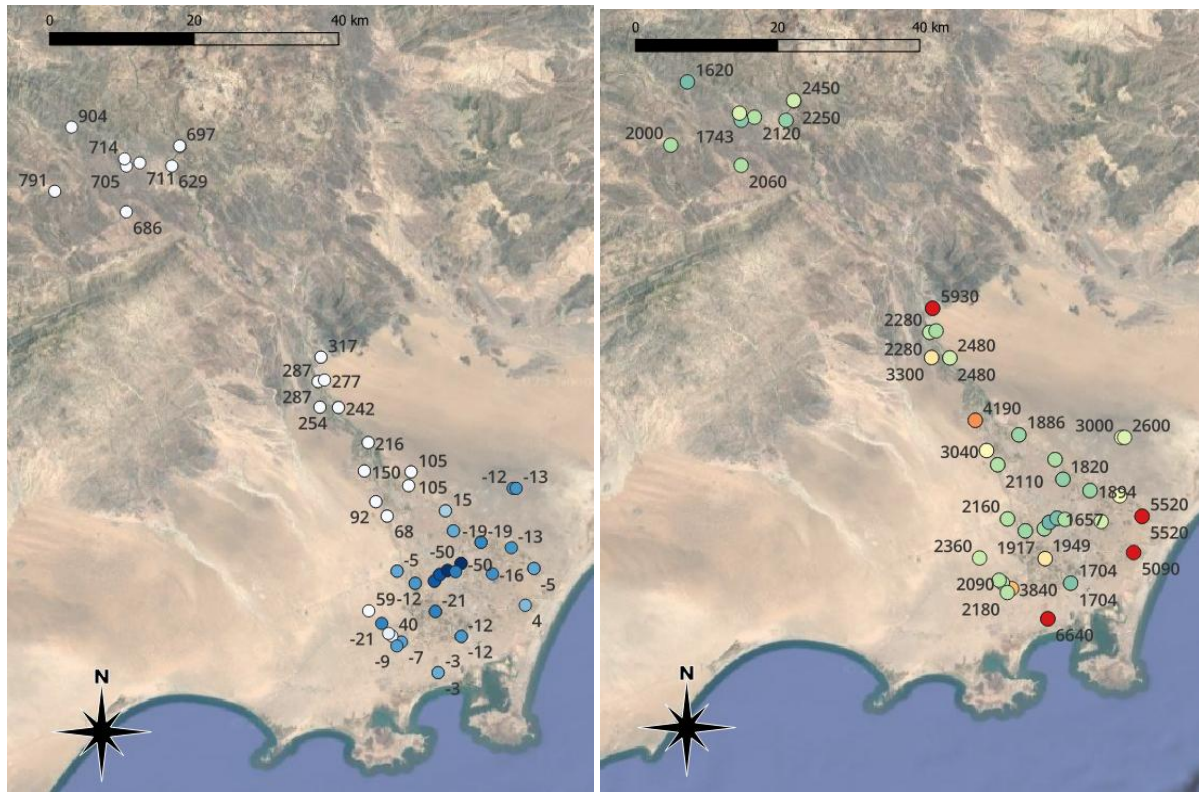


Figure 53. Phreatic hydraulic heads [m.a.s.l.] (left) and EC salinity [ $\mu\text{S cm}^{-1}$ ] (right) in boreholes measured during the UNDP reconnaissance mission in May 2025. The hydraulic heads are referenced to mean sea level. Blue dots indicate slightly positive (light blue) to strongly negative heads (dark blue), whereas white dots indicate heads well above mean sea level. The red dots indicate brackish water with high EC values, whereas blue dots represent freshwater.

The locations of wells/boreholes were mapped on the land use map to show the relation to well locations and crop land classified as irrigated. A detailed map is shown in Figure 54. Most wells do not have water level information, and those that were repeatedly measured between 2009 and 2010 suggest a decrease in level 1.5 m in that period. However, this could be part of the normal variation in groundwater levels due to difference in precipitation. A groundwater flow model would need more water level information for calibration and validation. For a detailed model in an area with active groundwater abstractions, a time-series of water level and pumping rates from at least 50 - 70 wells is likely necessary. Pumping rates should be available on a monthly or at least seasonal level to account for variability in abstractions. The model presently developed is a first attempt to couple surface and groundwater processes using a combination of SWAT and MODFLOW (Langevin et al., 2003; Park et al., 2019; Sisay et al., 2023).

In Tuban District, a coupled SWAT and MODFLOW model was created using the QSWATMOD2 plugin in QGIS (Park et al., 2018). This software allows the recharge to the deep aquifer from the SWAT model to be used as an input in the MODFLOW model. Outputs from the SWAT model such as HRUs, SUB and river areas were loaded into the QSWATMOD interface. QSWATMOD creates copies of these SWAT model input files. The model was initially set up in a simple manner, with the parameters set as constant values across the model domain. The parameters were estimated from the results of the Komex, 2002 MODFLOW model. When convergence issues were encountered, some variables were left as default values, which produced better results (Table 16).

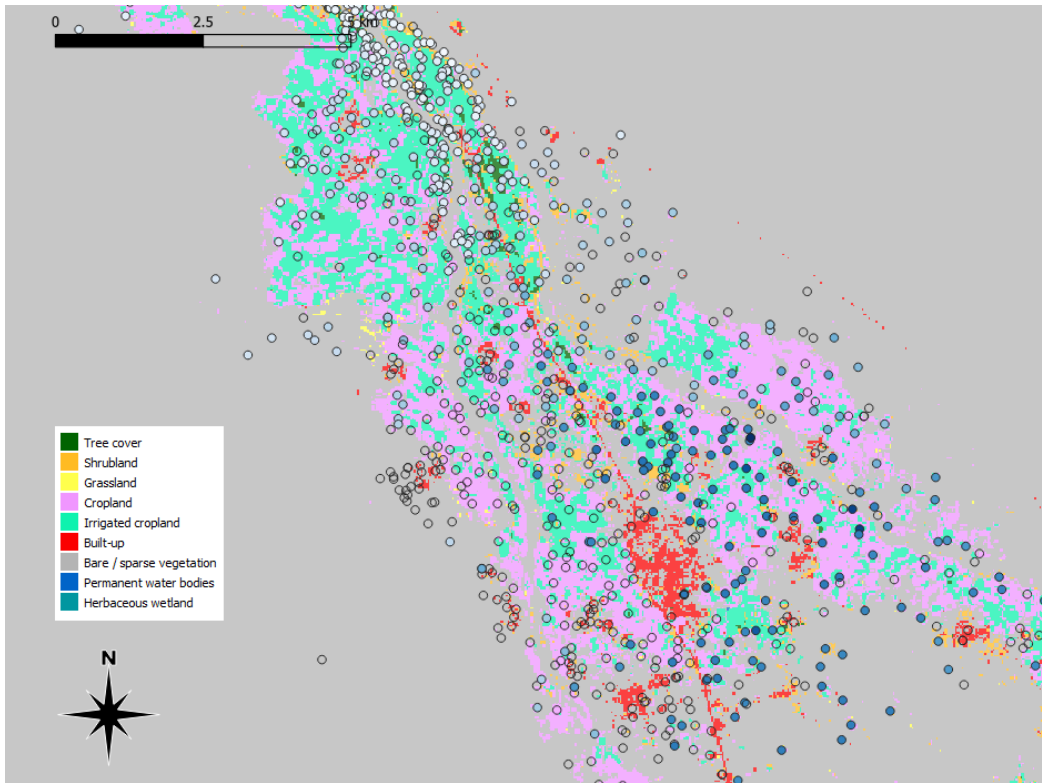


Figure 54. Map of the boreholes in the Tuban Delta and the land use classification. The colour of the well data points indicates the water level depths with dark blue representing deeper levels (up to 80 m below surface) and white colour shallow water levels.

Table 16. QSWATMOD MODFLOW model input variables.

Model Input Variable	Value	Source
Hydraulic conductivity of river bed material [m/d]	0.1	Default value
River bed thickness [m]	0.1	Default value
Depth to river bottom [m]	1.0	Default value
Aquifer thickness [m]	250	Komex, 2002
Hydraulic conductivity [m/d]	1	Default value
Horizontal anisotropy [-]	1	Komex, 2002
Specific storage [l/m]	1e-05	Default value
Specific Yield [-]	0.2	Default value
Initial hydraulic head [m amsl]	50	Komex, 2002

A one-layer groundwater model was constructed within the QSWATMOD2 plugin in QGIS. The model grid with 1000m x 1000m grid cells was created to follow the boundaries of the SWAT model of the Tuban District area. The rivers created in the SWAT model were overlayed on the grid, such that grid cells intersecting with rivers were designated as recharge zones.

The resulting hydraulic heads in December 2018, following a 17-year equilibration period and 20-year transient flow simulation period are shown in Figure 55. The pumping wells in the model area have not yet been included, so the hydraulic head remains constant

throughout the model run. For example, the heads at the red dot at the centre of the model domain remain steady around 129 m bgl (Figure 56).

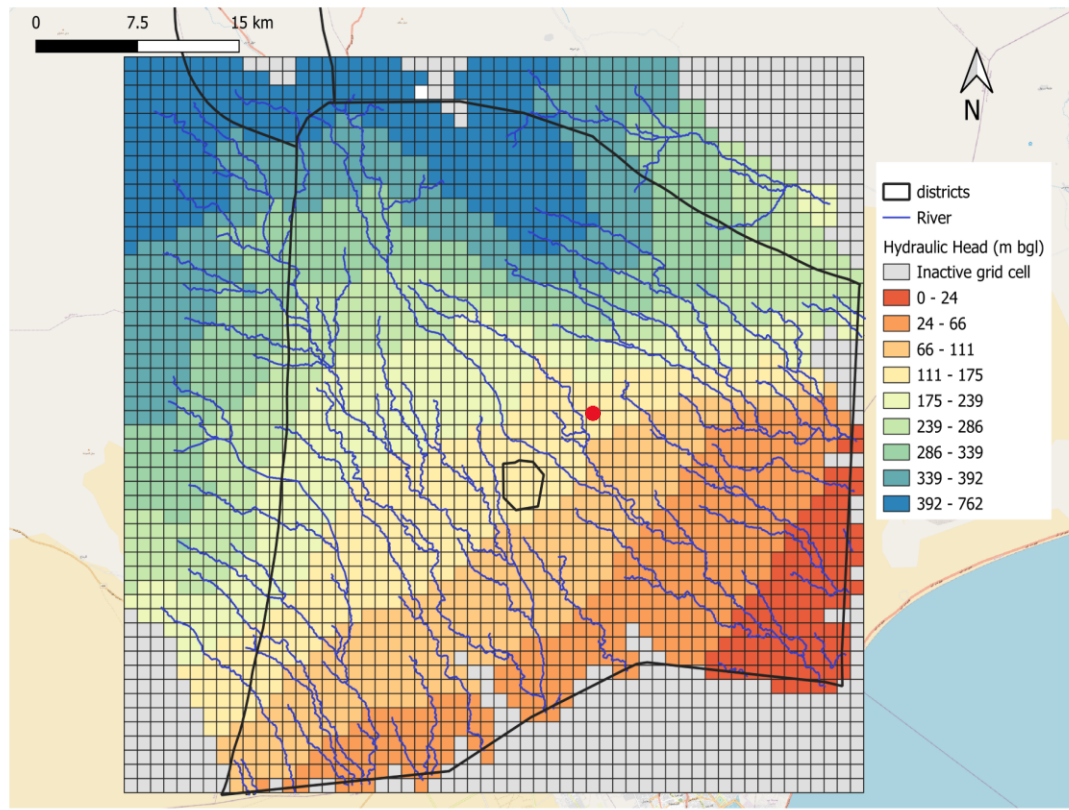


Figure 55. Hydraulic head in 2018 in the Tuban District. The MODFLOW model grid shows inactive cells in grey. The location of the example time series of hydraulic head without pumping is at the red dot.

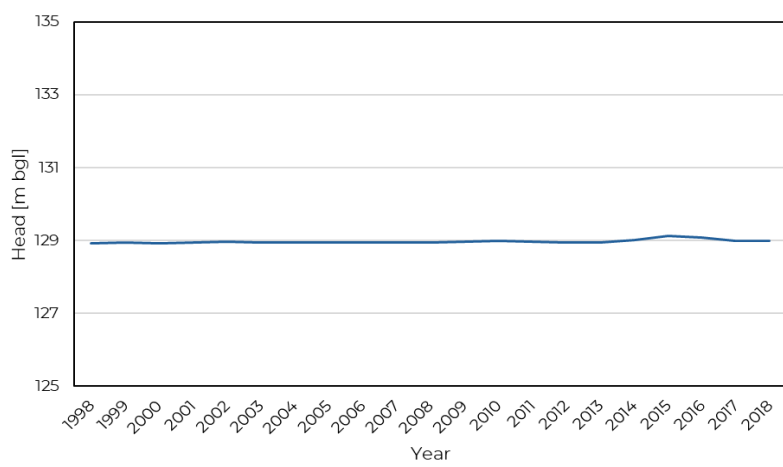


Figure 56. Modeled hydraulic head at observation point in [previous figure] from 1998 to 2017.

When pumping well and pumping rates are added to the model, the average annual drawdown of the groundwater table will be calculated. This will allow us to determine if the current groundwater abstraction rates are producing sustainable yields.

# **8. Water harvesting options**

Water harvesting basically implements temporary storage of water in a surface or subsurface reservoir for later use. In the Tuban Basin most of the stored water will be used for agricultural production in the dry period and sources include both water stored in surface water and in groundwater reservoirs. For surface water artificial storage reservoirs (dam reservoirs) have been constructed, whereas groundwater recharge only occurs through natural processes. However, surface water reservoirs may also replenish aquifers below the reservoirs through enhanced bed infiltration.

## **8.1 Current surface water harvesting**

Current water harvesting of surface water occurs uphill in terrace agriculture and by dam construction in stream channels, with diversions of river water occurring for spate irrigation in the wet season. Reservoirs have been mapped in the field study of this project and an overview of the reservoirs in the Tuban Basin is shown in Figure 57. The structures in the Tuban Delta are diversion barrier structures, whereas the structures in the hilly uplands are dams and ponds. In total 96 structures were included, but many smaller ponds may not have been identified. Terrace agriculture is mainly in the headwater catchments and seems often to be receiving irrigation from groundwater sources as indicated by pump houses visible on satellite imagery.

Check dams, not higher than 15 m due to regulations, may be constructed in the upland part of the basin. This would force a slower travel of water through the channels thereby creating opportunities for increased bed infiltration. water and presumably groundwater recharge. The main water shortage, however, seems to be in the coastal delta where rainfall is much less than  $100 \text{ mm a}^{-1}$ . Model simulations of Tuban District show that recharge in the bare soils from infiltration at the land surface is negligible under these conditions.

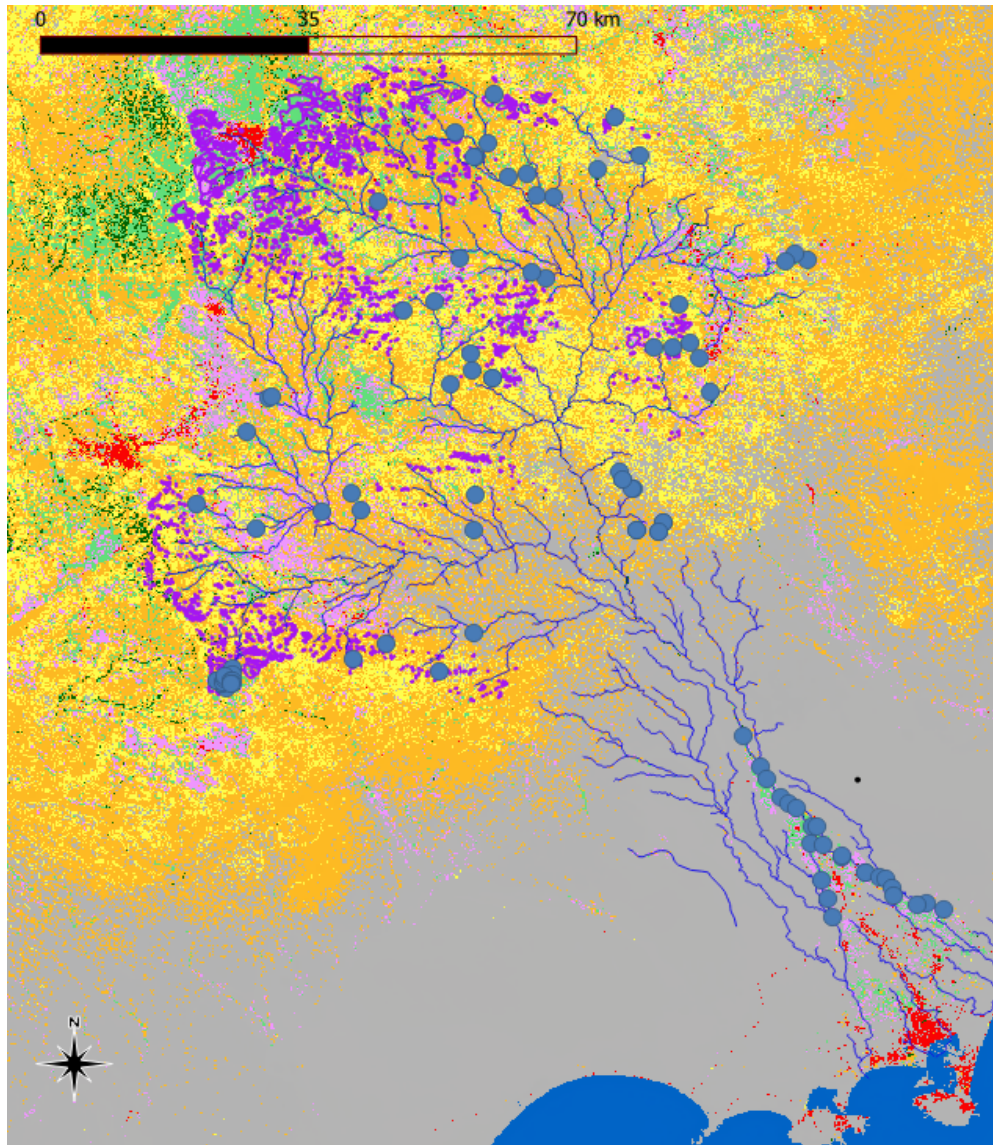


Figure 57. Map of rainwater harvesting structures (blue dots) and terrace agriculture (purple) displayed on the land use map.

## 8.2 Potential groundwater recharge and Integrated Water Harvesting approaches

This section presents potential groundwater recharge methods based on literature findings. These options have not been assessed within the scope of this study but are presented here to inform future planning and feasibility studies.

### 8.2.1 Managed Aquifer Recharge (MAR)

There are a number of options for enhanced groundwater recharge in rainwater harvesting projects (Abd-Elaty et al., 2024; CGWB, 2000; Gale et al., 2002; Gebreslassie et al., 2025). The process is called Managed Aquifer Recharge where conditions are created to enhance groundwater recharge. One of the main issues for successful application of infiltration enhancement techniques is the sediment concentration in the source water, as well as nutrient content that might lead to microbiological activity in the infiltration

structure. Sediment and microbiological activity can lead to clogging and reduce the infiltration capacity significantly (Kalwa et al., 2021).

These MAR systems include passive systems, where water flow towards the aquifer is governed by gravity flow, such as for:

- Spreading methods when groundwater is near the surface;
- Infiltration ditches;
- Infiltration ponds;
- Micro-dam reservoirs;
- Sand storage dams
- Sub-surface dams;
- River bank infiltration;
- Dry well infiltration systems;
- Hand dug well infiltration systems;
- Drilled well or borehole infiltration structures.

A more complex system would use a pump to actively inject source water into an aquifer through borehole screens.

Infiltration into wells with screens below the phreatic level seems to be the most direct and efficient way, but also requires pre-treatment of the infiltration source water to remove any suspended sediment (concentration  $<2 \text{ mg L}^{-1}$ ) or other substances that may cause clogging of the well screen and aquifer over time (Jeong et al., 2018; Martin, 2013; Ralph and Stevenson, 1995; Stuyfzand and Osma, 2019; Timmer et al., 2003; Zhao et al., 2009). In addition, if surface water is used, this may contain pollutants (e.g. nutrients, pesticides, industrial waste), which would be infiltrated into the aquifer and cause groundwater pollution. In The Netherlands regulations specify that these contaminants have to be removed before infiltration into groundwater reservoirs is allowed, which requires expensive and complicated slow sand – active carbon filter systems. In Yemen, the cost of such contaminant removal filters may be prohibitive and expertise may not be available to operate such a filter system. This procedure also requires the availability of laboratories that can measure pollutant concentrations, which may be difficult if low concentrations of pesticides or other organic pollutants need to be analysed.

In case desalination would be considered an option for producing drinking water and a surplus of desalination water would be available at times, this could also be a source for artificial infiltration into aquifers to serve as a buffer to the supply of drinking water (Alkhawlani et al., 2025; Ronen-Eliraz et al., 2017). However, this would not be a solution for the countering high extraction rates for agriculture.

### **8.2.2 Combined energy and water harvesting**

Innovative water harvesting approaches also include combining renewable energy infrastructure with water collection. A recent study by Waterloo et al. (2025) explored the potential of water harvesting using solar energy power plants for rainwater harvesting in the Sahel. They concluded that there was potential, especially for large plants that would be used to supply hydrogen for renewable energy supply. Although Yemen was included in their analysis, little information was given on the potentials for Yemen. However, if plans are being made for the deployment of solar energy plants in Yemen, this would be an

option to harvest water and potentially to reduce the groundwater needs for maintenance of these power plants in desert areas. Application of agrovoltaics (JRC, 2025) in combination with PV water harvesting could also contribute to the availability of water for agricultural use, but mostly in the uplands north of the Tuban District where annual precipitation totals exceed 200 mm a<sup>-1</sup>.

### 8.3 Water Harvesting Potential Areas

Figure 58 illustrates two types of water harvesting interventions across the Tuban Basin: upland (surface) interventions and stream (wadi-based) interventions. The classification is based on model-derived potentials for surface runoff reduction and wadi discharge.

The colored areas across the basin (Figure 58) represent the potential for surface runoff reduction, ranging from low (red) to high (dark blue). These areas reflect where upland measures, such as soil conservation, terracing, or micro-catchments can reduce runoff and increase infiltration. Reducing surface runoff not only mitigates erosion but also enhances groundwater recharge, contributing to Managed Aquifer Recharge (MAR) strategies. The southern portion of Tuban District (outlined in black) shows low to moderate potential, while the central and northern uplands exhibit moderately high to high potential, particularly where surface and subsurface conditions favor infiltration.

The river network is classified by wadi discharge potential (Figure 58), with line colors from red (low) to dark blue (high). These highlight potential zones for stream-based harvesting structures, such as check dams, infiltration weirs, or flood-spreading systems. The dark blue river segments indicate main contributors from tributaries and sub-basins, where flow volumes and geomorphology make them suitable for harvesting water and enhancing downstream recharge. Notably, the main tributaries exhibit high discharge, especially in the north and east, where stream harvesting is feasible. The southern Tuban District shows lower overall potential, but localized measures may still provide benefits.

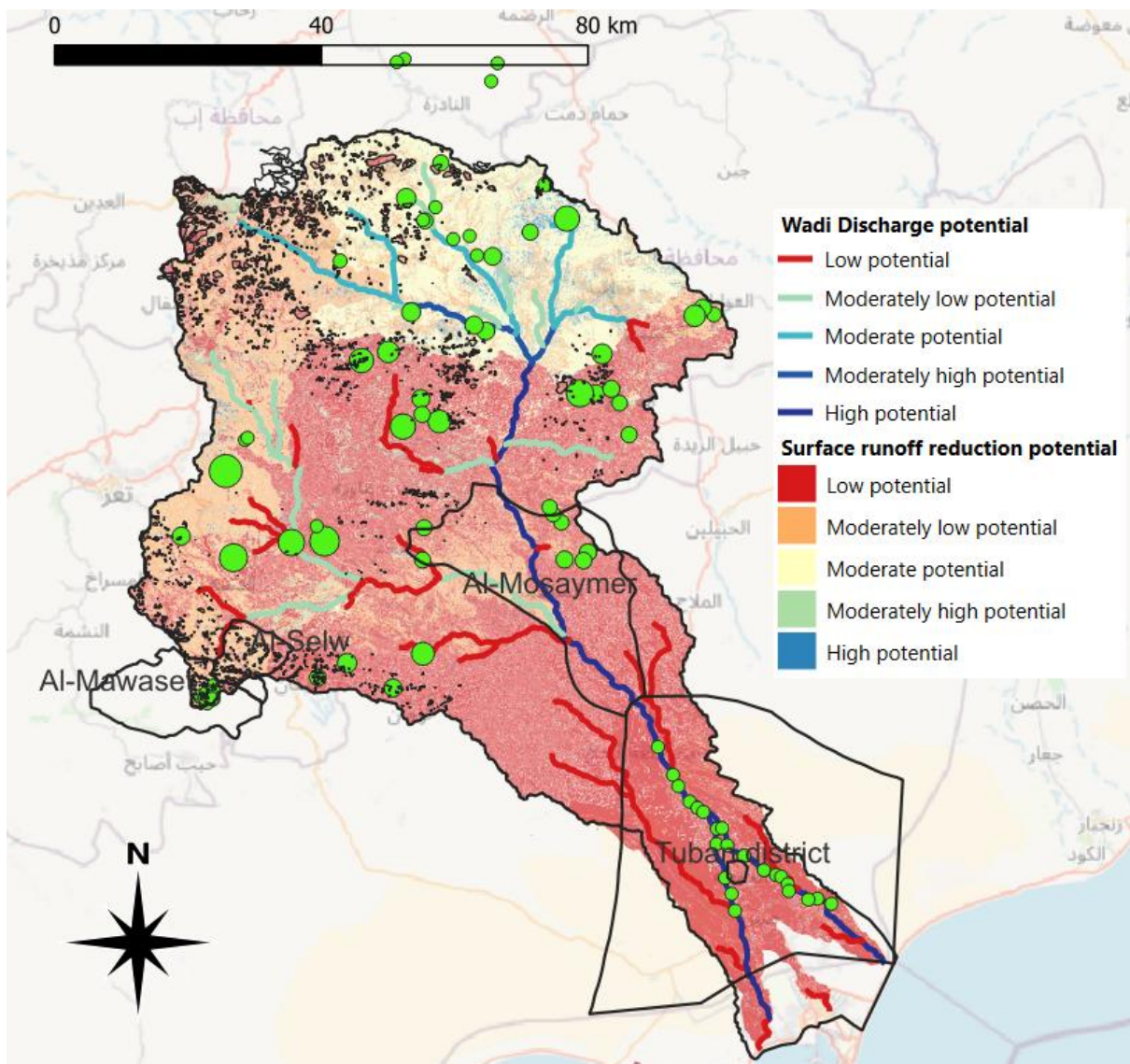


Figure 58. Map of potential water harvesting for Tuban Basin.

Figures 59, 60, and 61 present the district-level water harvesting potential areas. In addition, they illustrate the potential interventions proposed by stakeholders in the three districts of interest. These proposed measures include diversion barriers, pond rehabilitation, installation and rehabilitation of rain gauges, runoff gauges, new storage dams, and protection walls. All these interventions are mapped and visualized in Figures 59, 60, and 61 for each of the three districts.

The combined map of Al Selw and Al Mawaset Districts (Figure 59 )shows a mosaic of upland and wadi-based water harvesting potentials:

- Eastern and central areas exhibit moderate to high surface runoff potential, indicating good opportunities for upland interventions such as soil bunds, micro-catchments, or small terraces. These measures can enhance infiltration, reduce erosion, and support local groundwater recharge.
- The wadi network, particularly in the eastern part, shows moderate discharge potential, with some segments reaching high discharge levels. These are suitable

for infiltration weirs, check dams, or small sand dams, especially where topography and sediment transport allow accumulation and infiltration.

- Western areas show lower runoff potential, suggesting limited benefit from large-scale interventions, but localized measures may still be effective near cultivated zones or along intermittent streams.
- Black polygons in the map represent existing terraced areas. These terraces already support water retention and erosion control. Expanding or rehabilitating these terraces especially in zones with high runoff potential could further increase their effectiveness.

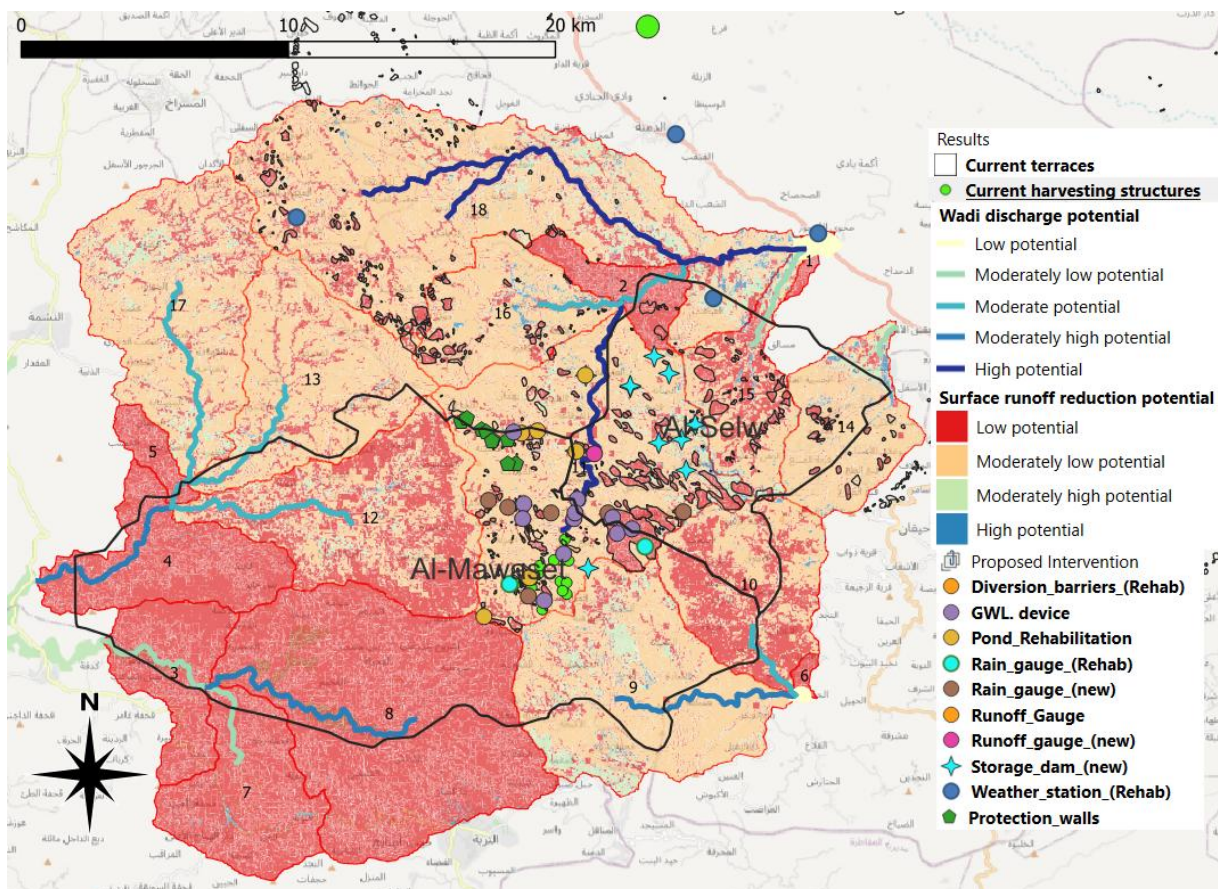


Figure 59. Map of potential water harvesting for Al Selw / Al Mawaset Districts.

Mosaymer District presents strong potential for both upland and stream-based harvesting water interventions (Figure 60):

- High surface runoff potential is observed in the northern and northeastern uplands, ideal for upland interventions such as contour bunds, hillside terraces, or semi-circular bunds. These could help improve soil moisture retention and reduce peak flows during rainfall events.
- The central and eastern wadi network shows high discharge potential, especially along major tributaries. These areas are well-suited for stream interventions, such as check dams, flood-spreading structures, or subsurface infiltration systems.

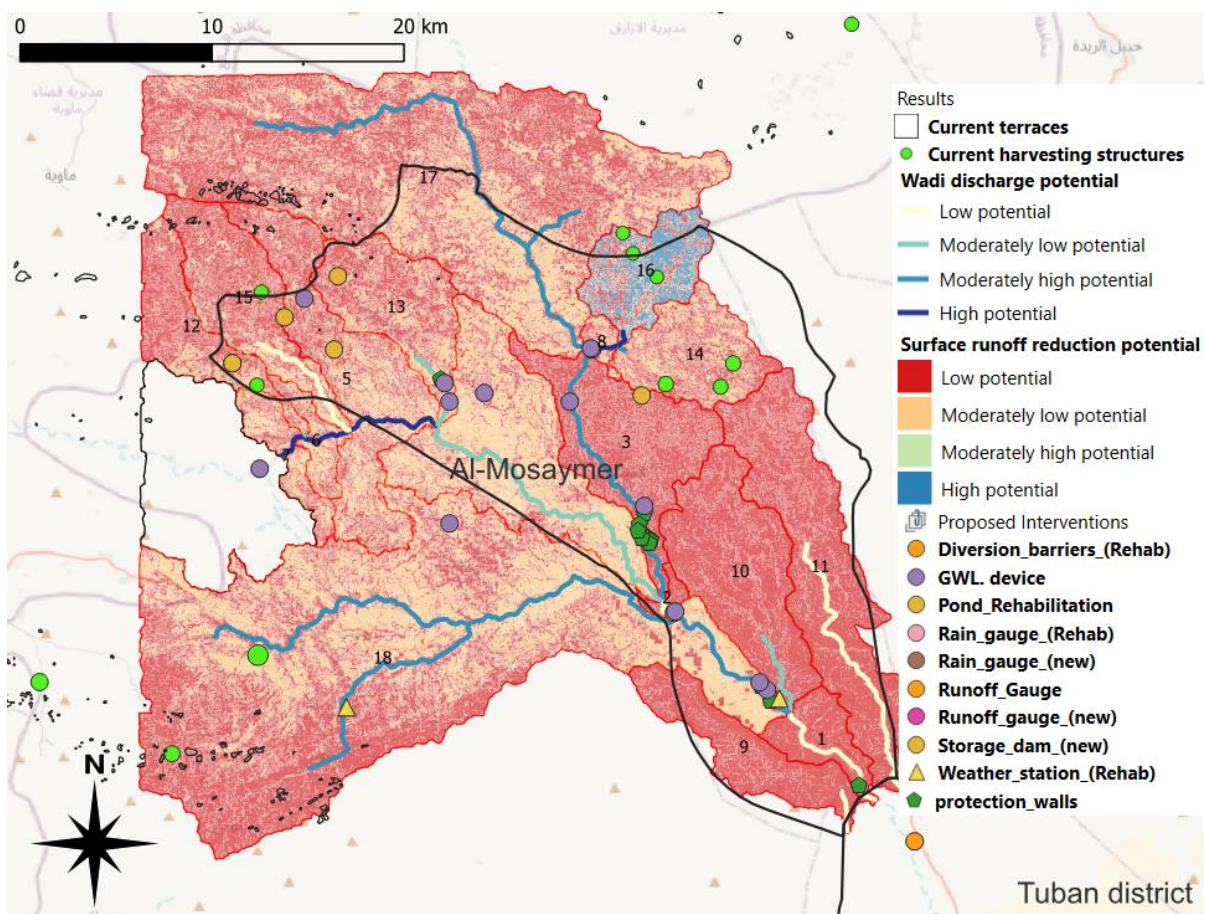


Figure 60. Map of potential water harvesting for Mosaymer District.

The Tuban District includes a mix of upland and lowland zones with variable harvesting water potential areas (Figure 61):

- The northern uplands show moderate to high runoff potential, particularly near elevated ridges and sloped terrain, making them well-suited for terracing, stone bunds, or infiltration pits.
- Central and western wadis display high discharge potential, indicating feasibility for wadi-based harvesting techniques such as infiltration weirs or sand dams, which can retain water and enhance aquifer recharge downstream.
- The southern district has lower overall potential, but targeted measures may still be viable near cultivated areas or degraded lands.

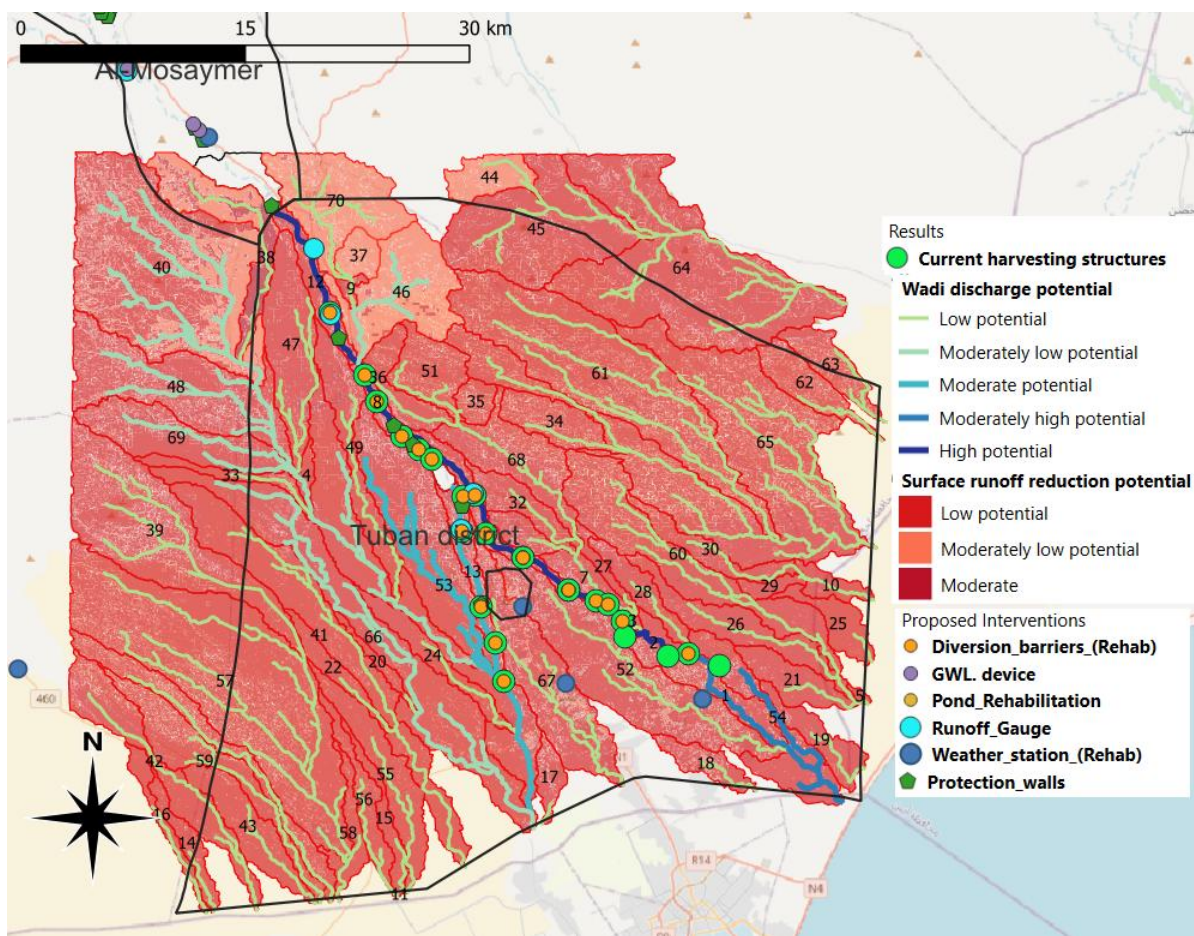


Figure 61. Map of potential water harvesting for Tuban District.

## 8.4 Water Harvesting Potential Areas under Climate Change Scenario

Climate change analysis for water resources resilience evaluation consists of historical and future change analyses. This provides information on the trends in temperature and precipitation in project areas and allows an assessment for the sustainability of proposed measures in view of climate change.

While identifying surface or groundwater resources for water resources development, future changes are important as these determine the robustness of the sources to supply water in view of climate change. For future climate projections, five scenarios describing possible land use development, alternative energy developments and reductions in fossil fuel and other greenhouse gas emissions have been developed (Meinshausen et al., 2020; Riahi et al., 2017). These Shared Socioeconomic Pathway scenarios have been labelled SSP1 – SSP5, where SSP1 represents an optimal pathway to sustainability, SSP2 the “middle of the road” pathway and SSP5 the scenario for further fossil fuel development representing the worst-case scenario. The change in global CO<sub>2</sub> emissions for different scenarios for the period 2000 – 2100 is shown in Figure 62.

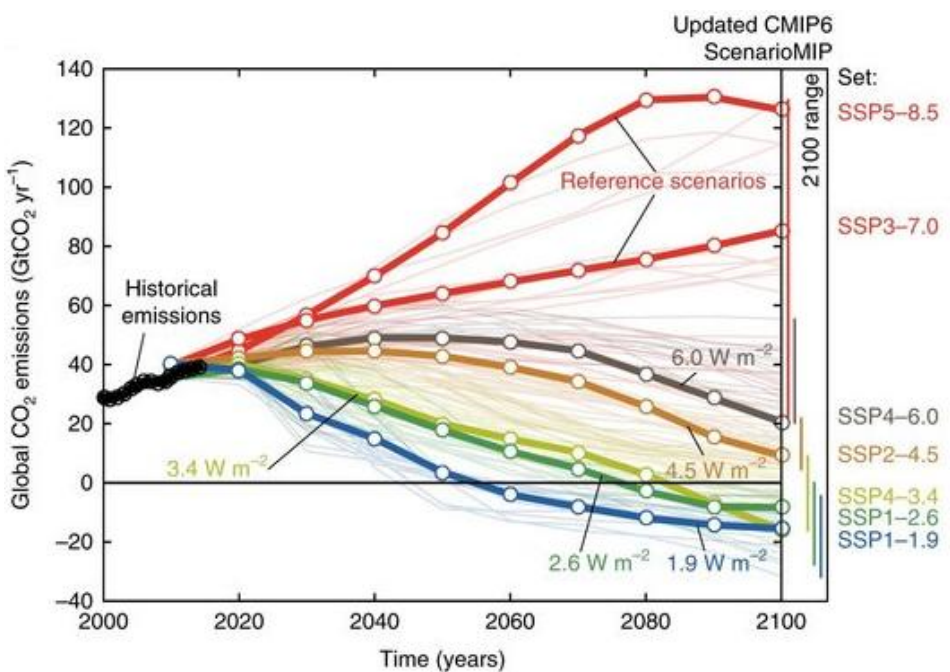


Figure 62. Global CO<sub>2</sub> emissions of SSP scenarios (Rogelj et al., 2018).

These SSP scenarios have been used for climate change modelling in the Coupled Model Intercomparison Project (CMIP) climate modelling experiments, including the SSP2-4.5 “middle of the road” scenario. The latest model results are from CMIP phase 6 (CMIP6) (Eyring et al., 2016), in which 40 general circulation models were selected and different ensembles were run to create a monthly data set of about 68 model runs for the different scenarios. The GCM runs in CMIP6 were developed and used in support of the Sixth Assessment Report of the Intergovernmental Panel on Climate Change (IPCC AR6).

The CMIP6 data, with a resolution of 2.5°, can be used to provide insight into future temperature and precipitation trends and are available for download at the KNMI Climate Explorer ([https://climexp.knmi.nl/selectfield\\_cmip6.cgi](https://climexp.knmi.nl/selectfield_cmip6.cgi)). These data were used to compile time series of monthly and annual trends at specific locations and assess confidence bands and the significance of observed changes.

In response to the need for downscaled CMIP6 data NASA Earth Exchange has developed the NEX-GDDP global, high resolution (0.25°), bias-corrected daily climate change projections for the CMIP6 historical scenario and the SSP1-2.6, SSP2-4.5, SSP3-7.0 and SSP5-8.5 scenarios. The bias-corrected downscaled data are better suited than the original CMIP6 data for use by the scientific community to determine spatial and temporal variations in climate change related to finer-scale climate gradients and the effects of local topography on climate conditions.

The total monthly change as predicted by the CMIP6 runs for the SSP2-4.5 scenario for temperature and precipitation are shown below for precipitation (Figure 63) and for temperature (Figure 64). The areas where changes were statistically not significant over this period were blanked. As can most parts of the Yemen are predicted not to have any significant increase in precipitation. An exception is the Southern part of the Tumbat which might experience a 1 mm decrease in precipitation.

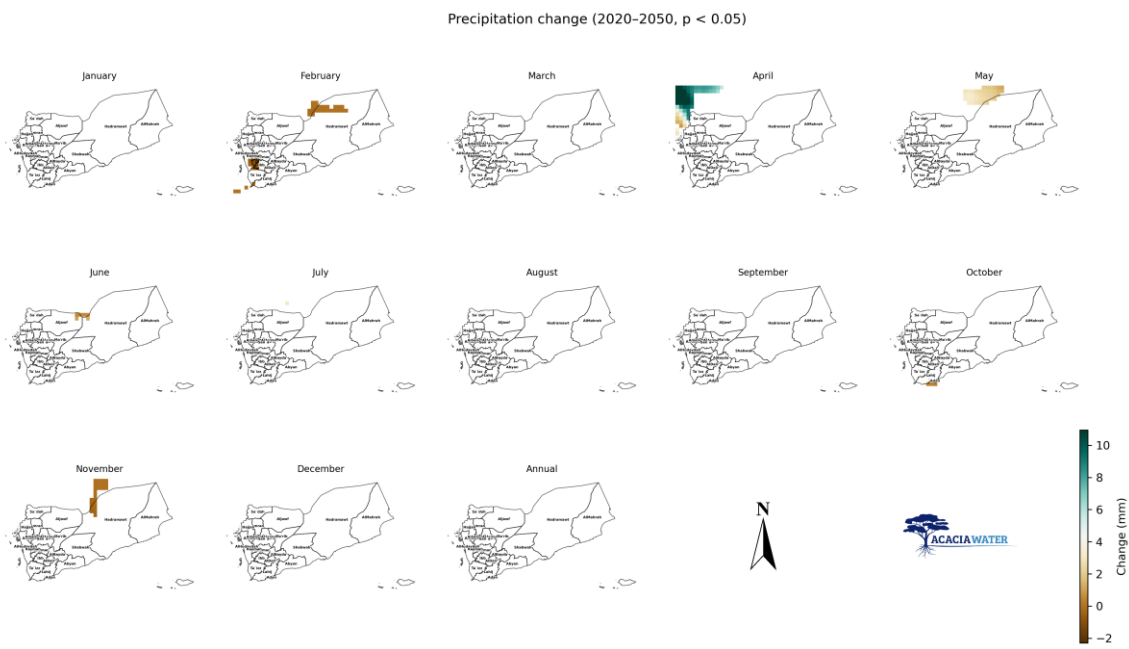


Figure 63. Map of potential precipitation change under SSP2-4.5 Climate Change Scenario for Yemen.

The temperature maps do indicate significant increase with monthly temperatures increasing by 0.9 – 1.0 °C in 2050. This will have a small influence in the evaporative demand of the air.

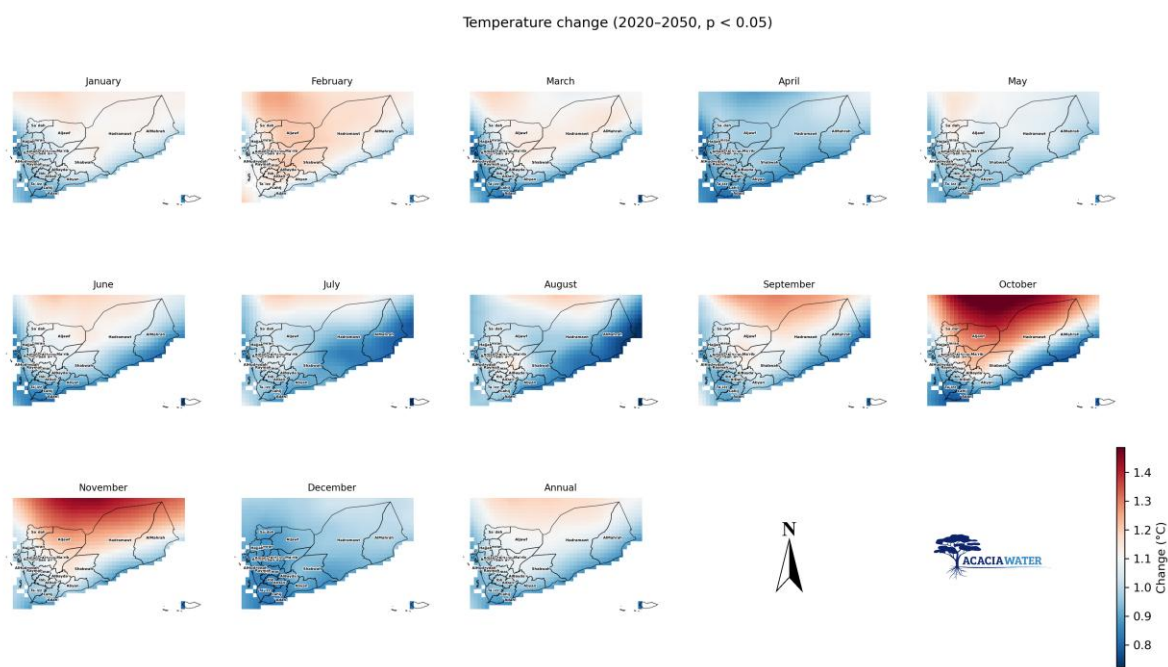


Figure 64. Map of potential temperature change under ssp2-4.5 Climate Change Scenario for Yemen.

A climate change simulation was run for the entire basin to assess changes due to a minimum and maximum temperature increase of 1.0 °C as predicted for 2050. The impacts on the annual water balance components of the Tuban Basin are shown in Figure 65.

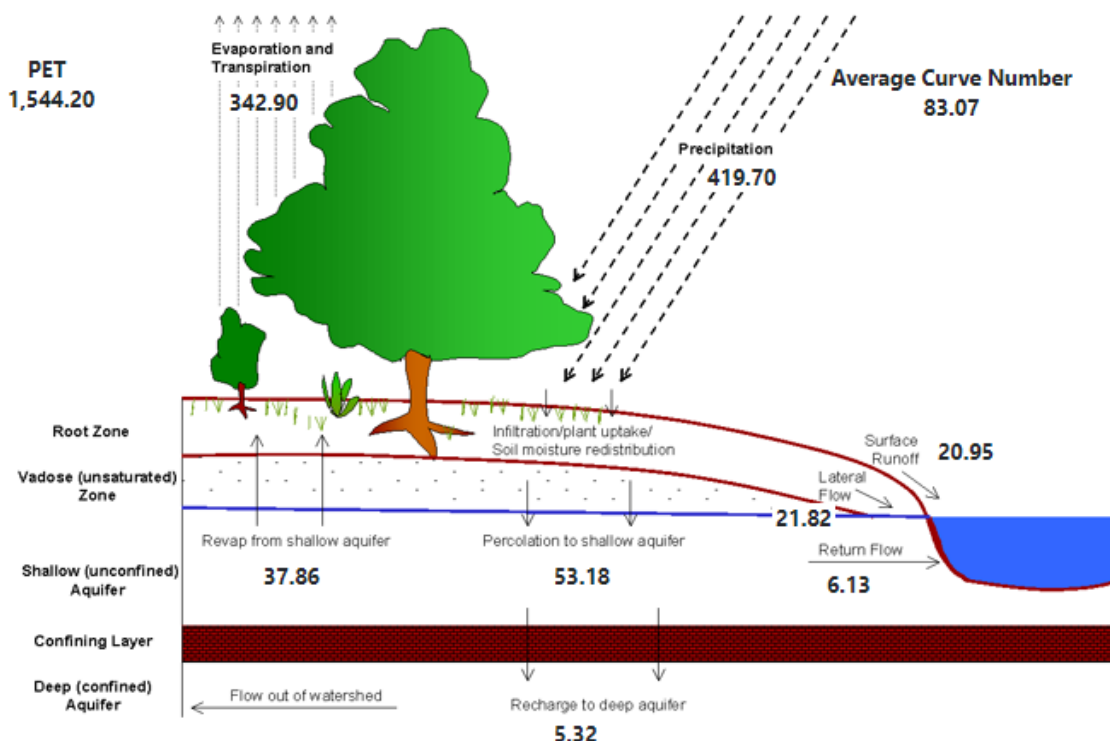
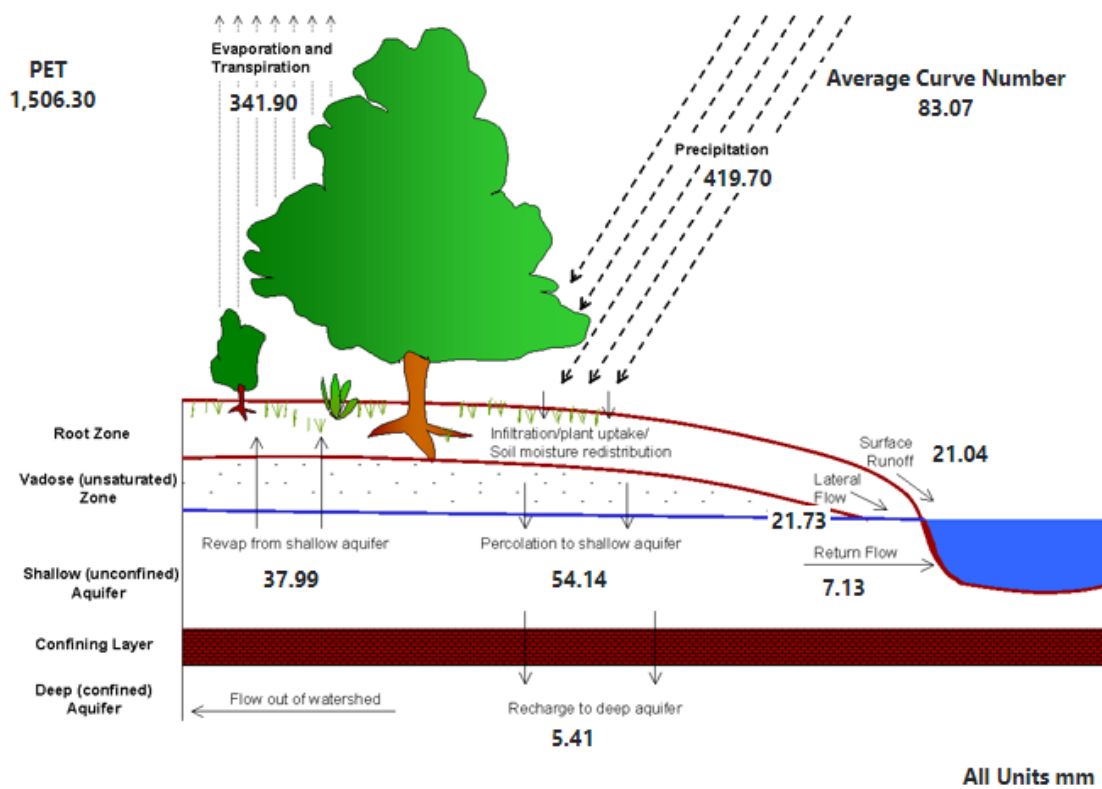


Figure 65. Comparison between current (upper) and future (lower) climate with a +1.0 °C temperature increase for water balance components for the Tuban Basin in the period 1999 – 2018.

The temperature increase of 1.0 °C causes an increase in PET of about  $38 \text{ mm a}^{-1}$ , but only a  $1.0 \text{ mm a}^{-1}$  increase in actual evaporation as the latter is limited by soil water availability and irrigation status. This increase in actual ET causes a 2% decrease in predicted deep

aquifer recharge, a decrease of less than 0.5% in surface runoff and of 1.4% in baseflow after 2050.

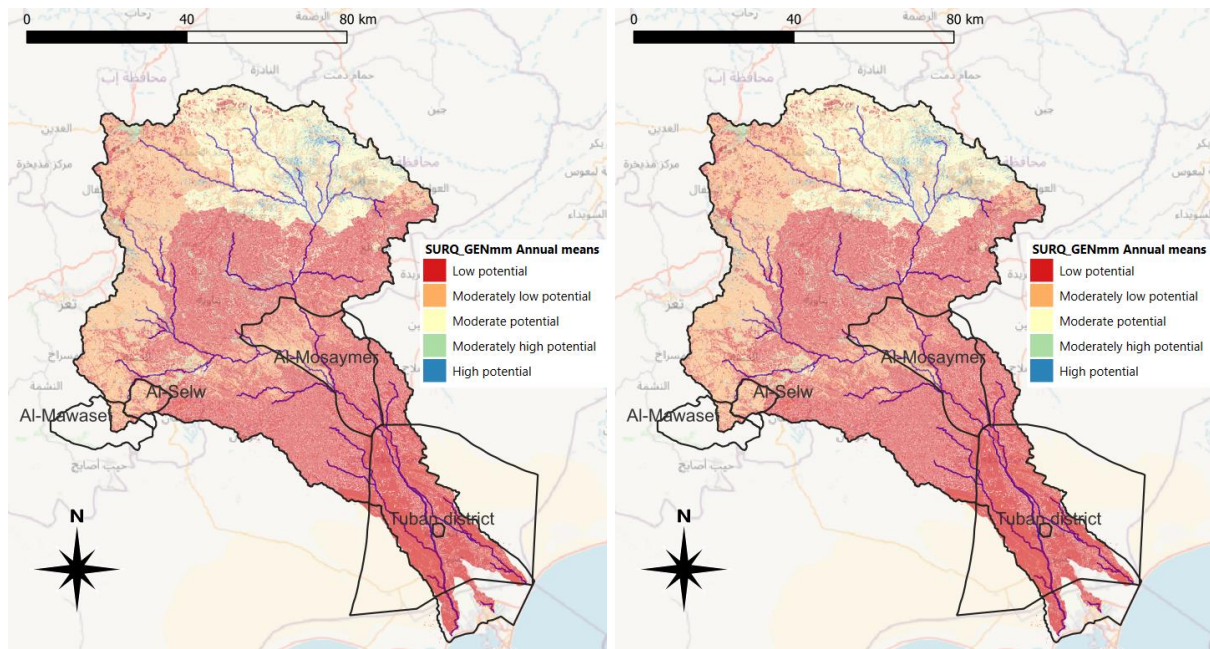


Figure 66. Comparison of current climate potential water harvesting map (left) and map for a significant temperature increase of 1.0 °C as predicted for 2050 by the CMIP6 dataset. Simulation data periods 1999-2018.

The potential maps for current and future climates are shown in Figure 66. There is no difference in the maps with respect to water harvesting potentials as the influence of temperature on surface runoff is small and surface runoff is much more related to precipitation input and land use and soil type. With the small changes in water balance components there will therefore be no impact on the water harvesting potentials in comparison with current climate simulations, although river flows and groundwater recharge may show a small decrease.

## 9. Conclusions

A recognizable SWAT model was developed for the entire Tuban Basin, providing an initial water balance overview for the region. Input data were obtained from public sources and a short field campaign, which—due to security and permission restrictions—could not reach the northern part of the basin. Global datasets were used for topography, land use, soil descriptions, weather inputs, and evaporation data for model calibration. However, there is a notable lack of continuous daily precipitation data in many areas of the basin to validate the satellite precipitation estimates derived from the CHIRPS dataset used in this study.

The simulations reveal a decreasing availability of water from the higher rainfall northern parts of the basin towards the coastal desert zone in the south. A significant gap between rainfall and potential evapotranspiration (PET) confirms the basin's high evaporative losses and seasonal water deficit. Most rainfall is quickly lost to evapotranspiration, emphasizing the urgent need for water storage solutions (such as harvesting during wet months) and improved irrigation efficiency to better utilize limited water resources.

To address these challenges with greater detail, three different SWAT models were developed that provide water balance information for the Tuban Basin and for four target districts. These models incorporate field data on land use, crop types, irrigation methods, and water use. Among them, only the Tuban district model includes a dedicated groundwater component, allowing for more in-depth analysis of aquifer dynamics. The simulations show a decreasing availability of water travelling from the higher rainfall parts of the basin in the North towards the coastal desert zone in the South. In addition a coupled surface – groundwater model was developed for the Tuban District.

Typically, models are calibrated against observed data, but this was limited in the current work due to a lack of recent data (e.g., streamflow) and time constraints caused by the short project duration and delays in field data collection. This lack of data also restricts model validation, meaning the results should be seen as a starting point rather than a finalized product.

Limited data availability severely restricts the validation of the models. As such these models should not be viewed as a final stage, but rather as a starting point from which improvements can be made. This also supports the training program developed for specialists in Yemen, including those from the academic institutions. Their involvement is crucial in developing a model community in Yemen that can provide input into management plans.

The role of groundwater recharge in the upland Tuban Basin and its contribution to regional groundwater flow in the delta area remain unknown, as no information is available on the deep groundwater system's functioning. Terraces are important for water harvesting and agriculture, often irrigated using deep groundwater, especially in the northern basin. These structures can increase infiltration, supporting groundwater replenishment. In the Al Mosaymer district water yields from terraces were significantly higher than those from the surrounding landscape.

Groundwater replenishment can occur in combination with surface water structures because the extended duration of water on the surface facilitates infiltration towards shallow and deep groundwater reservoirs. This can be done through construction of check dams and infiltration ponds, but the latter method does have the disadvantage that evaporation removes part of the water stored in the pond. An alternative is to use MAR systems in which surface water is directly infiltrated into the aquifer. However, this requires treatment of the infiltration source water to avoid clogging of the infiltration boreholes or wells.

Despite its limitations, the reconnaissance model provides a valuable first estimate of the basin's water balance and key hydrological patterns. It helps to guide where further detailed analysis and data collection are needed. The results from this reconnaissance-level model were used to define and develop the more detailed models for the targeted districts. These detailed models offer a strategic foundation for water management interventions but still require further calibration before they can be used for site-specific planning.

The impacts of climate change seem to be limited to a significant increase in temperature of 1.0 °C in the Tuban Basin, with no significant changes being predicted in the average CMIP6 model scenarios for the SSP2-4.5 'middle of the road' scenario. Although this increase had impact of the PET, changes in other water balance components were less than 2% decrease in quantities. With these small changes there will be no impact on the water harvesting potentials in comparison with current climate simulations.

Global HAWQS provides a platform in which less experienced users can do scenario modelling. However, the resolution of 1 km is less suitable for modelling impacts of small structures in the landscape such as terraces or check dams. As such, detailed analysis will still need to be done by specialists, which may be found through involvement of the academic community and providing options for MSc and PhD students to become involved in water management. The academic sector could also provide more data on groundwater changes if a monitoring network can be set up and providing the public access to data.

## 10. Recommendations

More time should be taken to tweak the developed models and to compare results with the general assumption that transmission losses in the main wadi channels contribute to groundwater recharge. The parametrization of terraces could also be improved and would presumably reveal more contrast in the water balance characteristics of the HRUs.

The mapping of terraces has not been completed in this study due to time constraints, and no borehole information is available for the upland part of the basin. As terraces are very important—also as water harvesting structures—mapping should continue to provide a complete overview of terraces in the basin. Similarly, boreholes should be identified, which could be done through remote sensing analysis combined with ground verification. However, this would require the purchase of high-resolution imagery.

Due to the large elevation differences in the basin, isotope studies of precipitation, river runoff, and deep groundwater could provide useful information on the origin of groundwater in the coastal delta (upland vs. local infiltration).

The development of a good hydrometeorological monitoring network providing daily precipitation and runoff records is important. The option of using citizen science to collect such data (e.g., through schools) should be explored. It is important that the wadi station at Dukeim is being maintained as this branch of the river forms the main input in the Tuban Delta. A monitoring plan and hydrometeorological network should be designed such as to provide information at key locations in the Tuban Basin.

Both surface and groundwater monitoring stations need to be installed, both in the upland areas of the basin and in the coastal delta where significant decreases in groundwater levels were already observed, leading to salt water intrusion along the coast. Automatic data logger stations would be needed for surface water monitoring, while manual stations could be used for groundwater measurements at monthly or quarterly intervals.

Hydrochemical measurements of groundwater may be used to assess if upland groundwater feeds into the coastal delta of the Tuban Basin. Analysis should then include EC, pH, major cations and anions, Si and when possible hydrogen and oxygen isotopes. These could then be used in a cluster or PCA analysis to detect similarities.

In the coastal delta, many boreholes have been developed for irrigation purposes. However, monitoring of groundwater levels and salinity changes has been minimal. A number of locations along the main wadis and in the surrounding drylands should be selected to establish time series of groundwater level and salinity. Collecting such data is essential to detect saltwater intrusion and aquifer depletion.

To enhance groundwater recharge, the use of Managed Aquifer Recharge (MAR) systems should be investigated. A small pilot project could be developed to test infiltration of wadi flows or water from a storage reservoir. For the design and successful implementation of such systems, water quality data—such as turbidity and ion concentrations (e.g., Fe, Mn)—are needed.

# References

- Abd-Elaty, I., Kuriqi, A., Ahmed, A., Ramadan, E.M., 2024. Enhanced groundwater availability through rainwater harvesting and managed aquifer recharge in arid regions. *Appl Water Sci* 14, 121. <https://doi.org/10.1007/s13201-024-02166-7>
- Al-Darwish, K.A., 2023. Groundwater Monitoring at Yemen.
- Alkhawlan, Q., Sabeeh, S., Algburi, S., Alsubih, M., Islam, S., Khan, R.A., 2025. Coupling solar-powered desalination and Managed Aquifer Recharge for integrated groundwater management in Central Saudi Arabia. *Desalination* 614, 119188. <https://doi.org/10.1016/j.desal.2025.119188>
- Arnold, J.G., Fohrer, N., 2005. SWAT2000: current capabilities and research opportunities in applied watershed modelling. *Hydrological Processes* 19, 563–572.
- Arnold, J.G., Moriasi, D.N., Gassman, P.W., Abbaspour, K.C., White, M.J., Srinivasan, R., Santhi, C., Harmel, R.D., Griensven, A. van, Liew, M.W. van, Kannan, N., Jha, M.K., 2012. SWAT: Model use, calibration and validation. *Transactions of the ASABE* 55, 1491–1508.
- Arnold, J.G., Srinivasan, R., Muttiah, R.S., Williams, J.R., 1998. Large Area Hydrologic Modeling and Assessment Part I: Model Development1. *JAWRA Journal of the American Water Resources Association* 34, 73–89. <https://doi.org/10.1111/j.1752-1688.1998.tb05961.x>
- CGWB, 2000. Guide on Artificial Recharge to Ground Water. Central Ground Water Board, Ministry of Water Resources, New Delhi, India.
- Climate Hazards Centre, n.d. CHIRPS: Rainfall Estimates from Rain Gauge and Satellite Observations | Climate Hazards Center - UC Santa Barbara [WWW Document]. CHIRPS: Rainfall Estimates from Rain Gauge and Satellite Observations. URL <https://www.chc.ucsb.edu/data/chirps> (accessed 4.10.20).
- Eyring, V., Bony, S., Meehl, G.A., Senior, C.A., Stevens, B., Stouffer, R.J., Taylor, K.E., 2016. Overview of the Coupled Model Intercomparison Project Phase 6 (CMIP6) experimental design and organization. *Geoscientific Model Development* 9, 1937–1958. <https://doi.org/10.5194/gmd-9-1937-2016>
- FAO, 2020. WaPOR Database Methodology. Version 2 release. (Technical Report), Methodology Series. FAO, Rome, Italy. <https://doi.org/10.4060/ca9894en>
- Gale, I., Neumann, I., Calow, R., Moench, M., 2002. The effectiveness of Artificial Recharge of groundwater: a review (Commissioned report No. CR/02/108N). British Geological Survey, Keyworth, Nottingham, UK.
- Gebreslassie, H., Berhane, G., Gebreyohannes, T., Hagos, M., Hussien, A., Walraevens, K., 2025. Water Harvesting and Groundwater Recharge: A Comprehensive Review and Synthesis of Current Practices. *Water* 17, 976. <https://doi.org/10.3390/w17070976>
- Gevaert, A.I., Merton, L., Bashir, Y., Uribe, N., 2024. Hydrological study of Wadi Tuban (No. AW24\_230-3\_NU\_241547). Gouda, The Netherlands.
- HAWQS, 2020. HAWQS System and Data to model the lower 48 conterminous U.S using the SWAT model. <https://doi.org/10.18738/T8/XN3TE0>
- Hengl, T., Jesus, J.M. de, Heuvelink, G.B.M., Gonzalez, M.R., Kilibarda, M., Blagotić, A., Shangguan, W., Wright, M.N., Geng, X., Bauer-Marschallinger, B., Guevara, M.A., Vargas, R., MacMillan, R.A., Batjes, N.H., Leenaars, J.G.B., Ribeiro, E., Wheeler, I., Mantel, S., Kempen, B., 2017. SoilGrids250m: Global gridded soil information based on machine learning. *PLOS ONE* 12, e0169748. <https://doi.org/10.1371/journal.pone.0169748>
- Hersbach, H., Bell, B., Berrisford, P., Hirahara, S., Horányi, A., Muñoz-Sabater, J., Nicolas, J., Peubey, C., Radu, R., Schepers, D., Simmons, A., Soci, C., Abdalla, S., Abellán, X., Balsamo, G., Bechtold, P., Biavati, G., Bidlot, J., Bonavita, M., De Chiara, G., Dahlgren, P., Dee, D., Diamantakis, M., Dragani, R., Flemming, J., Forbes, R., Fuentes, M., Geer, A., Haimberger, L., Healy, S., Hogan, R.J., Hólm, E., Janisková, M., Keeley, S., Laloyaux, P., Lopez, P., Lupu, C., Radnoti, G., de Rosnay, P., Rozum, I., Vamborg, F., Villaume, S.,

- Thépaut, J.-N., 2020. The ERA5 global reanalysis. *Quarterly Journal of the Royal Meteorological Society* 146, 1999–2049. <https://doi.org/10.1002/qj.3803>
- Jeong, H.Y., Jun, S.-C., Cheon, J.-Y., Park, M., 2018. A review on clogging mechanisms and managements in aquifer storage and recovery (ASR) applications. *Geosci J* 22, 667–679. <https://doi.org/10.1007/s12303-017-0073-x>
- JRC, 2025. Agrivoltaics alone could surpass EU photovoltaic 2030 goals [WWW Document]. JRC News and Updates. URL [https://joint-research-centre.ec.europa.eu/jrc-news-and-updates/agrivoltaics-alone-could-surpass-eu-photovoltaic-2030-goals-2023-10-12\\_en](https://joint-research-centre.ec.europa.eu/jrc-news-and-updates/agrivoltaics-alone-could-surpass-eu-photovoltaic-2030-goals-2023-10-12_en) (accessed 7.17.25).
- Kalwa, F., Binder, M., Händel, F., Grüneberg, L., Liedl, R., 2021. Biological and Physical Clogging in Infiltration Wells: Effects of Well Diameter and Gravel Pack. *Groundwater* 59, 819–828. <https://doi.org/10.1111/gwat.13104>
- Langevin, C.D., Shoemaker, W.B., Guo, W., 2003. MODFLOW-2000, the U.S. Geological Survey Modular Ground-Water Model--Documentation of the SEAWAT-2000 Version with the Variable-Density Flow Process (VDF) and the Integrated MT3DMS Transport Process (IMT) (USGS Numbered Series), Open-File Report.
- Li, Y., Tian, F., Zhang, M., Zeng, H., Ahmed, S., Qin, X., Liu, Y., Wang, L., Fan, R., Wu, B., 2025. A 10-meter global terrace mapping using sentinel-2 imagery and topographic features with deep learning methods and cloud computing platform support. *International Journal of Applied Earth Observation and Geoinformation* 139, 104528. <https://doi.org/10.1016/j.jag.2025.104528>
- Martin, R. (Ed.), 2013. Clogging issues associated with managed aquifer recharge methods. IAH Commission on Managing Aquifer Recharge, Australia.
- Meinshausen, M., Nicholls, Z.R.J., Lewis, J., Gidden, M.J., Vogel, E., Freund, M., Beyerle, U., Gessner, C., Nauels, A., Bauer, N., Canadell, J.G., Daniel, J.S., John, A., Krummel, P.B., Luderer, G., Meinshausen, N., Montzka, S.A., Rayner, P.J., Reimann, S., Smith, S.J., van den Berg, M., Velders, G.J.M., Vollmer, M.K., Wang, R.H.J., 2020. The shared socio-economic pathway (SSP) greenhouse gas concentrations and their extensions to 2500. *Geoscientific Model Development* 13, 3571–3605. <https://doi.org/10.5194/gmd-13-3571-2020>
- Mu, Q., Zhao, M., Running, S.W., n.d. MODIS Global Terrestrial Evapotranspiration (ET) Product MOD16A2 Collection 5.
- Park, S., Bailey, R., Bieger, K., 2019. QGIS Interface for SWAT-MODFLOW (QSWATMOD) (No. Version 1.2). Texas A&M AgriLife Research, Texas, USA.
- Ralph, D.E., Stevenson, J.M., 1995. The role of bacteria in well clogging. *Water Research* 29, 365–369. [https://doi.org/10.1016/0043-1354\(94\)E0077-J](https://doi.org/10.1016/0043-1354(94)E0077-J)
- Riahi, K., van Vuuren, D.P., Kriegler, E., Edmonds, J., O'Neill, B.C., Fujimori, S., Bauer, N., Calvin, K., Dellink, R., Fricko, O., Lutz, W., Popp, A., Cuaresma, J.C., Kc, S., Leimbach, M., Jiang, L., Kram, T., Rao, S., Emmerling, J., Ebi, K., Hasegawa, T., Havlik, P., Humpenöder, F., Da Silva, L.A., Smith, S., Stehfest, E., Bosetti, V., Eom, J., Gernaat, D., Masui, T., Rogelj, J., Strefler, J., Drouet, L., Krey, V., Luderer, G., Harmsen, M., Takahashi, K., Baumstark, L., Doelman, J.C., Kainuma, M., Klimont, Z., Marangoni, G., Lotze-Campen, H., Obersteiner, M., Tabeau, A., Tavoni, M., 2017. The Shared Socioeconomic Pathways and their energy, land use, and greenhouse gas emissions implications: An overview. *Global Environmental Change* 42, 153–168. <https://doi.org/10.1016/j.gloenvcha.2016.05.009>
- Rogelj, J., Popp, A., Calvin, K.V., Luderer, G., Emmerling, J., Gernaat, D., Fujimori, S., Strefler, J., Hasegawa, T., Marangoni, G., Krey, V., Kriegler, E., Riahi, K., van Vuuren, D.P., Doelman, J., Drouet, L., Edmonds, J., Fricko, O., Harmsen, M., Havlík, P., Humpenöder, F., Stehfest, E., Tavoni, M., 2018. Scenarios towards limiting global mean temperature increase below 1.5 °C. *Nature Clim Change* 8, 325–332. <https://doi.org/10.1038/s41558-018-0091-3>
- Ronen-Eliraz, G., Russak, A., Nitzan, I., Guttman, J., Kurtzman, D., 2017. Investigating geochemical aspects of managed aquifer recharge by column experiments with

- alternating desalinated water and groundwater. *Science of The Total Environment* 574, 1174–1181. <https://doi.org/10.1016/j.scitotenv.2016.09.075>
- Running, S., Mu, Q., Zhao, M., Moreno, A., 2021. MODIS/Terra Net Evapotranspiration Gap-Filled 8-Day L4 Global 500m SIN Grid V061.
- Sisay, B.M., Nedaw, D., Birhanu, B., Gigar, A.G., 2023. Application of SWAT and MODFLOW models for characterization of surface–groundwater interaction in the Modjo River catchment, central Ethiopia. *Environ Earth Sci* 82, 341. <https://doi.org/10.1007/s12665-023-10988-y>
- Stuyfzand, P.J., Osma, J., 2019. Clogging Issues with Aquifer Storage and Recovery of Reclaimed Water in the Brackish Werribee Aquifer, Melbourne, Australia. *Water* 11, 1807. <https://doi.org/10.3390/w11091807>
- Takaku, J., Tadono, T., Tsutsui, K., 2014. Generation of High Resolution Global DSM from ALOS PRISM. *Int. Arch. Photogramm. Remote Sens. Spatial Inf. Sci.* XL-4, 243–248. <https://doi.org/10.5194/isprsarchives-XL-4-243-2014>
- Timmer, H., Verdel, J., Jongmans, A., 2003. Well clogging by particles in Dutch well fields. *Journal American Water Works Association* 95 (2003) 8 95. <https://doi.org/10.1002/j.1551-8833.2003.tb10434.x>
- Waterloo, M.J., Arshad, R., la Loma González, B., Monente, G.S., 2025. Rainwater harvesting potential from photovoltaic energy systems in the Sahel. *Water-Energy Nexus*. <https://doi.org/10.1016/j.wen.2025.04.002>
- Zanaga, D., Van De Kerchove, R., Daems, D., De Keersmaecker, W., Brockmann, C., Kirches, G., Wevers, J., Cartus, O., Santoro, M., Fritz, S., Lesiv, M., Herold, M., Tsendbazar, N.-E., Xu, P., Ramoino, F., Arino, O., 2022. ESA WorldCover 10 m 2021 v200. <https://doi.org/10.5281/zenodo.7254221>
- Zhao, L., Zhu, W., Tong, W., 2009. Clogging processes caused by biofilm growth and organic particle accumulation in lab-scale vertical flow constructed wetlands. *Journal of Environmental Sciences* 21, 750–757. [https://doi.org/10.1016/S1001-0742\(08\)62336-0](https://doi.org/10.1016/S1001-0742(08)62336-0)

## **Annex 1 – Desk Review**

## **Annex 2 - Input Data Preparation and Processing for the SWAT Model**

## **Annex 3 – Monte Carlo Calibration**

**Global Head Office**

Van Hogendorpplein 4  
Gouda, 2805 BM  
The Netherlands

**Regional Office  
East Africa**

Woreda 03, Bole Sub city  
House No. 4/020  
Addis Ababa  
Ethiopia

[www.acaciawater.com](http://www.acaciawater.com)